Open access • Journal Article • DOI:10.1190/1.2035909

The Electromagnetic Response of a Conductive Inhomogeneity in a Layered Earth

J. J. Lajoie, Gordon F. West

Institutions: University of Toronto

Published on: 01 Dec 1976 - Geophysics (Society of Exploration Geophysicists)

Topics: Integral equation

RESEARCH
IN
APPLIED GEOPHYSICS

THE ELECTROMAGNETIC RESPONSE OF A CONDUCTIVE INHOMOGENEITY IN A LAYERED EARTH

BY

JULES J. LAJOIE

NO. 6

OCT. 1973

GEOPHYSICS LABORATORY
DEPARTMENT OF PHYSICS
UNIVERSITY OF TORONTO

THE ELECTROMAGNETIC RESPONSE OF A CONDUCTIVE INHOMOGENEITY IN A LAYERED EARTH.

BY

JULES J. LAJOIE

A thesis submitted in conformity with
the requirements for the degree of
Doctor of Philosophy in the University
of Toronto, Department of Physics

1973

ACKNOWLEDGEMENTS

During the course of this research, it has been a pleasure to work with the staff and graduate students of the Geophysics Lab. at the University of Toronto, and, in particular, with my supervisor, Dr. G.F. West. I am deeply indebted to him for his guidance, ideas, and unfailing enthusiasm.

I wish to thank Yves Lamontagne and Peter Annan for many hours of stimulating discussions on the theoretical and practical aspects of the research. Dr. West and Yves Lamontagne are responsible for the idea of separating the current flow in the anomalous conductor into divergence free and curl free types. This formulation eventually led to the successful numerical simulation of the problem. Also, it has been a pleasure to work with J. Alfonso-Roche during the development of the FFT filtering approach.

I am grateful to Dr. Misac Nabighian of the Newmont Exploration Co. for correcting the final version of the manuscript.

Dr. Ted Clee's help and advice with programming problems is sincerely appreciated. The authors of some of the computer programs used in the thesis are as follows: Gaussian quadrature integration routines: Peter Annan; Contouring Package: Yves Lamontagne; Perspective plotting routine: Dr. Nigel Edwards.

I wish to thank Noranda Mines Ltd. for their generous financial support through the Noranda Graduate Research Fellowship. The computing bill was borne by the National Research Council of Canada.

ABSTRACT

In this thesis, the integral equation technique is used to model the electromagnetic prospecting problem of a conductive inhomogeneity embedded in a layered earth environment. Basically, it consists of replacing the anomalous conductor, which is simplified to a finite vertical thin plate, by a surface of scattering currents. The plate is sampled on a sqare grid and the number of points is kept to a minimum by using a fifth degree spline moment function to interpolate between them. In order to bypass the numerical problems encountered when attempting to solve directly for the components of electric field at each grid point, the integral equation is expressed in terms of two potentials representing divergence free current flow inside the plate and curl free current flow through its surface. Calculations involving the layered earth are done with a new Fast Fourier transform approach which basically consists of solving this problem in the Catesian wavenumber domain, i.e. the 2-D Fourier transform of the horizontal plane.

The results show that a conductive host and/or overburden will affect the amplitude, phase and width of the conductor's free air anomaly. Both the host and the overburden will cause an attenuation and phase rotation of the source fields to the plate and the anomalous fields from the plate. When the target conductor is in contact with a conductive host, the channelling of currents induced in the host is found to increase the anomally amplitude substantially.

Computation costs do not permit the generation of high accuracy type curves, but the model examples presented demonstrate the basic physics of conductive earth effects in electromagnetic prospecting.

CONTENTS

CHAPTER 1

INTRODUCTION

1.1 Electromagnetic Methods in Geophysics

The electromagnetic method is a powerful technique in exploring for electrically conductive mineral deposits in the first two hundred or so metres of the earth's crust, and it is the subject of continuing research and development. It's major use is in base metal exploration but other applications of the method have been found in such areas as geological mapping, petroleum exploration and engineering. Through attrition, the search for new metal deposits is obviously becoming more difficult and progress must constantly be made in equipment, the optimization of field survey methods, and data processing. Multifrequency electromagnetic systems are presently being developed to give a 'three-dimensional view' of the earth's conductivity structure. To interpret the data from such systems it is necessary to have a better understanding of how electromagnetic fields propagate in a typical geological environment. This may be achieved by laboratory scale model studies and numerical modelling with the aid of a computer.

Other disciplines of exploration geophysics such as

gravity, magnetics and seismology are more advanced than electromagnetics. In these areas, optimal inversion schemes and computer interactive interpretation methods are now being applied. In electromagnetic and induced polarization methods, however, we are still attempting to model and understand the direct problem, the EM field pattern of a source in a realistic geological setting.

The numerical modelling of the electromagnetic response of the earth is a difficult task, a fact which is certainly not apparent upon first inspection of Maxwell's equations. Much has been accomplished by analytical methods in computing the EM response of models where boundaries between media of different electrical properties are defined by a constant on a coordinate axis; e.g. constant depth for problems involving a layered earth (Sunde, 1949; Wait, 1970; Frischknecht, 1967; and others), constant spherical radius (Negi, 1967; Nabighian, 1971), and constant angles for problems with cylindrical symmetry (Geyer, 1972). For such geometries, the setting up of boundary conditions for the electromagnetic fields is greatly simplified.[1]

[1] The literature of EM theory with geophysical applications is so vast it is impossible to reference all the important contributions here. Only a selection of more recent or general papers is given here and in what follows.

Numerical methods have been used to obtain solutions for two-dimensional structures and sources. Finite difference, finite element and integral equation techniques have been employed (Swift, 1971; Coggon, 1971; Parry, 1969; Hohmann, 1970). Lamontagne (1971) has computed the response of a rectangular thin plate in air to a Turam loop source.

Another approach is to study model conductors in the laboratory (West, 1960). Ghosh and West (1972) have produced a suite of type curves for the response of sheet-like conductors to several airborne EM systems. Modelling in an electrolytic tank (Dosso, 1966) is very useful for studying the response of odd shaped conductors in a solution that represents a background homogeneous earth. Goldstein (1971) has modelled two quarter spaces of different conductivity by building a special retainer wall that satisfies the EM boundary conditions at the interface.

The theoretical solutions have greatly increased our understanding of the physical processes in the electromagnetic methods. In mining geophysics, however, the geometry most closely resembling actual field conditions is a local source near a finite electrically conductive inhomogeneity which is embedded in a layered earth environment, and it has not yet been possible to solve this problem.

1.2 Thesis Objectives and Outline

A good deal of ground and airborne EM interpretation is based on data from scale model experiments using thin sheet-like conductors in air to represent target conductive zones in the ground. The effect of the rock surrounding the conductor and overlying soil has been largely neglected in practical interpretation, although there has been considerable recent research interest in this area. Due to numerical and computational problems, most of the research has been directed to laboratory model studies (Lowrie, 1965; Gupta, 1973; Ward, 1973; and Wong, 1973). This research work clearly demonstrates that in many situations the host rock and overburden will have a significant effect on the free air anomaly, making the standard interpretation techniques erroneous.

The search for new orebodies is presently retreating to classically unsuitable areas of higher overburden and host rock conductivity such as the plains of Western Australia. Current instrumentation development of the low frequency type (Paterson, 1972) and time domain ground systems (Lamontagne, 1973) are geared to attacking these areas. There is obviously a need for guidance and direction from theoretical studies. The field geophysicist requires an understanding of host rock and conductive overburden effects to optimize the information return from field surveys.

The purpose of this thesis, therefore, is to study the combined effects of host rock and conductive overburden so that the basic physical processes can be better understood and to develop the computational capability to solve these problems with the aid of the computer. To this end, the thesis is divided into two main sections. One concerns the development of a FFT (Fast Fourier Transform) filtering approach for solving the electromagnetic response of a layered earth. This technique takes advantage of the Fast Fourier Transform program to solve the layered earth induction problem in the wavenumber domain. In many circumstances it requires much less computation time than the standard methods available to date, and has greater flexibility. The other section consists of solving the problem of an electrical inhomogeneity within the stack of layers. In order to make the computation manageable, the inhomogeneity is taken as a thin vertical plate. This implies that the electric field perpendicular to the plate in uncoupled from the two field components in the plane of the plate. The general solution for the electromagnetic fields in the plate is found by an integral equation technique. The FFT filtering approach is used in solving the integral equation to transmit the fields through the layers and to

solve for the interaction between the layers and the plate.

The number of independent variables in such problems is very large and hence this thesis makes no attempt to present a complete catalogue of type curves. Rather, the computational techniques and mathematical development are presented in detail, with the example solutions intended to demonstrate the scope of the methods and physics of the problem.

The remainder of this chapter introduces the basic concepts for the computational techniques used in the thesis. Chapter 2 is divided into two sections. One concerns the theory of the FFT filtering approach for the layered earth problem and the other the integral equation formulation for the conductive inhomogeneity. In Chapter 3 examples of solutions for the layered earth problem are presented to demonstrate the limits and scope of the FFT filtering approach. Chapter 4 is a heuristic presentation of some solutions for a plate embedded in a conducting host medium of infinite extent. Chapter 5 presents solutions for the plate in a layered earth environment. Chapter 6 includes the general conclusions and a discussion of the possible extensions and applications of the work presented in the thesis.

1.3 The Layered Earth Problem

In the previously quoted references and in most of the published material attacking the problem of EM induction in a layered earth, the approach is to express the EM response in an integral of the general form:

$$\int_0^\infty \Psi(\lambda)\, e^{-z(\lambda^2+\gamma^2)^{1/2}}\, J(\lambda\rho)\, d\lambda$$

where ψ is a complex function involving the layered earth and the source parameters, J is a Bessel function, λ the variable of integration, and γ is the propagation constant $= (-\omega^2\mu\varepsilon + i\sigma\mu\omega)^{1/2}$. The integral which usually must be evaluated by numerical integration, gives a field value at one point in space. For any other point it must be reevaluated. Since the integrand is oscillatory and complex, and in some cases converges slowly as a function of λ, the numerical integration can be costly and is subject to truncation errors. Also, when formulating the problem in this manner, it is practical to deal only with sources having a simple geometry, such as dipoles and lines.

In contrast to this, the FFT filtering approach solves the layered earth EM induction problem in the Cartesian wavenumber domain, i.e. the two dimensional

Fourier transform of the horizontal x-y plane, and allows a completely arbitrary source current distribution. As shown in Figure 1-1, the horizontal (x,y) distribution of the vectors $\overline{E}$ and $\overline{H}$ can be defined on a grid in the x-y plane of the space domain or, equivalently, in the u-v plane of the wavenumber domain, via the 2-D Fast Fourier Transform. This approach then considers the complete distribution in one plane at the same time.

There are three reasons why a wavenumber domain solution is preferable. The first and most important is that the induction problem becomes multiplicative, i.e.

$$\left\{\begin{matrix}\text{EM}\\ \text{RESPONSE}\end{matrix}\right\} = \left\{\begin{matrix}\text{SOURCE}\\ \text{TERM}\end{matrix}\right\} \text{ x } \left\{\begin{matrix}\text{TRANSFER FUNCTION}\\ \text{OF}\\ \text{EARTH MODEL}\end{matrix}\right\}$$

where the source term and transfer function are completely independent. The wavenumber domain multiplication corresponds to the integration or convolution of the space domain. Secondly, it is desirable in the theoretical development to reduce the number of variables by using potentials, and the components of electric and magnetic field are expressed as various derivatives of Hertz potentials. In the wavenumber domain, the derivative operators become

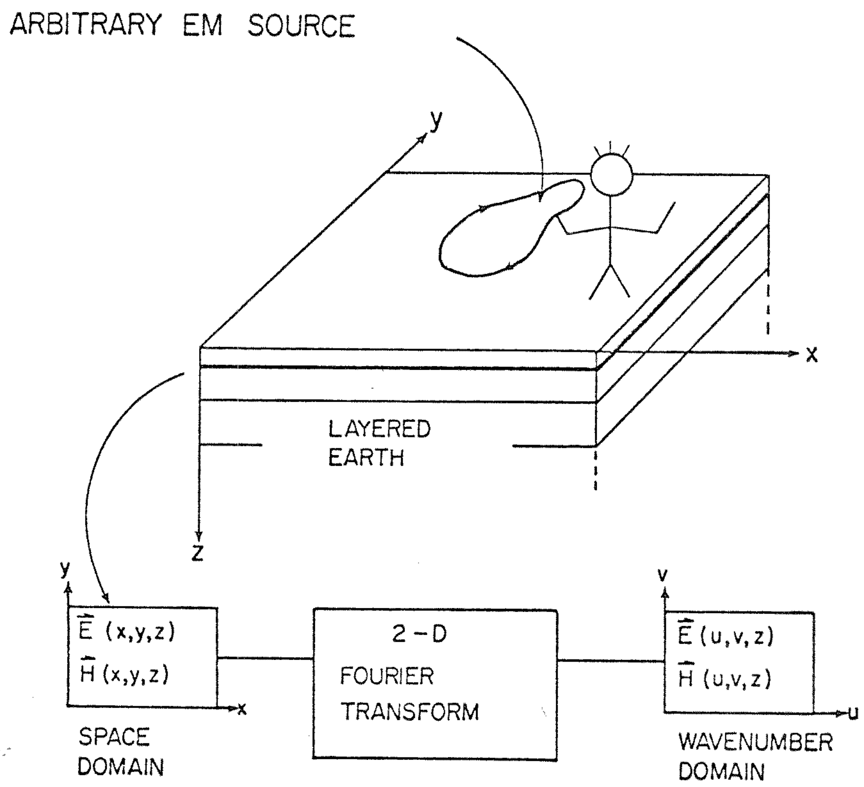

Fig. 1-1: The space domain and wavenumber domain

simple multiplicative operators:

e.g. Space Domain:

$$E_y(x,y,z) = i\omega \frac{\partial}{\partial x} \Gamma(x,y,z)$$

Wavenumber Domain:

$$E_y(u,v,z) = i\omega(iu)\Gamma(u,v,z)$$

where Γ is the magnetic Hertz potential. Finally, the wavenumber domain solution can be continued up or down by applying the standard exponential continuation operator of the form

$$e^{-(u^2+v^2+\gamma^2)^{1/2}z}$$

where γ is the propagation constant of the medium.

Figure 1-2 is a flow chart for the FFT filtering approach. In steps 1 to 3 the source fields are transformed to the wavenumber domain via FFT. In step 4 the source Hertz potentials are obtained by multiplication with the appropriate derivative operators. For simple sources such as dipoles and lines, the source Hertz potentials may be computed directly in the wavenumber domain, thereby eliminating the first four steps. Next, the source potentials are multiplied with the appropriate layered earth transfer function to obtain the total potentials. The transfer function is a function of the number of layers, their conductivities, thicknesses etc. and also contains the continuation operator

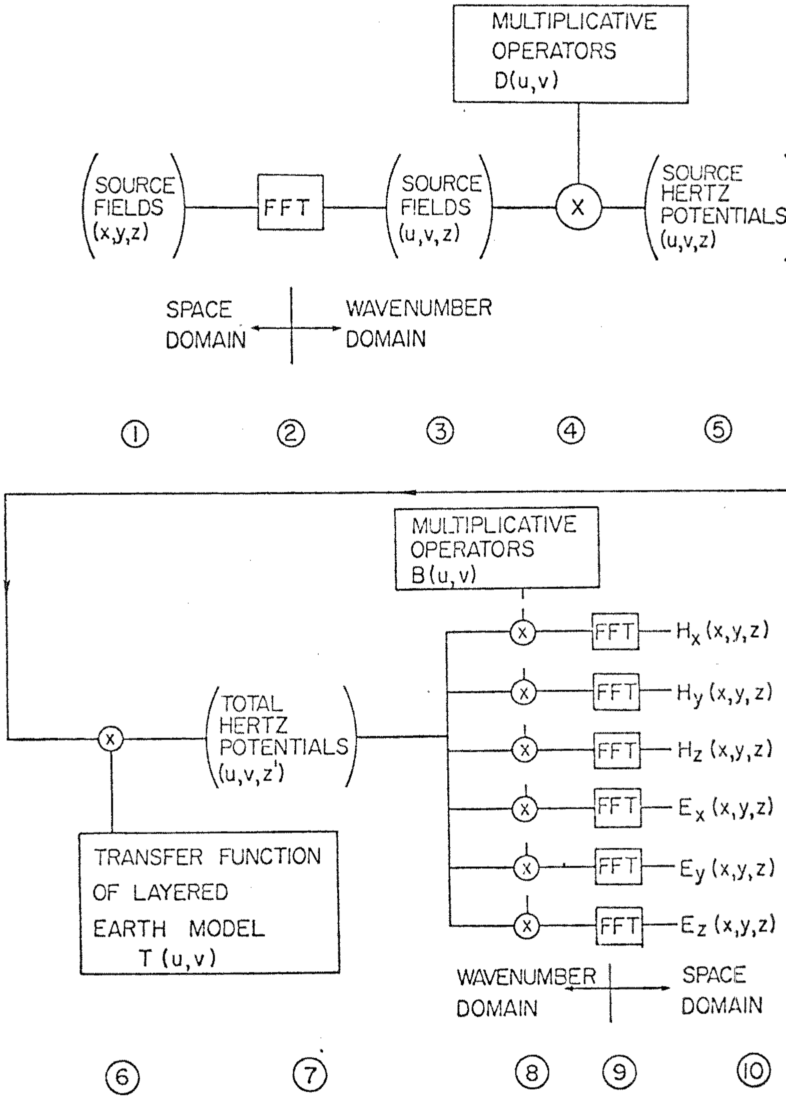

Fig. 1-2: Flow chart of the FFT filtering approach.

for continuation to the observation plane. This is the crucial point in the approach as it relates INPUT and OUTPUT potentials in the wavenumber domain. The next step is to multiply by the appropriate derivative operators for the field components desired, and transform back to the space domain. The output is the complete horizontal distribution of any component of the electromagnetic field. Figure 1-2 represents the most general sequence of events. In most cases, we can include steps 4, 6 and 8 into one filter operator.

The FFT filtering approach allows much more flexibility in solving layered earth models. For example, when attempting to fit field data, the source potentials may be stored onto computer disk and repeatedly multiplied by the transfer functions of the various earth models until a suitable fit is obtained. The computer programming is simple and straightforward. As will be shown later, numerical accuracy is limited only by considerations of sampling interval and record length in common with any discrete Fourier technique. Weaver (1970) describes the basic theory for this approach by solving analytically for the response of the homogeneous earth in terms of a Fourier integral rather than a Hankel transform.

1.4 Numerical Modelling of a Finite Conductive Inhomogeneity In a Layered Earth

The 2-D solutions for structures extending to infinity in one direction are undoubtedly very useful for studying the responses of geological features of large strike extent such as faults and dykes. They may have limited application in mining geophysics, however, where the strike extent can be a fraction of the distance to the source. Also none of the published techniques to date can handle a three dimensional source field.

Three dimensional electromagnetic modelling can be an obscure and costly undertaking. The many difficulties arise from the necessity of representing the electromagnetic equations for continuous media with a finite number of points. Many of the problems of 3-D modelling do not occur in 2-D modelling. The numerics in 3-D may not adequately represent the curl and divergence operators and the interaction between them. For example $\bar{\nabla}\cdot\bar{\nabla}\mathrm{x}\bar{A} \equiv 0$ analytically, but this may not be exactly satisfied numerically and small errors may produce large effects. In 2-D this particular difficulty does not occur because the problem may be broken down into two independent polarizations representing the current flowing either parallel or perpendicular to the strike of the surfaces of conductivity contrast. Another problem is that the simple approximations used for generating the 2-D Green's dyadic simply do not work in 3-D.

If a three dimensional conductive inhomogeneity is represented by N sampling points, there are 3N unknowns in the problem,viz. the three components of electric field at each sampling point. Therefore a 3N X 3N matrix must be generated and solved. A great saving in computation cost may be achieved by reducing the inhomogeneity to a thin plate. 'Thin' implies that the current component perpendicular to the plate is unaffected by the plate and uncoupled from the two components in the plane of the plate. This effectively reduces the problem to 2N unknowns, the two components of electric field in the plane of the plate.

In this thesis, the numerical modelling is done using the integral equation technique. Basically, it consists of expressing the solution for the total electric field inside a region of anomalous conductivity, in integral form. The procedure then is to express the equations digitally, form a matrix equation, and solve for the total field in the anomalous region. The source vector for the matrix equation is the field that would exist in the region of the inhomogeneity if it were absent. The anomalous field outside the region is then found by integrating over the scattering field inside the region.

Obviously thin plates do not occur in nature. However, this model has served very well in the past to represent many types of conductive veins, shears or dipping strata, and it does offer an opportunity to study the combined effects of conduction and induction for a finite inhomogeneity in a layered earth environment, and at reasonable cost on present day computers. If suites of type curves for a buried inhomogeneity were to be made for interpretation purposes the thin plate would be the first choice for a model.

CHAPTER 2

THEORY

2.1 Mathematical Notation

Symbols

x,y,z	coordinate axes; z positive down
r	$\sqrt{(x^2 + y^2)}$
R	$\sqrt{(x^2 + y^2 + z^2)}$
$\overline{i},\overline{j},\overline{k}$	unit vectors for coordinate axes
u,v	wavenumbers in x and y directions respectively
ρ	$\sqrt{(u^2 + v^2)}$
$\overline{E}(x,y,z)$	electric field intensity
$\overline{B}(x,y,z)$	magnetic induction
$\overline{H}(x,y,z)$	magnetic field intensity
$\overline{\Pi}(x,y,z)$	electric Hertz potential
$\overline{\Gamma}(x,y,z)$	magnetic Hertz potential
$\hat{\overline{E}}(u,v,z)$	Fourier transform of $\overline{E}(x,y,z)$
$\hat{\overline{B}}(u,v,z)$	Fourier transform of $\overline{B}(x,y,z)$
$\hat{\overline{H}}(u,v,z)$	Fourier transform of $\overline{H}(x,y,z)$
$\hat{\overline{\Pi}}(u,v,z)$	Fourier transform of $\overline{\Pi}(x,y,z)$
$\hat{\overline{\Gamma}}(u,v,z)$	Fourier transform of $\overline{\Gamma}(x,y,z)$
$\overline{J}$	electric current density
$\overline{M}$	magnetic current density

σ	conductivity
μ_0	permeability
ε_0	permittivity
ω	angular frequency
Y	admittivity = $\sigma+i\omega\varepsilon$
Z	impedivity = $i\omega\mu$
γ	propagation constant = $\surd(ZY)$
k	$\surd(\rho^2 + \gamma^2)$

Partial Derivative Notation

To simplify the mathematical text, the partial derivatives of the Hertz potentials are indicated by the subscripts 1,2,3 corresponding to differentiation with respect to x,y,z respectively:

e.g. $\bar{\Pi} = \bar{\Pi}(x,y,z)$,

then $\partial\bar{\Pi}/\partial x = \bar{\Pi}_1$

and $\partial^2\Pi/\partial z\partial y = \bar{\Pi}_{32}$

On the other hand, x,y,z subscripts refer to the vector components.

Derivative and Integral Operators

Space Domain — Wavenumber Domain

$$\partial/\partial x\,,\ \int dx \longleftrightarrow \{iu\}\,,\ \{iu\}^{-1}$$

$$\partial/\partial y\,,\ \int dy \longleftrightarrow \{iv\}\,,\ \{iv\}^{-1} \qquad 2.1\text{-}1$$

Compact Notation

if $\bar{r} = x\bar{i} + y\bar{j}$ and $\bar{\rho} = u\bar{i} + v\bar{j}$,

then $\phi(\bar{r},z) = \phi(x,y,z)$ and $\phi(\bar{\rho},z) = \phi(u,v,z)$,

and $r = |\bar{r}| = \sqrt{(x^2+y^2)}$ and $\rho = |\bar{\rho}| = \sqrt{(u^2+v^2)}$.

The Fourier Transform Pair

$$\bar{F}(u,v,z) = \int_{-\infty}^{\infty}\int_{-\infty}^{\infty} \bar{\phi}(x,y,z)\, e^{-i(ux+vy)}\, dx\, dy$$

$$\bar{\phi}(x,y,z) = \frac{1}{(2\pi)^2}\int_{-\infty}^{\infty}\int_{-\infty}^{\infty} \bar{F}(u,v,z)\, e^{+i(ux+vy)}\, du\, dv \qquad 2.1\text{-}2$$

2.2 Integral Equation Formulation for a 'Thin' Plate In a Layered Earth

a) General Case

Figure 2-1 shows the layered earth model containing an anomalous region R of electrical properties (Y_P, Z_P) in a host medium (Y_H, Z_H).

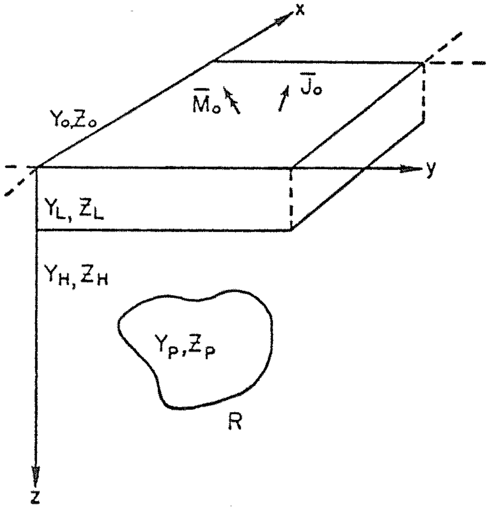

Fig. 2-1. The layered earth model with an anomalous region R of electrical properties (Y_P, Z_P).

In a homogeneous medium of macroscopic properties (Y, Z), Maxwell's source equations may be written as

$$\bar{\nabla} \times \bar{H} = Y\bar{E} + \bar{J} \qquad 2.2\text{-}1$$

and

$$\bar{\nabla} \times \bar{E} = -Z\bar{H} - \bar{M}, \qquad 2.2\text{-}2$$

where $\bar{J}$ is any impressed electric source current and $\bar{M}$ any "magnetic current" source.

In region H, the curl equations for the total field may be written as

$$\bar{\nabla} \times \bar{H} = Y_H \bar{E} + \bar{J}_{EQ} \qquad 2.2\text{-}3$$

and

$$\bar{\nabla} \times \bar{E} = -Z_H \bar{H} - \bar{M}_{EQ}, \qquad 2.2\text{-}4$$

where $\bar{J}_{EQ}$ and $\bar{M}_{EQ}$ are written to represent the equivalent sources for region H. Equivalent source distributions are required because the actual source currents may be located in regions having $Y \neq Y_H, Z \neq Z_H$.

Inside R, the total field equations are

$$\bar{\nabla} \times \bar{H} = Y_P \bar{E} \qquad 2.2\text{-}5$$

and

$$\bar{\nabla} \times \bar{E} = -Z_P \bar{H} \qquad 2.2\text{-}6$$

Alternatively, they may be written in the form

$$\bar{\nabla} \times \bar{H} = Y_H \bar{E} + \bar{J}_I \qquad 2.2\text{-}7$$

and

$$\bar{\nabla} \times \bar{E} = -Z_H \bar{H} - \bar{M}_I \quad , \qquad 2.2\text{-}8$$

where $\bar{J}_I = (Y_P - Y_H)\bar{E}$ and $\bar{M}_I = (Z_P - Z_H)\bar{H}$ represent the induced or impressed electric and magnetic sources inside R. As far as the electromagnetic problem in concerned, the impressed sources $\bar{J}_I$ and $\bar{M}_I$ effectively replace the inhomogeneity (Y_P, Z_P).

Combining the above equations, the following relations are valid throughout the halfspace H including the region R:

$$\bar{\nabla} \times \bar{H} = Y_H \bar{E} + \bar{J}_{EQ} + \bar{J}_I \qquad 2.2\text{-}9$$

and

$$\bar{\nabla} \times \bar{E} = -Z_H \bar{H} - \bar{M}_{EQ} - \bar{M}_I \quad . \qquad 2.2\text{-}10$$

Since these equations are linear the fields may be separated into two parts:

$$\bar{E} = \bar{E}^P + \bar{E}^S \qquad 2.2\text{-}11$$

and

$$\bar{H} = \bar{H}^P + \bar{H}^S \quad , \qquad 2.2\text{-}12$$

where the primary fields E^P and H^P are due to $\bar{J}_{EQ}$ and $\bar{M}_{EQ}$ and the scattered fields $\bar{E}^S$ and $\bar{H}^S$ are due to $\bar{J}_I$ and $\bar{M}_I$.

Therefore

$$\bar{\nabla} \times \bar{H}^P = Y_H \bar{E}^P + \bar{J}_{EQ} \quad , \qquad 2.2\text{-}13$$

$$\bar{\nabla} \times \bar{E}^P = -Z_H \bar{H}^P - \bar{M}_{EQ} \quad , \qquad 2.2\text{-}14$$

$$\bar{\nabla} \times \bar{H}^S = Y_H \bar{E}^S + \bar{J}_I \quad , \qquad 2.2\text{-}15$$

and

$$\bar{\nabla} \times \bar{E}^S = -Z_H \bar{H}^S - \bar{M}_I \quad . \qquad 2.2\text{-}16$$

$\bar{J}_I$ and $\bar{M}_I$ are the scattering electric and magnetic currents which replace the inhomogeneity. They are zero outside R.

The problem is then to solve for the scattered fields in the region R, given the incident fields in this same region. The incident fields for the layered earth environment are readily obtained through the FFT filtering approach.

We now break from generality to consider only inhomogeneities in conductivity. The following derivation however would hold equally well for inhomogeneities in permeability and permittivity.

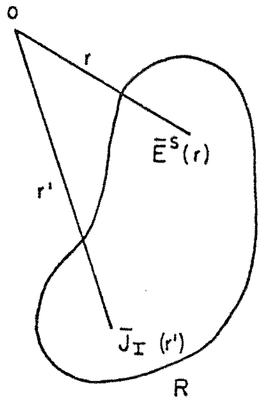

Fig. 2-2. The scattered electric field at r due to the impressed current at r'.

As outlined in Figure 2-2 the scattered electric field at any point r within the region R is due to the cumulative effect of the impressed currents $\bar{J}_I(r') = (Y_P - Y_H)\,\bar{E}(r')$ flowing throughout R, in the presence of the background medium. The background medium may be separated into two parts, the host layer acting as if it were infinite in extent, and the effect of the differing properties in the layers above. The second effect, called here the plate-layer interaction, may be found with the FFT filtering approach and will be dealt with later. For now, the host layer is

considered to be of infinite extent, and the problem is to solve for the scattered fields inside the inhomogeneity in the presence of an infinite host of finite conductivity.

The Infinite Host

In the presence of the infinite host medium, whose electrical properties are now denoted by the unsubscripted variables Y, Z, and γ, the scattered electric field at a point r, inside R, due to impressed currents $\bar{J}_I(r')$ throughout R, may be written as

$$\bar{E}^s(\bar{r}) = \iiint_{-\infty}^{\infty} \left\{ -\gamma^2\, \bar{\bar{\Pi}}(r,r') + \bar{\nabla}_r\, \bar{\nabla}_r \cdot \bar{\bar{\Pi}}(r,r') \right\} d^3r', \qquad 2.2\text{-}17$$

where the Hertz vector at r due to a current element $\bar{J}_I$ at r' is given by

$$\bar{\bar{\Pi}}(r,r') = \frac{1}{4\pi Y}\, \bar{\bar{J}}_I(r')\, \frac{e^{-\gamma|r-r'|}}{|r-r'|} \qquad 2.2\text{-}18$$

and $\bar{J}_I(r')$ is zero outside R.

Now, using the identity

$$\bar{\nabla}_r \cdot \left\{ \frac{e^{-\gamma R}}{R}\, \bar{J}_I(r') \right\} = \frac{e^{-\gamma R}}{R}\, \bar{\nabla}_{r'} \cdot \bar{J}_I(r') - \bar{\nabla}_{r'} \cdot \left\{ \frac{e^{-\gamma R}}{R}\, \bar{J}_I(r') \right\}, \qquad 2.2\text{-}19$$

where $R = |r-r'|$, and the property that $\bar{\nabla}_{r'} \cdot \bar{J}_I(r') \equiv 0$ inside a homogeneous conductor, equation 2.2-17 reduces to

$$\bar{E}^s(r) = -\frac{Z}{4\pi} \iiint_{-\infty}^{\infty} \frac{e^{-\gamma R}}{R}\, \bar{\bar{J}}_I(r')\, d^3r' - \frac{\bar{\nabla}_r}{4\pi Y} \iiint_{-\infty}^{\infty} \bar{\nabla}_{r'} \cdot \left\{ \frac{e^{-\gamma R}}{R}\, \bar{\bar{J}}_I(r') \right\} d^3r'. \qquad 2.2\text{-}20$$

Applying Gauss' law, equation 2.2-20 reduces to

$$\bar{E}^{s}(r) = -\frac{Z}{4\pi}\iiint_{-\infty}^{\infty}\frac{e^{-\gamma R}}{R}\,\bar{J}_{I}(r')\,d^{3}r' - \frac{1}{4\pi Y}\oiint_{S}\bar{\nabla}_{r}\left(\frac{e^{-\gamma R}}{R}\right)J_{I_{\hat{n}}}(r')\,d^{2}r' \qquad 2.2\text{-}21$$

where the second integral is over the surface of the conductor and $J_{I_{\hat{n}}}$ is the component of $\bar{J}$ which is the outward normal to the surface.

2.2 b) Thin Plate Approximation

We begin by confining the impressed currents $\bar{J}_{I}(r')$ to the region $-t/2 < y < +t/2$ for all x,z.

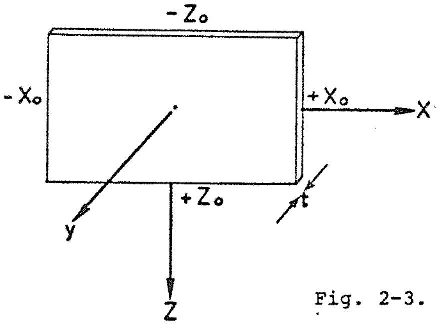

Fig. 2-3. The thin plate.

For this case equation 2.2-21 reduces to

$$\bar{E}^{s}(r) = -\frac{Z}{4\pi}\iint_{-\infty}^{\infty}\int_{-t/2}^{t/2}\frac{e^{-\gamma R}}{R}\,\bar{J}_{I}(r')\,d^{3}r' - \frac{1}{4\pi Y}\iint_{-\infty}^{\infty}\bar{\nabla}\left(\frac{e^{-\gamma R}}{R}\right)\left\{J_{I_y}(x',+\tfrac{t}{2},z') - J_{I_y}(x',-\tfrac{t}{2},z')\right\}d^{2}r' \qquad 2.2\text{-}22$$

In the thin sheet model, the assumption is that the impressed current sources are such that the components in the plane y=0 are the key variables, and they are assumed constant across the thickness of the plate $-t/2 < y < t/2$. Since we have assumed no permittivity contrast,

$$\bar{J}_I(r') = (Y_r - Y_H)\,\bar{E}(r') = \sigma_A(x',z')\,\bar{E}(r'), \qquad 2.2\text{-}23$$

where σ_A is the anomalous conductivity. $\sigma_A(x',z')$ may be expressed as

$$\sigma_A(x',z') = \sigma_A \cdot s(x',z'), \qquad 2.2\text{-}24$$

where s(x',z') is the unit gate window defined by

$$\begin{aligned} s(x',z') &= 1 \qquad -x_o < x < +x_o \\ &\qquad\quad\; -z_o < z < +z_o, \qquad 2.2\text{-}25 \\ &= 0 \qquad \text{otherwise.} \end{aligned}$$

Now, we may write

$$J_{I_y}(x,y,z) \cong J_{I_y}(x,0,z) + y\,\frac{\partial}{\partial y}\,J_{I_y}(x,0,z) \quad . \qquad 2.2\text{-}26$$

Since $\bar{\nabla}\cdot\bar{J} \equiv 0$ inside, equation 2.2-26 reduces to

$$J_{I_y}(x,y,z) \cong J_{I_y}(x,0,z) - y\left[\frac{\partial}{\partial x}J_{I_x}(x,0,z) + \frac{\partial}{\partial z}J_{I_z}(x,0,z)\right] \qquad 2.2\text{-}27$$

Substituting equation 2.2-27 into equation 2.2-22 we obtain

$$\begin{aligned} \bar{E}^s(r) = &-\frac{Zt}{4\pi}\iint_{-\infty}^{\infty}\frac{e^{-\gamma R}}{R}\,\bar{J}_I(r')\,d^2r' \\ &+\frac{t}{4\pi Y}\iint_{-\infty}^{\infty}\bar{\nabla}\left(\frac{e^{-\gamma R}}{R}\right)\left\{\frac{\partial}{\partial x}J_{I_x}(x,0,z) + \frac{\partial}{\partial z}J_{I_z}(x,0,z)\right\}d^2r' \end{aligned} \qquad 2.2\text{-}28$$

Thus we need only to know the impressed current in the central plane of the plate.

At this point, scalar potentials U and V are introduced to represent, respectively, the divergence free and curl free components of the impressed currents in the plane of the sheet. They are defined by

$$\frac{1}{\sigma_A}\,\bar{J}_I(x,z) = s(x,z)\,\bar{E}(x,z) = (\bar{\nabla}\times\bar{j}\,U_y)_{xz} - \bar{\nabla}_{xz}V \qquad 2.2\text{-}29$$

U is the same potential as used by Lamontagne (1971) in solving for induction in a finite plate in free space.

The introduction of potentials may seem an unnecessary complication. However, in a first computational attempt, the programs were set up to solve directly for the two components of total electric field in the plate. Although the results looked reasonable in form, the amplitude and phase were grossly incorrect. At first, this seemed to be a simple programming error. Upon closer inspection, however, it was found to result from solving for both inductive and conductive currents in each component of the field. For a reasonably resistive background, the conduction matrix operator $\left(\sim \frac{1}{4\pi\Upsilon}\right)$ was so much larger than the inductive matrix operator $(\sim \bar{a})$ that the latter was effectively lost when the two terms were added together to form the coefficient matrix. Solving for the two new variables U and V bypasses this problem. The electric field vectors may be obtained from the solutions of U and V by finite difference curl and gradient operators.

Substituting equation 2.2-29 into equation 2.2-27,

$$J_{I_y}(x, +t/2, z) = J_{I_y}(x, 0, z) + \frac{t}{2}\,\sigma_A\,\nabla^2 V$$

and

$$J_{I_y}(x, -t/2, z) = J_{I_y}(x, 0, z) - \frac{t}{2}\,\sigma_A\,\nabla^2 V \quad . \qquad 2.2\text{-}30$$

Substituting equation 2.2-30 into equation 2.2-22,

$$\bar{E}^s(r) = \frac{-2t}{4\pi}\iint_{-\infty}^{\infty}\frac{e^{-\gamma R}}{R}\,\bar{J}_I(r')\,d^2r' - \frac{t\,\sigma_A}{4\pi\Upsilon}\iint_{-\infty}^{\infty}\bar{\nabla}\left(\frac{e^{-\gamma R}}{R}\right)\nabla^2 V(r')\,d^2r' \qquad 2.2\text{-}31$$

Substituting equation 2.2-29 and 2.2-31 into 2.2-11 and writing for each component, x and z,

$$\frac{\partial U}{\partial z} + \frac{\partial V}{\partial x} + a\,s(x,z)\iint_{-\infty}^{\infty}\frac{e^{-\gamma R}}{R}\left(\frac{\partial U(r')}{\partial z'} + \frac{\partial V(r')}{\partial x'}\right)d^2r'$$
$$- b\,s(x,z)\iint_{-\infty}^{\infty}\frac{\partial}{\partial x}\left(\frac{e^{-\gamma R}}{R}\right)\nabla_{r'}^2 V(r')\,d^2r' = -s(x,z)\,E_x^{\,p} \,, \qquad 2.2\text{-}32$$

and

$$\frac{\partial U}{\partial x} - \frac{\partial V}{\partial z} + a\,s(x,z)\iint_{-\infty}^{\infty}\frac{e^{-\gamma R}}{R}\left(\frac{\partial U(r')}{\partial x'} - \frac{\partial V(r')}{\partial z'}\right)d^2r'$$
$$+ b\,s(x,z)\iint_{-\infty}^{\infty}\frac{\partial}{\partial z}\left(\frac{e^{-\gamma R}}{R}\right)\nabla_{r'}^2 V(r')\,d^2r' = s(x,z)\,E_z^{\,p} \,, \qquad 2.2\text{-}33$$

where $a = \frac{2t\,\sigma_A}{4\pi}$ and $b = \frac{t\,\sigma_A}{4\pi\Upsilon}$.

A set of integral equations for the U and V potentials may be obtained from the derivatives of equations 2.2-32 and 2.2-33 as follows:

$\underline{\partial\ /\partial z\ \ -\ 2.2\text{-}32}$:

$$\frac{\partial^2 U(r)}{\partial z^2} + \frac{\partial^2 V(r)}{\partial x\,\partial z}$$
$$+ \left[\delta(z+Z_0) - \delta(z-Z_0)\right]\left\{a\iint_{-\infty}^{\infty}\frac{e^{-\gamma R}}{R}\left(\frac{\partial U(r')}{\partial z'} + \frac{\partial V(r')}{\partial x'}\right)d^2r' - b\iint_{-\infty}^{\infty}\frac{\partial}{\partial x}\left(\frac{e^{-\gamma R}}{R}\right)\nabla_{r'}^2 V(r')\,d^2r'\right\}$$
$$+ a\oiint\frac{\partial}{\partial z}\,\frac{e^{-\gamma R}}{R}\left\{\frac{\partial U(r')}{\partial z'} + \frac{\partial V(r')}{\partial x'}\right\}d^2r' - b\oiint\frac{\partial^2}{\partial x\,\partial z}\,\nabla_{r'}^2 V(r')\,d^2r'$$
$$= -\left[\delta(z+Z_0) - \delta(z-Z_0)\right]E_x^{\,p}(r) - \frac{\partial}{\partial z}E_x^{\,p}(r) \quad . \qquad 2.2\text{-}34$$

$\underline{\partial\ /\partial x\ \ -\ 2.2\text{-}32}$:

$$\frac{\partial^2 U(r)}{\partial x\,\partial z} + \frac{\partial^2 V(r)}{\partial x^2}$$
$$+ \left[\delta(x+X_0) - \delta(x-X_0)\right]\left\{a\iint_{-\infty}^{\infty}\frac{e^{-\gamma R}}{R}\left(\frac{\partial U(r')}{\partial z'} + \frac{\partial V(r')}{\partial x'}\right)d^2r' - b\iint_{-\infty}^{\infty}\frac{\partial}{\partial x}\left(\frac{e^{-\gamma R}}{R}\right)\nabla_{r'}^2 V(r')\,d^2r'\right\}$$
$$+ a\oiint\frac{\partial}{\partial x}\left(\frac{e^{-\gamma R}}{R}\right)\left\{\frac{\partial U(r')}{\partial z'} + \frac{\partial V(r')}{\partial x'}\right\}d^2r' - b\oiint\frac{\partial^2}{\partial x^2}\,\nabla_{r'}^2 V(r')\,d^2r'$$
$$= -\left[\delta(x+X_0) - \delta(x-X_0)\right]E_x^{\,p}(r) - \frac{\partial}{\partial x}E_x^{\,p}(r) \,. \qquad 2.2\text{-}35$$

$\partial\ /\partial z$ 2.2-33:

$$\frac{\partial^2 U(r)}{\partial x\,\partial z} - \frac{\partial^2 V(r)}{\partial z^2}$$
$$+\left[\delta(z+Z_0)-\delta(z-Z_0)\right]\left\{a\iint_{-\infty}^{\infty}\frac{e^{-\gamma R}}{R}\left(\frac{\partial U(r')}{\partial x'}-\frac{\partial V(r')}{\partial z'}\right)d^2r' + b\iint_{-\infty}^{\infty}\frac{\partial}{\partial z}\left(\frac{e^{-\gamma R}}{R}\right)\nabla_{r'}^2 V(r')\,d^2r'\right\}$$
$$+\,a\oiint\frac{\partial}{\partial z}\left(\frac{e^{-\gamma R}}{R}\right)\left(\frac{\partial U(r')}{\partial x'}-\frac{\partial V(r')}{\partial z'}\right)d^2r' + b\oiint\frac{\partial^2}{\partial z^2}\left(\frac{e^{-\gamma R}}{R}\right)\nabla_{r'}^2 V(r')\,d^2r'$$
$$=\left[\delta(z+Z_0)-\delta(z-Z_0)\right]E_z^{p} + \frac{\partial}{\partial z}E_z^{p}\qquad. \qquad 2.2\text{-}36$$

$\partial\ /\partial x$ 2.2-33:

$$\frac{\partial^2 U(r)}{\partial x^2} - \frac{\partial^2 V(r)}{\partial x\,\partial z}$$
$$+\left[\delta(x+X_0)-\delta(x-X_0)\right]\left\{a\iint_{-\infty}^{\infty}\frac{e^{-\gamma R}}{R}\left(\frac{\partial U(r')}{\partial x'}-\frac{\partial V(r')}{\partial z'}\right)d^2r' + b\iint_{-\infty}^{\infty}\frac{\partial}{\partial z}\left(\frac{e^{-\gamma R}}{R}\right)\nabla_{r'}^2 V(r')\,d^2r'$$
$$+\,a\oiint\frac{\partial}{\partial x}\left(\frac{e^{-\gamma R}}{R}\right)\left(\frac{\partial U(r')}{\partial x'}-\frac{\partial V(r')}{\partial z'}\right)d^2r' + b\oiint\frac{\partial^2}{\partial x\,\partial z}\left(\frac{e^{-\gamma R}}{R}\right)\nabla_{r'}^2 V(r')\,d^2r'$$
$$=\left[\delta(x+X_0)-\delta(x-X_0)\right]E_z^{p} + \frac{\partial}{\partial x}E_z^{p}\qquad. \qquad 2.2\text{-}37$$

In the four previous equations, the parts multiplied by delta functions operate only on the edges of the plate while the remainder operates inside. The integrals over the primed variables, however, cover the whole plate, edges included. The U potential represents the divergence free current vortex that is constrained to flow within the plate. The boundary condition therefore must be that U is constant along the edges of the plate, and since only derivatives of U are required, U is set equal to zero along the edges of the plate. The V potential on the other hand represents the curl free component, that is, the current entering and leaving the plate through its surface and edges.

U interior

An integral equation for U applicable to the region inside the plate is obtained by adding equations 2.2-34 and 2.2-37:

$$\nabla_{xz}^2\, U(r)$$
$$+\,a\oiint\left\{\frac{\partial}{\partial z}\left(\frac{e^{-\gamma R}}{R}\right)\left(\frac{\partial U(r')}{\partial z'}+\frac{\partial V(r')}{\partial x'}\right)+\frac{\partial}{\partial x}\left(\frac{e^{-\gamma R}}{R}\right)\left(\frac{\partial U(r')}{\partial x'}-\frac{\partial V(r')}{\partial z'}\right)\right\}d^2r'$$
$$=\frac{\partial}{\partial x}E_z^{p}(r) - \frac{\partial}{\partial z}E_x^{p}(r) = Z\,H_y^{p}(r)\qquad. \qquad 2.2\text{-}38$$

V interior

Subtracting equation 2.2-36 and 2.2-35,

$$\nabla_r^2 V(r) - b \iint \nabla_r^2 \left(\frac{e^{-\gamma R}}{R} \right) \nabla_{r'}^2 V(r') \, d^2 r' + a \, I$$

$$= - \left[\frac{\partial E_x^p(r)}{\partial x} + \frac{\partial E_z^p(r)}{\partial z} \right] , \qquad 2.2\text{-}39$$

where

$$I = \iint \left\{ \frac{\partial}{\partial x} \left(\frac{e^{-\gamma R}}{R} \right) \left(\frac{\partial U(r')}{\partial z'} + \frac{\partial V(r')}{\partial x'} \right) - \frac{\partial}{\partial z} \left(\frac{e^{-\gamma R}}{R} \right) \left(\frac{\partial U(r')}{\partial x'} - \frac{\partial V(r')}{\partial z'} \right) \right\} d^2 r'$$

2.2-40

Expanding, equation 2.2-40 becomes

$$I = \iint \left\{ - \frac{e^{-\gamma R}}{R} \nabla_{r'}^2 V(r') \, d^2 r' - \bar{\nabla}_{r'} \cdot \left\{ \frac{e^{-\gamma R}}{R} \cdot \bar{E}(r') \right\} d^2 r' \right.$$

$$= - \iint \frac{e^{-\gamma R}}{R} \nabla_{r'}^2 V(r') \, d^2 r' - \oint \frac{e^{-\gamma R}}{R} E_n \, ds' \qquad 2.2\text{-}41$$

The line integral around the edge of the plate ($\oint$) in equation 2.2-41 may be set equal to zero from the thin plate approximation (Appendix A).

Equation 2.2-39 therefore reduces to

$$\nabla_r^2 V(r) + b \iint \frac{\partial^2}{\partial y^2} \left(\frac{e^{-\gamma R}}{R} \right) \nabla_{r'}^2 V(r') \, d^2 r' = \frac{\partial}{\partial y} E_Y^p$$

2.2-42

V edges

From equation 2.2-35,

$$-a \iint \frac{e^{-\gamma R}}{R} \left(\frac{\partial U(r')}{\partial z'} + \frac{\partial V(r')}{\partial x'} \right) d^2 r' + b \iint \frac{\partial}{\partial x} \left(\frac{e^{-\gamma R}}{R} \right) \nabla_{r'}^2 V(r') \, d^2 r'$$

$$= E_x^p(-X_o, 0, z) \quad \text{on the edge} \quad x = -X_o ,$$

$$= E_x^p(+X_o, 0, z) \quad \text{on the edge} \quad x = +X_o .$$

2.2-43

From equation 2.2-36,

$$a \iint \frac{e^{-\gamma R}}{R} \left(\frac{\partial U(r')}{\partial x'} - \frac{\partial V(r')}{\partial z'} \right) d^2 r' + b \iint \frac{\partial}{\partial z} \left(\frac{e^{-\gamma R}}{R} \right) \nabla_{r'}^2 (r') \, d^2 r'$$

$$= E_z^p(x, 0, +Z_o) \quad \text{on the edge} \quad z = +Z_o ,$$

$$= E_z^p(x, 0, -Z_o) \quad \text{on the edge} \quad z = -Z_o .$$

2.2-44

2.2 c) The Discrete Case

The integral equations for continuous media derived in the last section must now be expressed in digital form. The plate is to be sampled on a square grid, the outer points defining the edge of the thin plate. The potential amplitudes at the grid points must fully represent the potential in the region between. To achieve this, a suitable moment or weighting function must be chosen to distribute the potential around each sampling point. Its property should be such that, when the contributions from all the grid points are considered together, a realistic and smooth distribution for the potential is obtained everywhere within the plate. The properties of various moment functions have been investigated experimentally by convolving them with different data series. Since the integral equation involves derivatives, the moment must also give smooth derivative estimates.

The standard gate and triangle moment functions (Harrington, 1968) are shown in Figure 2-4 in one dimension only. This figure demonstrates the convolution of the

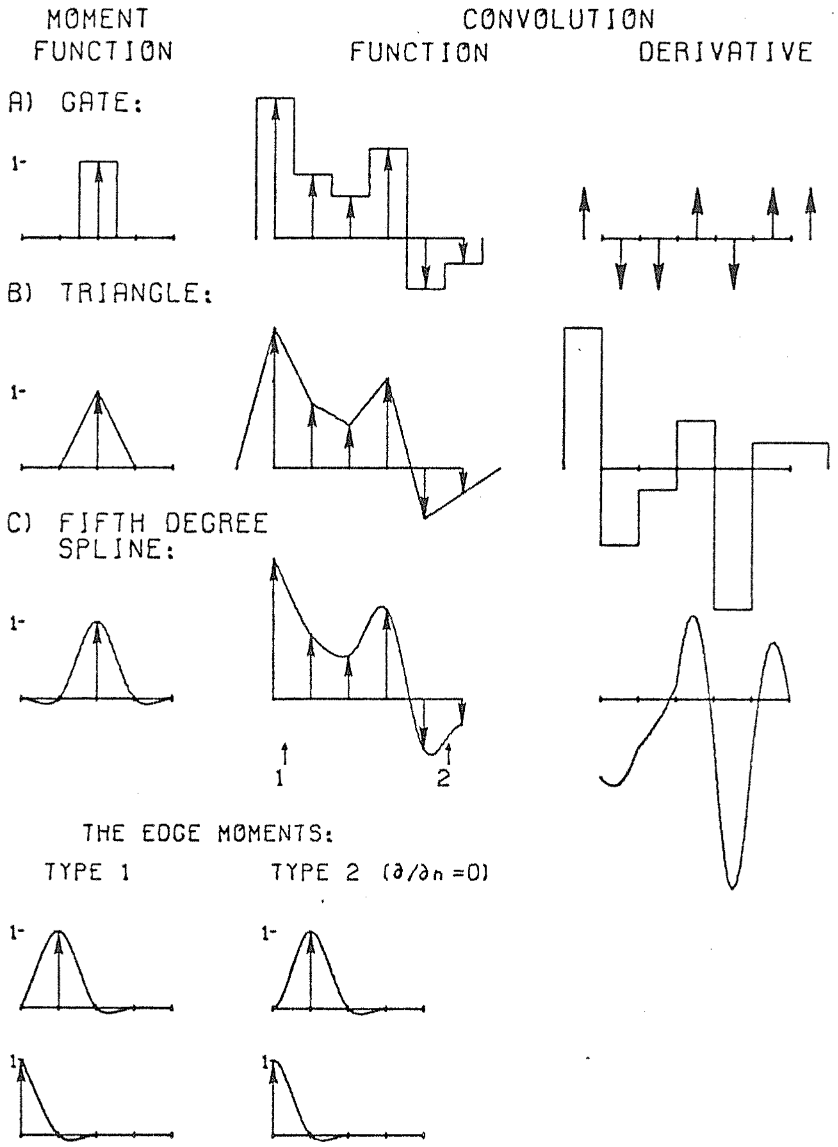

Fig. 2-4. Comparison of moment functions in 1-D only.

moment function with a data series, and the resultant derivative. These moments obviously give a poor interpolation of both the data series and its derivative. To improve on the interpolation, the number of sample points in the data series would have to be increased. This is a very important consideration, since it eventually fixes the size of the matrix that needs to be generated and inverted. For this reason, it is desirable to use a more sophisticated moment to reduce to a minimum the number of grid points required for a good solution.

Many moment functions were investigated, including bells, Parzen windows and bicubic splines, all without satisfactory results for interpolation of the function and its derivative. The best results were obtained with a two dimensional fifth degree spline extending over 16 subintervals (or 4 subintervals in one dimension). The spline, which was designed by Lamontagne (1972) for use in automatic contouring programs, is shown in Figure 2-4. The interpolation and derivative are obviously much improved. The shape of the moment differs for points close to an edge. Figure 2-5 gives a perspective view of the spline moment and its first derivative in the x direction. Figure 2-6 shows the type 1 moment for a grid point on a free edge of the plate and

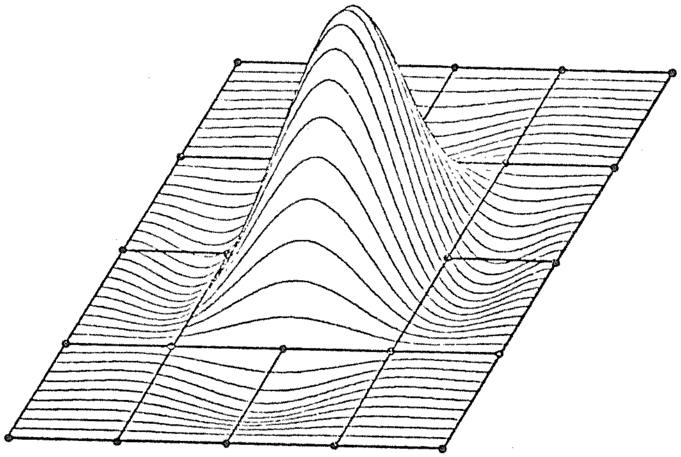

Fig. 2-5a. The normal 5th degree spline moment function.

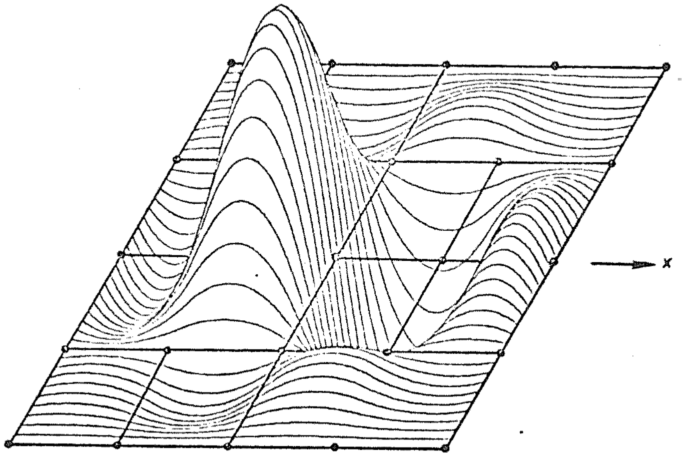

Fig. 2-5b. The first derivative in the x direction.

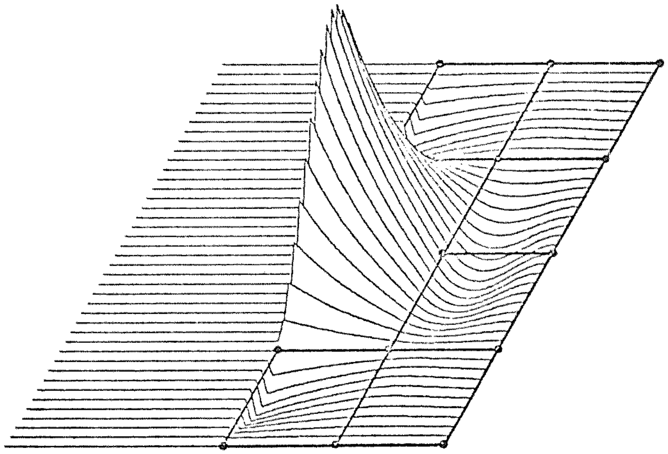

Fig. 2-6. 5th degree spline moment for a free edge of the plate.

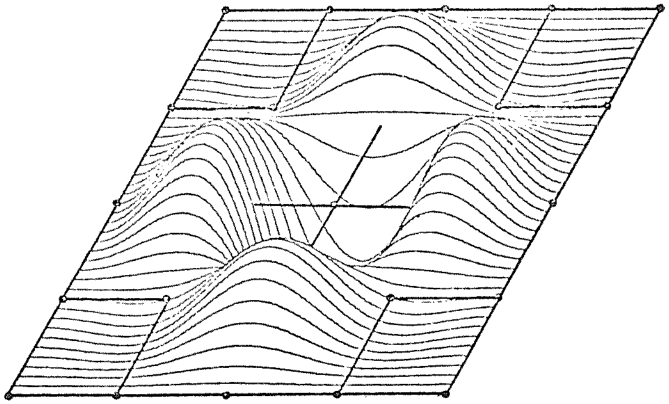

Fig. 2-7. 5th degree spline moment for the Laplacian operator.

Figure 2-7 shows the moment for the Laplacian operator. As shown in Figure 2-4, three different moments are required for a data series in one dimension. For the thin plate, 6 different moment functions are required to properly represent the interior, corners, and edges.

In applying the integral equations to a discrete set of points, a spline moment is associated with each grid point and is denoted by S(r'), remembering of course that the exact shape of S(r') depends on its position relative to the edge. Taking equation 2.2-38 as an example, the U_m potential at r_m due to potentials U_n and V_n at r_n only,

$$\nabla^2 U(r_m, r_n) + a \iint_{-\infty}^{\infty} \left\{ \frac{\partial}{\partial z} \frac{e^{-\gamma R}}{R} \left(U_n \frac{\partial S(r')}{\partial z'} + V_n \frac{\partial S(r')}{\partial x'} \right) + \frac{\partial}{\partial x} \frac{e^{-\gamma R}}{R} \left(U_n \frac{\partial S(r')}{\partial x'} - V_n \frac{\partial S(r')}{\partial z'} \right) \right\} d^2 r' = Z\, H_y^{\,r}(r_m) \,, \qquad 2.2\text{-}45$$

where $R = r_m - r_n$.

The integral in equation 2.2-45 is a convolution integral and may be represented by the standard notation:

$$f_1(R) * f_2(R) = \iint_{-\infty}^{\infty} f_1(r') \cdot f_2(R - r')\, d^2 r' \quad . \qquad 2.2\text{-}46$$

Summing over all the discrete points r_n , the discrete equation for the potential U at r_m may be written as

m inside:

$$\nabla_{xz}^2 U_m + a \sum_n \left\{ \frac{\partial}{\partial z} \frac{e^{-\gamma|R|}}{|R|} * \left(U_n \frac{\partial S(R)}{\partial z} + V_n \frac{\partial S(R)}{\partial x} \right) + \frac{\partial}{\partial x} \frac{e^{-\gamma|R|}}{|R|} * \left(U_n \frac{\partial S(R)}{\partial x} - V_n \frac{\partial S(R)}{\partial z} \right) \right\} = Z\, H_Y^P(r_m) \; . \qquad 2.2\text{-}47$$

Similarly, the other integral equations reduce to:

m inside:

$$\nabla_{xz}^2 V_m + b \sum_n \frac{\partial^2}{\partial y^2} \frac{e^{-\gamma R}}{R} * V_n \nabla^2 S(R) = \frac{\partial}{\partial y} E_Y^P \; . \qquad 2.2\text{-}48$$

m; edge x constant:

$$- a \sum_n \left\{ \frac{e^{-\gamma R}}{R} * \left(U_n \frac{\partial S(R)}{\partial z} + V_n \frac{\partial S(R)}{\partial x} \right) \right\} + b \sum_n \left\{ \frac{\partial}{\partial x} \frac{e^{-\gamma R}}{R} * V_n \nabla^2 S(R) \right\}$$

$$= E_x^P(-X_0, 0, z) \qquad \text{at} \quad x = -X_0 \qquad 2.2\text{-}49$$

$$= E_x^P(+X_0, 0, z) \qquad \text{at} \quad x = +X_0 \; .$$

m; edge z constant:

$$a \sum_n \left\{ \frac{e^{-\gamma R}}{R} * \left(U_n \frac{\partial S(R)}{\partial x} - V_n \frac{\partial S(R)}{\partial z} \right) \right\} + b \sum_n \left\{ \frac{\partial}{\partial z} \left(\frac{e^{-\gamma R}}{R} \right) * V_n \nabla^2 S(R) \right\}$$

$$= E_z^P(x, 0, -Z_0) \qquad \text{at} \quad z = -Z_0 \qquad 2.2\text{-}50$$

$$= E_z^P(x, 0, Z_0) \qquad \text{at} \quad z = +Z_0 \; .$$

2.2 d) The Matrix Equation

If we let $\bar{\phi}$ be a generalized vector whose two components are the potentials U and V, the integral equations may be represented by the general relation:

$$\bar{L}\ \bar{\phi}(r_m) + \sum_n \bar{\bar{G}}(r_m, r_n)\,\bar{\phi}(r_n) = \bar{\phi}^P(r_m) \quad , \qquad 2.2\text{-}51$$

where

$$\bar{\bar{G}}(r_m, r_n) = \begin{bmatrix} G_{vv} & G_{vu} \\ G_{uv} & G_{uu} \end{bmatrix}$$

is the Green's tensor and $\bar{L}$ is either the Laplacian operator or is equal to zero.

For example,

a) m inside:

$$G_{uv}(r_m, r_n) = a\left(\frac{\partial}{\partial z}\frac{e^{-\gamma R}}{R}\right) * \frac{\partial S(R)}{\partial x} - a\left(\frac{\partial}{\partial x}\frac{e^{-\gamma R}}{R}\right) * \frac{\partial S(R)}{\partial z} , \qquad 2.2\text{-}52$$

b) m on the edge, $x = x_0$:

$$G_{uv}(r_m, r_n) = a\left\{\frac{e^{-\gamma R}}{R} * \frac{\partial S(R)}{\partial x}\right\} + b\left\{\left(\frac{\partial}{\partial x}\frac{e^{-\gamma R}}{R}\right) * \nabla^2 S(R)\right\} . \qquad 2.2\text{-}53$$

Equation 2.2-51 may be written in the matrix notation:

$$\underbrace{\| \bar{L} + \bar{G} \|}_{\|A\|} \ X\ |\phi| = |\phi|^P \quad ,$$

where $\|A\|$ is now called the coefficient matrix.

To generate the coefficient matrix, the Green's tensor convolution arrays must be computed for the six different moment functions making up the plate. The convolution integrals are evaluated by Gaussian quadrature numerical integration using computer routines written by Annan (1973).

For an MxN plate, the size of the coefficient matrix is AxA where

$$A = MN + (M-2)(N-2) ,$$

since the U potentials at the edge grid points are equal to zero and therefore need not be included in the matrix. For M odd and a symmetric source field distribution about the grid line m = (M+1)/2,   may be set equal to zero on this line and the size of the coefficient matrix reduces to BxB where B = (M-1)(N-1).

2.3 The Layered Earth Induction Problem in the Wavenumber Domain

In this section, the solution of the electromagnetic induction problem for the layered earth is expressed in the wavenumber domain, i.e. the 2-D Fourier transform of the horizontal x-y plane. As there may be many different possible approaches for presenting the theoretical development, the particular format herein was chosen in order to facilitate the direct computer application of the FFT filtering approach.

The earth model is shown in Figure 2-8. The stack of layers is bounded by two half spaces with the z=0 plane defining the top of the first layer. The time dependence is $e^{i\omega t}$ and is implicit throughout.

2.3 a) Magnetic and Electric Hertz Potentials

The source free Maxwell's equations may be written in the form:

$$\bar{\nabla} \times \bar{E} = -Z \bar{H} \quad , \qquad 2.3\text{-}1$$

and

$$\bar{\nabla} \times \bar{H} = Y \bar{E} \quad . \qquad 2.3\text{-}2$$

Following Wait (1951), the electric and magnetic Hertz vectors $\bar{\Pi}$ and $\bar{\Gamma}$, respectively, are given by

$$\bar{E} = -\gamma^2 \bar{\Pi} + \bar{\nabla}(\bar{\nabla}\cdot\bar{\Pi}) - Z\ \bar{\nabla}\times\bar{\Gamma} \qquad 2.3\text{-}3$$

and

$$\bar{H} = Y\bar{\nabla}\times\bar{\Pi} - \gamma^2\bar{\Gamma} + \bar{\nabla}(\bar{\nabla}\cdot\bar{\Gamma}) \ , \qquad 2.3\text{-}4$$

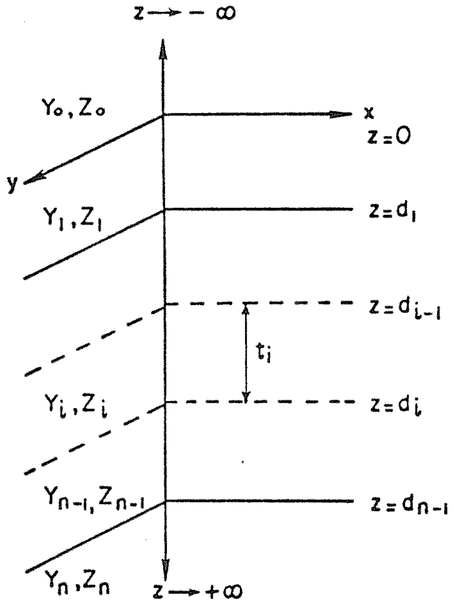

Fig. 2-8. The layered earth model.

where $\bar{E}$, $\bar{H}$, $\bar{\Pi}$, and $\bar{\Gamma}$ are functions of position (x,y,z), and γ is the propagation constant of the medium. All the components of $\bar{E}$, $\bar{H}$, $\bar{\Pi}$, and $\bar{\Gamma}$ satisfy the source free diffusion equation,

$$(\nabla^2 - \gamma^2)\,\bar{\theta} = 0 \quad . \qquad 2.3\text{-}5$$

Hence from 2.3-5 and using the familiar identity,

$$\bar{\nabla}\times\bar{\nabla}\times\bar{\theta} = \bar{\nabla}(\bar{\nabla}\cdot\bar{\theta}) - \nabla^2\bar{\theta} \quad , \qquad 2.3\text{-}6$$

equations 2.3-3 and 2.3-4 may be simplified to

$$\bar{E} = \bar{\nabla}\times\bar{\nabla}\times\bar{\pi} - Z\,\bar{\nabla}\times\bar{\Gamma} \qquad 2.3\text{-}7$$

and

$$\bar{H} = Y\,\bar{\nabla}\times\bar{\pi} + \bar{\nabla}\times\bar{\nabla}\times\bar{\Gamma} \; . \qquad 2.3\text{-}8$$

The induction theorem now allows equations 2.3-7 and 2.3-8 to be simplified for the particular case of the layered earth. The theorem as derived by Harrington (1961) and Jordan and Balmain (1968) considers two regions of different electrical properties as shown in Figure 2-9. The sources are contained in region 1. For this geometry the induction theorem states that the induced or scattered fields in both regions may be uniquely specified by electric and magnetic current sheets over the surface S. In turn, these surface currents may be uniquely represented by a distribution of the normal component of electric and magnetic Hertz vectors over the surface.

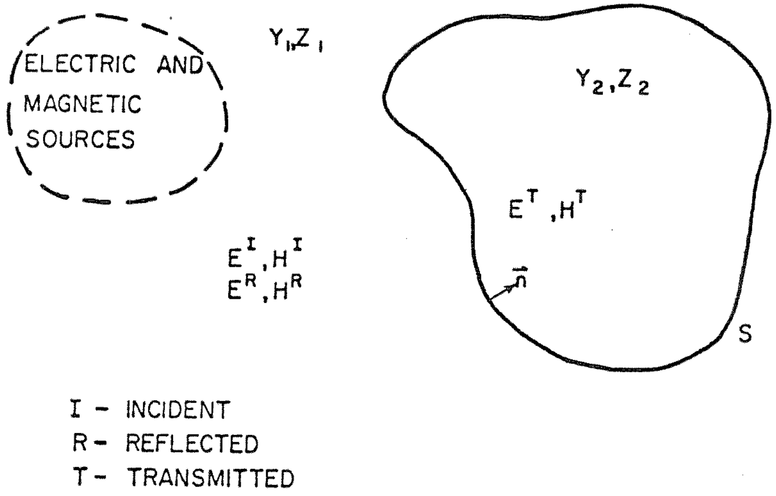

Fig. 2-9. The geometry for the induction theorem.

In the layered earth model, the boundary surfaces reduce to planes defined by z=constant. Therefore it is only necessary to consider the z component of electric and magnetic Hertz vectors. In the remainder of the thesis Π and Γ will denote the z component of the electric and magnetic Hertz potentials, and they will be treated as scalars.

Using the partial derivative notation, equations 2.3-7 and 2.3-8 reduce to

$$\begin{aligned}\bar{E}(x,y,z) = {} & \bar{i}\left[\Pi_{31}(r,z) - Z\,\Gamma_{2}(r,z)\right] \\ & + \bar{j}\left[\Pi_{32}(r,z) + Z\,\Gamma_{1}(r,z)\right] \\ & - \bar{k}\left[\Pi_{11}(r,z) + \Pi_{22}(r,z)\right]\end{aligned} \qquad 2.3\text{-}9$$

and

$$\begin{aligned}\bar{H}(x,y,z) = {} & \bar{i}\left[Y\,\Pi_{2}(r,z) + \Gamma_{31}(r,z)\right] \\ & + \bar{j}\left[-Y\,\Pi_{1}(r,z) + \Gamma_{32}(r,z)\right] \\ & - \bar{k}\left[\Gamma_{11}(r,z) + \Gamma_{22}(r,z)\right]\end{aligned} \qquad 2.3\text{-}10$$

2.3 b) Boundary Conditions

The boundary conditions for the Hertz potentials are now considered at the plane interface (z=d) between two media of electrical properties (Y_1, Z_1) and (Y_2, Z_2).

The boundary conditions for the field variables $\bar{E}$ and $\bar{H}$ are stated as the continuity across the boundary of normal YE and ZH, and tangential E and H.

Electric Hertz Potential Π

From equation 2.3-9 the continuity of normal $Y\bar{E}$ implies that

$$Y_1\left[\Pi_{11}(r,d^-) + \Pi_{22}(r,d^-)\right] = Y_2\left[\Pi_{11}(r,d^+) + \Pi_{22}(r,d^+)\right]. \qquad 2.3\text{-}11$$

If we let

$$\Theta(r,d) = Y_2\,\Pi(r,d^+) - Y_1\,\Pi(r,d^-)\,, \qquad 2.3\text{-}12$$

equation 2.3-11 reduces to

$$\Theta_{11}(r,d) + \Theta_{22}(r,d) = 0\ . \qquad 2.3\text{-}13$$

θ is therefore a harmonic function in the plane z=d. Since there are no sources on this plane and the fields must vanish as $r \to \infty$, θ must be zero everywhere on the plane z=d.

Therefore

$$Y_2\,\Pi(r,d^+) = Y_1\,\Pi(r,d^-)\ . \qquad 2.3\text{-}14$$

Also, from equation 2.3-9, the continuity of tangential $\bar{E}$ requires that

$$\Pi_{13}(r,d^+) = \Pi_{13}(r,d^-) \quad ,$$

and 2.3-15

$$\Pi_{23}(r,d^+) = \Pi_{23}(r,d^-) \quad .$$

Equations 2.3-15 may be differentiated and added to obtain the harmonic function

$$\Theta = \Pi_3(r,d^+) - \Pi_3(r,d^-) \qquad 2.3\text{-}16$$

on the plane z=d. This therefore implies that

$$\Pi_3(r,d^+) = \Pi_3(r,d^-) \quad . \qquad 2.3\text{-}17$$

Magnetic Hertz Potential Γ

From equation 2.3-10, the continuity of normal ZH implies that

$$Z_1\left[\Gamma_{11}(r,d^-) + \Gamma_{22}(r,d^-)\right] = Z_2\left[\Gamma_{11}(r,d^+) + \Gamma_{22}(r,d^-)\right] \quad , \qquad 2.3\text{-}18$$

and the continuity of tangential H implies that

$$\Gamma_{13}(r,d^+) = \Gamma_{13}(r,d^-)$$

and 2.3-19

$$\Gamma_{23}(r,d^+) = \Gamma_{23}(r,d^-) \quad .$$

These relations are analogous to equations 2.3-11 and 2.3-15 for the electric potential Π and the boundary conditions are therefore written as

$$Z_2 \; \Gamma(r,d^+) = Z_1 \; \Gamma(r,d^-)$$

2.3-20

and

$$\Gamma_3(r,d^+) = \Gamma_3(r,d^-) \quad .$$

2.3 c) Wavenumber Domain Reflection and Transmission Filters

The electromagnetic induction problem for the layered earth is now expressed in the wavenumber domain, the two dimensional Fourier transform of the horizontal x-y plane.

The wavenumber domain equivalents for the horizontal derivative operators are defined in relation 2.1-1. Since Π, Γ, and all the components of $\bar{E}$ and $\bar{H}$ satisfy the source free diffusion equation 2.3-5, the z derivative operator becomes

$$\left\{ \frac{\partial}{\partial z} \right\} \longleftrightarrow \left\{ \sqrt{(\rho^2 + \gamma^2)} \right\} , \qquad 2.3\text{-}21$$

where $\longleftrightarrow$ denotes a Fourier transform pair.

With the help of these operators, the electromagnetic field vectors may be expressed in terms of Hertz Potentials in the space domain or the wavenumber domain. For example, the x component of electric field $\bar{E}$ is written in the space domain as

$$E_x(x,y,z) = \frac{\partial^2}{\partial z \partial x} \Pi(r,z) - z \frac{\partial}{\partial y} \Gamma(r,z), \qquad 2.3\text{-}22$$

or, in the wavenumber domain as

$$E_x(u,v,z) = \{iu\}\left\{\sqrt{(\rho^2+\gamma^2)}\right\} \Pi(\rho,z) - Z\,\{iv\}\,\Gamma(\rho,z), \qquad 2.3\text{-}23$$

where $E_x(x,y,z) \longleftrightarrow E_x(u,v,z)$, 2.3-24

and $\Pi(x,y,z) \longleftrightarrow \Pi(u,v,z)$. 2.3-25

The advantage of expressing the electromagnetic problem in terms of Hertz potentials in the wavenumber domain is that, given a source electromagnetic field distribution, it is only necessary to consider its Hertz potential as a scalar distribution in the u-v wavenumber plane. The scalar distribution may be continued up or down throughout the stack of layers, after matching boundary conditions of course. At any depth, the complete horizontal distribution of the field vectors $\bar{E}$ and $\bar{H}$ are obtained by applying the appropriate wavenumber domain derivative operators and constants, and computing the inverse Fourier transform.

The boundary conditions for the Hertz potentials may be expressed in the wavenumber domain as the continuity of

$$Y\Pi,\ \Pi_3,\ Z\Gamma, \text{ and } \Gamma_3 . \qquad 2.3\text{-}26$$

The usual approach for obtaining the solution of the Hertz potential in a stack of layers is to define upward and downward propagating components in each layer, match boundary conditions, and obtain a coefficient matrix. The inversion of the matrix will define the solution everywhere in the stack. This technique is applicable equivalently in the space domain (Ward, 1967) and in the wavenumber domain (Alfonso-Roche, 1973). The method in this thesis however, was chosen to optimize and simplify the computer programming for the plate in a stratified medium problem. For the FFT filtering approach, wavenumber domain reflection and transmission <u>filters</u> are defined.

These are different from the usual reflection and transmission coefficients for a plane wave at a boundary. Given the spatially dependent incident Hertz potential on a stack of layers, the transmission and reflection filters will give the Hertz potential transmitted through the stack and the potential reflected from the stack, respectively, in the wavenumber domain. This technique effectively bypasses the solution within the stack.

To generalize the problem, we let $X(\rho,z)$ denote either $\Pi(\bar{\rho},z)$ or $\Gamma(\bar{\rho},z)$, and the boundary conditions are written in the form

$$B^- X(\bar{\rho}, d^-) = B^+ X(\bar{\rho}, d^+)$$

and $$C^- X_3(\bar{\rho}, d^-) = C^+ X_3(\bar{\rho}, d^+) \,, \qquad 2.3\text{-}27$$

where B and C are either Y,Z or unity depending on the Hertz potential.

We first begin by deriving the reflection and transmission filter at the boundary to a half space as shown in Figure 2-10. This may represent the boundary at the bottom of the stack in the layered earth model.

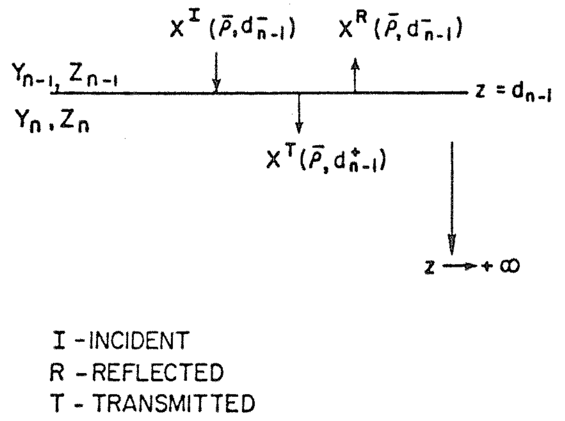

Fig. 2-10 The boundary to a half space

In the wavenumber domain, the diffusion equation becomes

$$X_{33}(\bar{\rho}, z) = k^2 X(\bar{\rho}, z) \,, \qquad 2.3\text{-}28$$

where

$$k = (\rho^2 + \gamma^2)^{1/2} \,.$$

Solutions to the diffusion equation for the two regions are:

$\underline{z \leq d_{n-1}}$

$$X(\bar{\rho}, z) = X^I(\bar{\rho}, d^-_{n-1})\, e^{-k_{n-1}(z-d_{n-1})} + X^R(\bar{\rho}, d^-_{n-1})\, e^{k_{n-1}(z-d_{n-1})}$$

$$X_3(\bar{\rho}, z) = -k_{n-1} X^I(\bar{\rho}, d^-_{n-1})\, e^{-k_{n-1}(z-d_{n-1})} + k_{n-1} X^R(\bar{\rho}, d^-_{n-1})\, e^{k_{n-1}(z-d_{n-1})} \,, \qquad 2.3\text{-}29$$

$\underline{z \geq d_{n-1}}$

$$X(\bar{\rho},z) = X^{T}(\bar{\rho}, d_{n-1}^{+})\, e^{-k_n (z-d_{n-1}^{+})} \qquad 2.3\text{-}30$$

$$X_3(\bar{\rho},z) = -k_n\, X^{T}(\bar{\rho}, d_{n-1}^{+})\, e^{-k_n (z-d_{n-1}^{+})} \; .$$

Letting $z \to d_{n-1}^{-}$ in equation 2.3-29 and $z \to d_{n-1}^{+}$ in equation 2.3-30,

$\underline{z \leq d_{n-1}}$

$$X(\bar{\rho}, d_{n-1}^{-}) = X^{I}(\bar{\rho}, d_{n-1}^{-}) + X^{R}(\bar{\rho}, d_{n-1}^{-}) \qquad 2.3\text{-}31$$

$$X_3(\bar{\rho}, d_{n-1}^{-}) = -k_{n-1}\, X^{I}(\bar{\rho}, d_{n-1}^{-}) + k_{n-1}\, X^{R}(\bar{\rho}, d_{n-1}^{-}) \; ,$$

$\underline{z \geq d_{n-1}}$

$$X(\bar{\rho}, d_{n-1}^{+}) = X^{T}(\bar{\rho}, d_{n-1}^{+}) \qquad 2.3\text{-}32$$

$$X_3(\bar{\rho}, d_{n-1}^{-}) = -k_{n-1}\, X^{I}(\bar{\rho}, d_{n-1}^{-}) + k_{n-1}\, X^{R}(\bar{\rho}, d_{n-1}^{-}) \; .$$

Applying the boundary conditions from 2.3-26 to equations 2.3-31 and 2.3-32,

$$B^{-} X^{I}(\bar{\rho}, d_{n-1}^{-}) + B^{-} X^{R}(\bar{\rho}, d_{n-1}^{-}) = B^{+} X^{T}(\bar{\rho}, d_{n-1}^{+}) \qquad 2.3\text{-}33$$

and

$$-C^{-} k_{n-1}\, X^{I}(\bar{\rho}, d_{n-1}^{-}) + C^{-} k_{n-1}\, X^{R}(\bar{\rho}, d_{n-1}^{-}) = -C^{+} k_n\, X^{T}(\bar{\rho}, d_{n-1}^{+}) \; . \qquad 2.3\text{-}34$$

Eliminating X^{T} from equations 2.3-33 and 2.3-34,

$$X^{R}(\bar{\rho}, d_{n-1}^{-}) = \left\{ \frac{k_{n-1} C^{-} B^{+} - k_n C^{+} B^{-}}{k_{n-1} C^{-} B^{+} + k_n C^{+} B^{-}} \right\} X^{I}(\bar{\rho}, d_{n-1}^{-}) \; . \qquad 2.3\text{-}35$$

Eliminating X^{R},

$$X^{T}(\bar{\rho}, d_{n-1}^{+}) = \frac{2 k_{n-1} B^{-} C^{-}}{k_{n-1} C^{-} B^{+} + k_n C^{+} B^{-}} \; X^{I}(\bar{\rho}, d_{n-1}^{-}) \; . \qquad 2.3\text{-}36$$

From equations 2.3-35 and 2.3-36, the reflection and transmission filters for the one boundary model as shown in Figure 2-10 may be defined as

$$RF(\rho, d_{n-1}) = \frac{k_{n-1} C_{n-1} B_n - k_n C_n B_{n-1}}{k_{n-1} C_{n-1} B_n + k_n C_n B_{n-1}} \; , \qquad 2.3\text{-}37$$

and

$$TF(\rho, d_{n-1}) = \frac{2 k_{n-1} C_{n-1} B_{n-1}}{k_{n-1} C_{n-1} B_n + k_n C_n B_{n-1}} \; , \qquad 2.3\text{-}38$$

respectively.

A recursion relation is now required to obtain the reflection and transmission filters for a stack of layers. With reference to Figure 2-11, the recursion relation will relate the reflection and transmission filters at the $z = d_{i-1}$ boundary to those at the $z = d_i$ boundary, i.e.

$$\left\{ \begin{matrix} RF(\bar{\rho}, d_{i-1}) \\ TF(\bar{\rho}, d_{i-1}) \end{matrix} \right\} = f \left\{ \begin{matrix} RF(\bar{\rho}, d_i) \\ TF(\bar{\rho}, d_i) \end{matrix} \right\} \; .$$

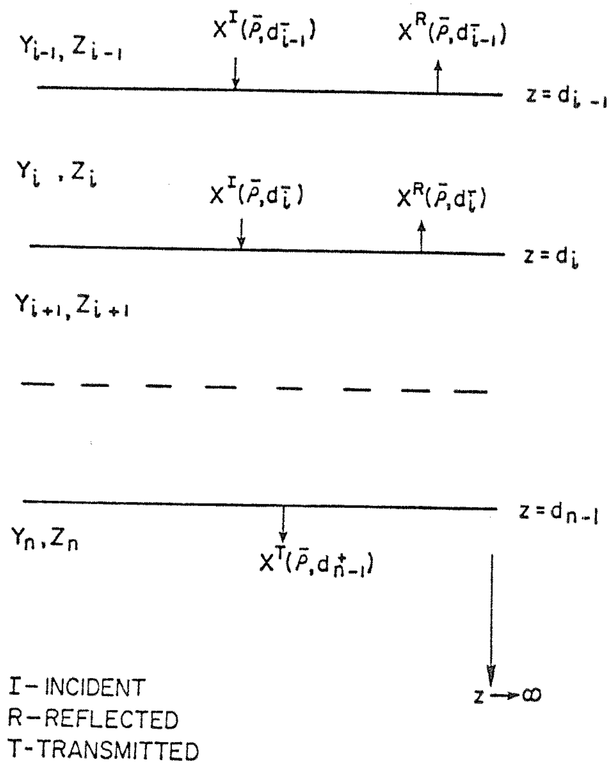

Fig. 2-11. Boundaries for the recursion relation.

Recursion Relation-Reflection

Given $\dfrac{X^R(\bar{\rho}, d_i)}{X^I(\bar{\rho}, d_i)}$, find $\dfrac{X^R(\bar{\rho}, d_{i-1})}{X^I(\bar{\rho}, d_{i-1})}$.

In the $i-1$ layer, letting $z \to d_{i-1}^-$, the generalized Hertz potential and its z derivative are written as:

$$X(\bar{\rho}, d_{i-1}^-) = X^I(\bar{\rho}, d_{i-1}^-) + X^R(\bar{\rho}, d_{i-1}) , \qquad 2.3\text{-}39$$

and

$$X_3(\bar{\rho}, d_{i-1}^-) = -k_{i-1} X^I(\bar{\rho}, d_{i-1}^-) + k_{i-1} X^R(\bar{\rho}, d_{i-1}^-), \qquad 2.3\text{-}40$$

respectively.

In the i layer, letting $z \to d_{i-1}^+$,

$$X(\bar{\rho}, d_{i-1}^+) = X^I(\bar{\rho}, d_{i-1}^+) + X^R(\bar{\rho}, d_{i-1}^+) \qquad 2.3\text{-}41$$

and

$$X_3(\rho, d_{i-1}^+) = -k_i X^I(\bar{\rho}, d_{i-1}^+) + k_i X^R(\bar{\rho}, d_{i-1}^+) . \qquad 2.3\text{-}42$$

But

$$\begin{aligned} X^R(\bar{\rho}, d_{i-1}^+) &= X^R(\bar{\rho}, d_i^-)\, e^{-k_i t_i} \\ &= RF(\rho, d_i)\, X^I(\bar{\rho}, d_i^-)\, e^{-k_i t_i} \qquad 2.3\text{-}43 \\ &= RF(\rho, d_i)\, X^I(\bar{\rho}, d_{i-1}^+)\, e^{-2 k_i t_i} . \end{aligned}$$

Substituting equation 2.3-43 into 2.3-41 and 2.3-42,

$$X(\bar{\rho}, d_{i-1}^{+}) = X^{I}(\bar{\rho}, d_{i-1}^{+})\left\{1 + RF(\rho, d_i)\, e^{-2k_i t_i}\right\} \qquad 2.3\text{-}44$$

and

$$X_3(\bar{\rho}, d_{i-1}^{+}) = k_i\, X^{I}(\bar{\rho}, d_{i-1}^{+})\left\{-1 + RF(\rho, d_i)\, e^{-2k_i t_i}\right\} \qquad 2.3\text{-}45$$

The generalized boundary conditions are

$$B_{i-1}\, X(\bar{\rho}, d_{i-1}^{-}) = B_i\, X(\bar{\rho}, d_{i-1}^{+}) \qquad 2.3\text{-}46$$

and

$$C_{i-1}\, X_3(\bar{\rho}, d_{i-1}^{-}) = C_i\, X_3(\bar{\rho}, d_{i-1}^{+}) . \qquad 2.3\text{-}47$$

Substituting equations 2.3-39, 2.3-40, 2.3-44 and 2.3-45 into equations 2.3-46 and 2.3-47, and eliminating $X^{I}(\bar{\rho}, d_{i-1}^{+})$, we obtain

$$RF(\rho, d_{i-1}) = \frac{(1-D) + RE(1+D)}{(1+D) + RE(1-D)} , \qquad 2.3\text{-}48$$

where $RE = RF(\rho, d_i)\, e^{-2k_i t_i}$,

and $D = \dfrac{B_{i-1}\, C_i\, k_i}{B_i\, C_{i-1}\, k_{i-1}}$.

Recursion Relation-Transmission

Given $\dfrac{X^{T}(\bar{\rho}, d_{n-1}^{+})}{X^{I}(\bar{\rho}, d_i)}$, find $\dfrac{X^{T}(\bar{\rho}, d_{n-1}^{+})}{X^{I}(\bar{\rho}, d_{i-1})}$.

Following a derivation similar to that shown in the last section, it may be shown that

$$TF(\rho, d_{i-1}) = \frac{2\, TF(\rho, d_i)\, e^{-k_i t_i}}{\left\{\dfrac{B_i}{B_{i-1}}(1+RE) + \dfrac{C_i k_i}{C_{i-1} k_{i-1}}(1-RE)\right\}} , \qquad 2.3\text{-}49$$

where $RE = RF(\rho, d_i)\, e^{-2k_i t_i}$.

This general formulation is particularly useful from a programming point of view. The filter functions TF and RF may be applied in subprograms where the recursion relation operates in a loop. The layer parameters and boundary conditions are entered in the form of arrays. In many cases, since the electromagnetic fields are derivable from Hertz potentials using linear operators in the wavenumber domain, the above filters may be applied directly to the Fourier transform of the incident field component.

2.3 d) The Plate-Layer Interaction Matrix

When one or more layers of different electrical properties are introduced in the background or host medium, the reflection from the stack will alter the coefficient matrix for the plate in the infinite host. Since Maxwell's equations are linear, this effect is considered separately in a plate-layer interaction matrix which is to be added to the basic coefficient matrix.

The FFT approach may be used for computing the interaction coefficients. The procedure consists of finding the potential distribution on the layer interface, transforming to the wavenumber domain, multiplying by the appropriate reflection filter as derived in section 2.3 c), continuing to the desired level and inverting back to the space domain.

In order to define the reflection filters in the wavenumber domain the boundary conditions for $U, \frac{\partial U}{\partial z}$, V, and $\frac{\partial V}{\partial z}$ are required.

Since $\bar{E} = \bar{\nabla} \times \bar{j}\, U_y$,

$$E_y = -\frac{\partial U}{\partial z} \qquad \text{and} \qquad E_z = \frac{\partial U}{\partial x} \qquad 2.3\text{-}50$$

From equation 2.3-9 and 2.3-10, E_z may be represented only by an electric Hertz potential Π. From equation 2.3-14, $Y\Pi$ is continuous across the boundary. This implies therefore that YU is continuous at least to within some integration constant. However, since the potential on both sides of the boundary must vanish as $r \to \infty$, the constant may be equated to zero and YU is continuous across the boundary. Using similar arguments for the V potential and the vertical derivatives, the boundary conditions reduce to the continuity of

$$YU,\ \frac{\partial U}{\partial z},\ V,\ \text{and}\ \frac{\partial V}{\partial z} \qquad 2.3\text{-}51$$

across the interface.

Figure 2-12 summarizes the steps in obtaining a solution for the thin plate in a layered earth environment. The Green's function matrix is unique for a plate of given size, at a given frequency and in a host medium of given conductivity. Changing any of these parameters requires regenerating the matrix. The same applies to the plate-layer interaction matrix. The same matrices however may be used for plates of varying conductivity. In order to save computation time, it is convenient to store various matrices onto computer disk space so that they may be used many times.

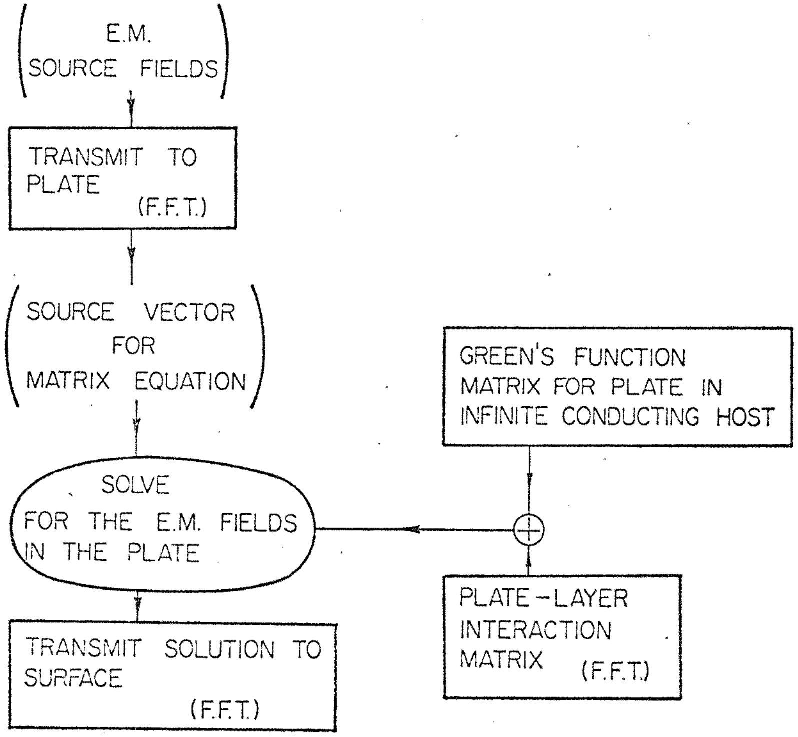

Fig. 2-12. Numerical steps for the solution of the plate in a layered earth.

CHAPTER 3

Numerical Results for Electromagnetic Induction in a Layered Earth Using the FFT Filtering Approach

3.1 Qualitative Results for an Odd-Shaped Current Loop Source

This first example is purposely non-quantitative to demonstrate the INPUT-OUTPUT nature of the FFT filtering approach and how it can deal with any arbitrary finite source current distribution.

The layered earth model consists of two layers over a half-space. In grid units, the skin depths and layer thicknesses are chosen as:

$\delta_1 = 7.$, $t_1 = 3.$,

$\delta_2 = 2.$, $t_2 = 4.$,

$\delta_3 = 10.$, $t_3 = \infty$.

The current source is an odd-shaped four sided loop raised two grid units above the surface z=0. A 128 x 128 grid is used in the Fourier transform.

First, the source magnetic field $H_z(x,y,0^-)$ due to the current loop alone is computed and is shown in Figure 3-1 a). The source electric fields generating dielectric displacement currents in the air is neglected.

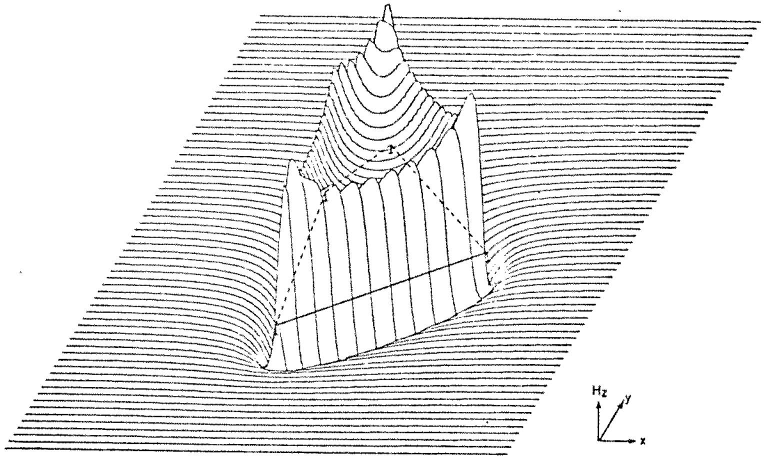

Fig. 3-1a. The $H_z(x,y,o^-)$ source magnetic field.

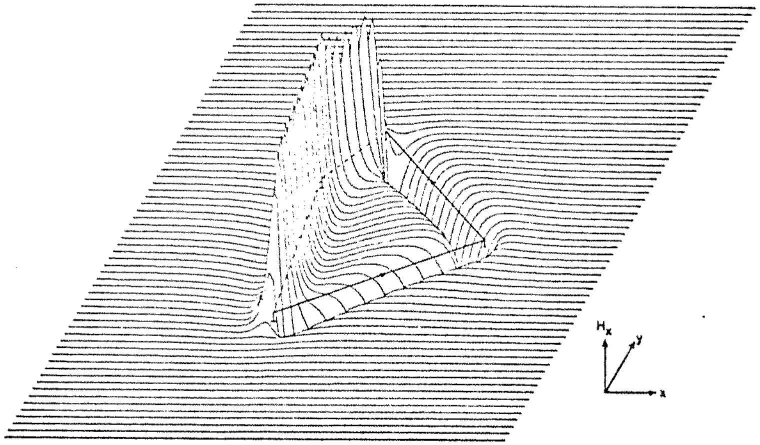

Fig. 3-1b. The $H_x(x,y,o^-)$ total magnetic field in-phase.

The Fourier transform $H_z(u,v,0^-)$ is found via FFT. By using the wavenumber domain derivative operators and by adding the constant 1 to the layered earth reflection filter derived in section 2.3 c), the total (i.e. both source and reflected) magnetic Hertz potential $\Gamma^T(u,v,0^-)$ may be found directly. Making use of the boundary condition (equation 2.3-20) for Γ, and equations 2.3-9 and 2.3-10, the electromagnetic fields may be found directly on both sides of the z=0 boundary. Figures 3-1 b) and 3-1 c) show respectively the responses of $H_x(x,y,0^-)$ total field in phase, and $H_y(x,y,0^-)$ quadrature. The spatial resolution of the total in-phase component is obviously much higher since it contains the primary field.

The stream potential $\phi(x,y,0^+)$ for the quadrature current flow in the plane $z=0^+$ is shown in Figure 3-1 d). The stream potential's contours may be visualized as lines of circulating induced current flow. It is defined by

$$\sigma_1 \bar{E}(x,y,0^+) = \bar{\nabla} \times \bar{\Phi}(x,y,0^+) \quad . \qquad 3.1\text{-}1$$

From equation 2.3-10, the stream potential is simply given by

$$\phi(x,y,0^+) = -i\omega\mu\Gamma(x,y,0^+) \quad , \qquad 3.1\text{-}2$$

or, in the wavenumber domain,

$$\hat{\phi}(u,v,0^+) = -i\omega\mu\Gamma(u,v,0^+) \quad . \qquad 3.1\text{-}3$$

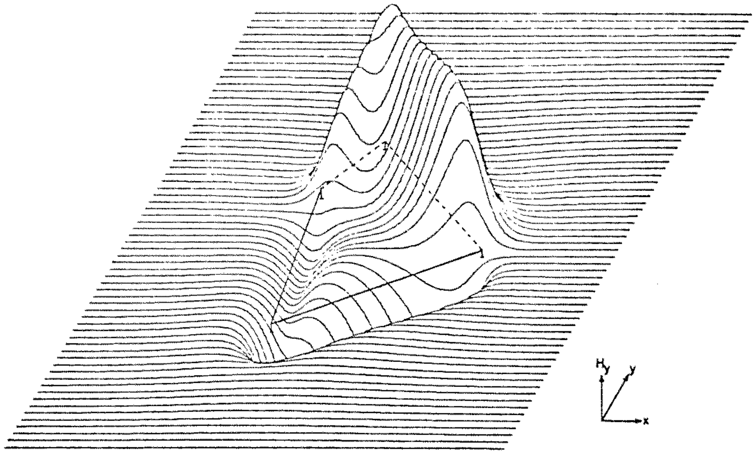

Fig. 3-1c. The $H_y(x,y,0^-)$ anomalous magnetic field, quadrature.

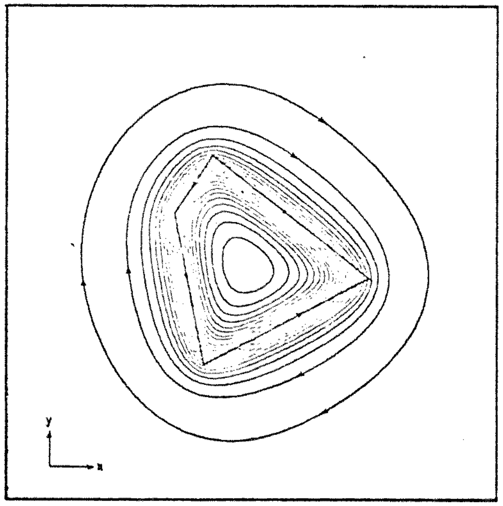

Fig. 3-1d. The quadrature current flow pattern in the plane $z = 0^+$.

3.2 Comparison of Quantitative Results for the Coaxial Dipole Exploration System

In order to investigate the accuracy and limitations of the FFT filtering approach, it is convenient to compare results with those readily available for the coaxial dipole system (Frischnecht, 1967) shown in Figure 3-2.

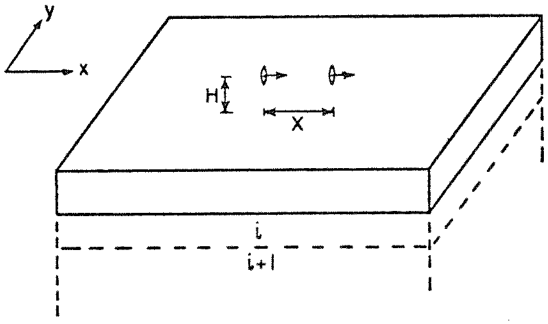

Fig.3-2 An elevated coaxial dipole system.

In this example, the source is ungrounded and the dielectric currents are neglected so that only the magnetic Hertz potential is considered. A wavenumber domain expression for the source field is easily derived. Consequently, FFT is used only in executing the inversion to the space domain. Choosing the x axis as the axis of the coaxial system, a grid of size 256 x 64 is used to increase the accuracy in the x direction at the expense of that in the y direction.

The free space magnetic field of a horizontal x-oriented dipole at the origin is given by:

$$\bar{H}(r) = -\frac{m}{4\pi}\,\bar{\nabla}\left(\frac{x}{R^3}\right) \qquad 3.2\text{-}1$$

where m is the magnetic dipole moment and $R = \sqrt{(X^2+Y^2+Z^2)}$.

The corresponding wavenumber domain expression for the source magnetic Hertz potential on the surface $z=0^-$ due to a horizontal x-oriented dipole at (x=0, z=-h) is

$$\hat{\Gamma}(u,v,0^-) = -2\pi m\left(\frac{iu}{\rho^2}\right)e^{-\rho h} \qquad 3.2\text{-}2$$

From equation 2.3-10, we have that

$$H_x(\bar{r},z) = \Gamma_{13}(\bar{r},z) \qquad 3.2\text{-}3$$

In the wavenumber domain, equation 3.2-3 becomes

$$H_x(\bar{\rho},0^-) = (-iu)(\rho)\,\Gamma(\bar{\rho},0^-) \qquad 3.2\text{-}4$$

Multiplying the source field by the appropriate reflection filter $RF(\rho,0^-)$ as derived in section 2.3 c) and upward continuing to z=-h, the Fourier transform of the anomalous magnetic field for the coaxial dipole

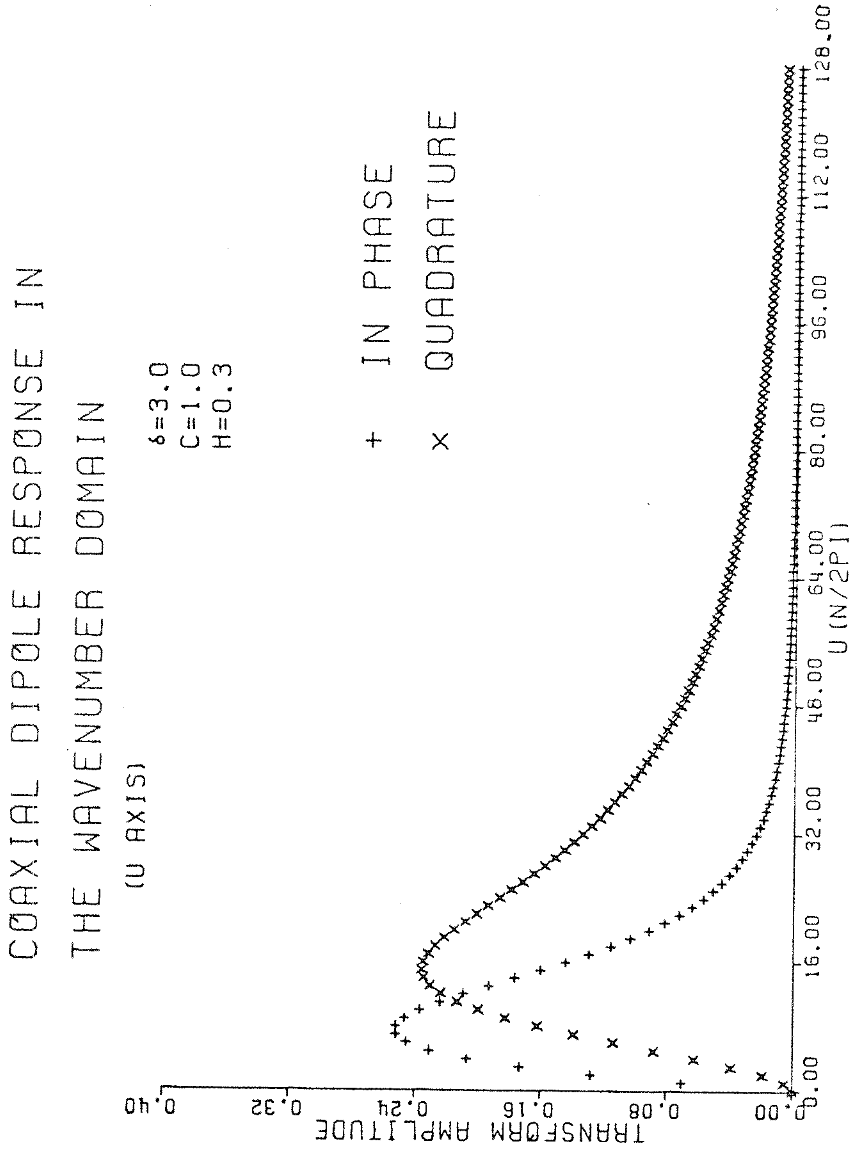

Fig. 3-3a. Wavenumber domain response on the u axis.

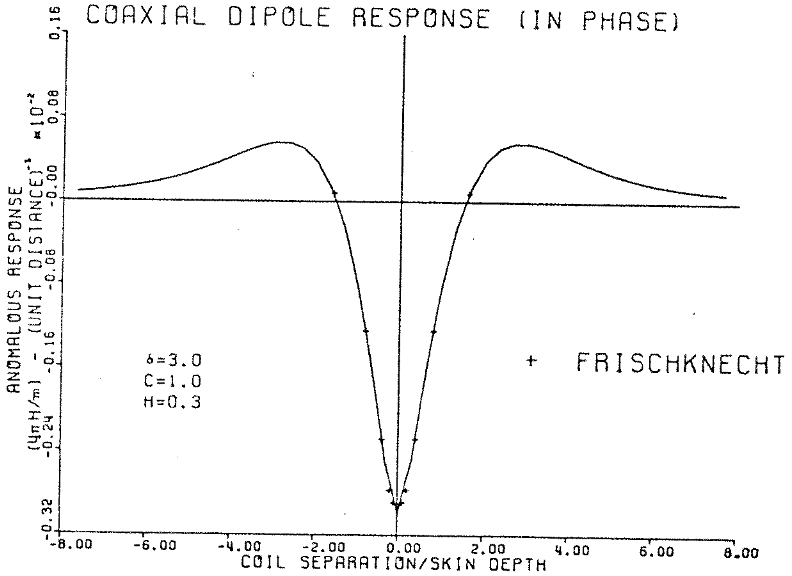

Fig. 3-3b. Inverse transform of Figure 3-3a (IP).

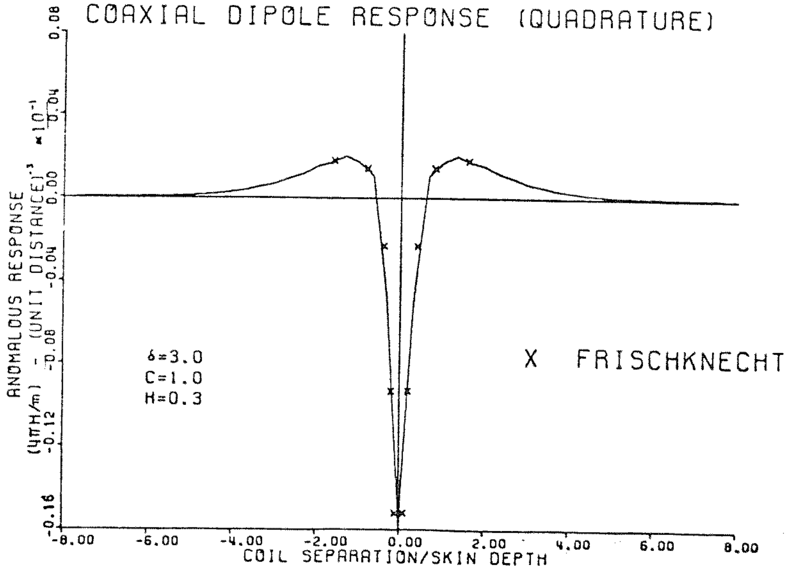

Fig. 3-3c. Inverse transform of Figure 3-3a (Quad.).

system is given by

$$\hat{H}_x^A(\bar{\rho},-h) = 2\pi m \frac{u^2}{\rho} e^{-2\rho h} \cdot RF(\rho,\sigma) \qquad 3.2\text{-}5$$

To obtain $H_x^A(r,-h)$, the anomalous spatial distribution, equation 3.2-5 is generated in the wavenumber domain and then transformed to the space domain.

The data tabulated by Frischknecht is in the form of mutual coupling ratios. The anomalous in phase and quadrature components were extracted by specifying a source field with the appropriate magnetic moment.

In the following examples, skin depth (δ), source height (H), and layer thickness (D) are all in units of the sampling interval ΔX=ΔY=1. The conductivity contrast (C) is that of the half space with respect to that of the first layer.

Figure 3-3 a) is a plot of equation 3.2-5, the anomalous response of the coaxial dipole system in the wavenumber domain, shown along the u wavenumber axis only. The earth model is homogeneous (C=1), with skin depth of three sampling units (δ=3.) and coil height of 0.3 sampling units (H=0.3). For this case, the wavenumber response is seen to be well behaved, that is, the low wavenumber peaks are adequately sampled and the response decays smoothly to near zero at the Nyquist wavenumber. Figures 3-3b and 3-3c compare the

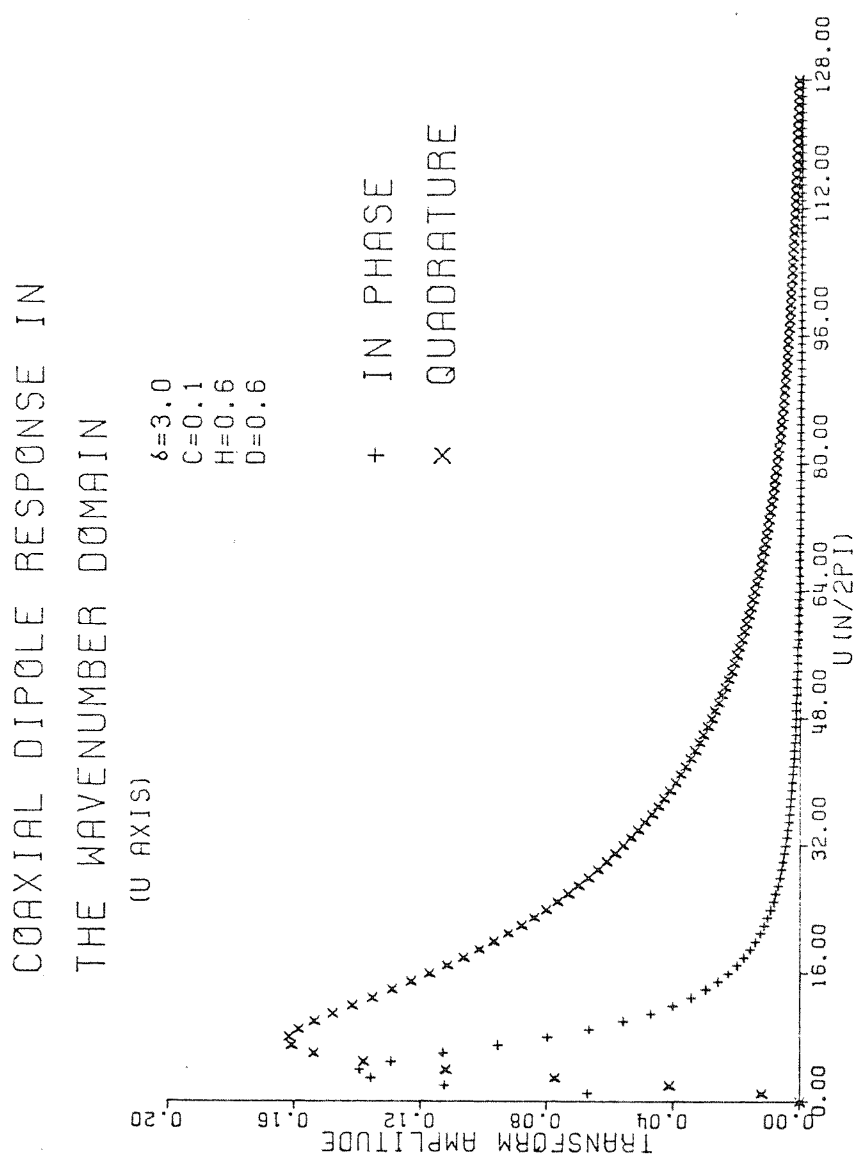

Fig. 3-4a. Wavenumber domain response on the u axis.

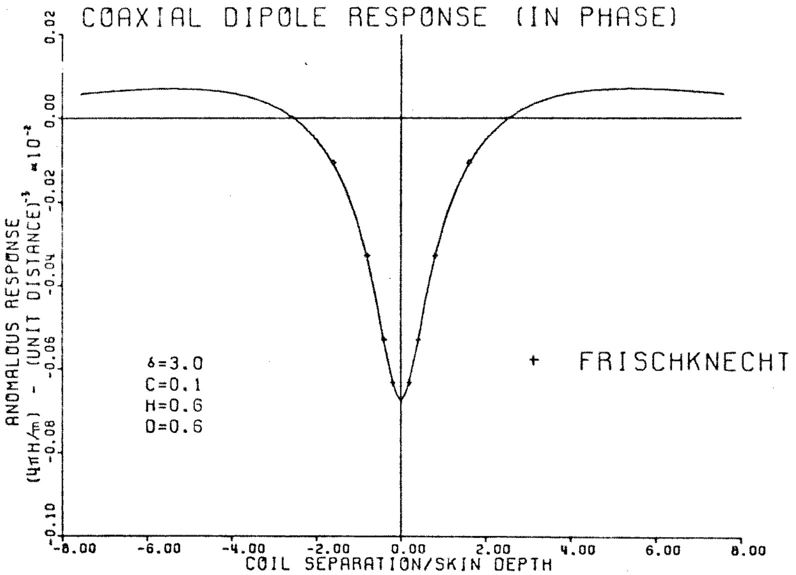

Fig. 3-4b. Splined inverse transform of Figure 3-3a (IP).

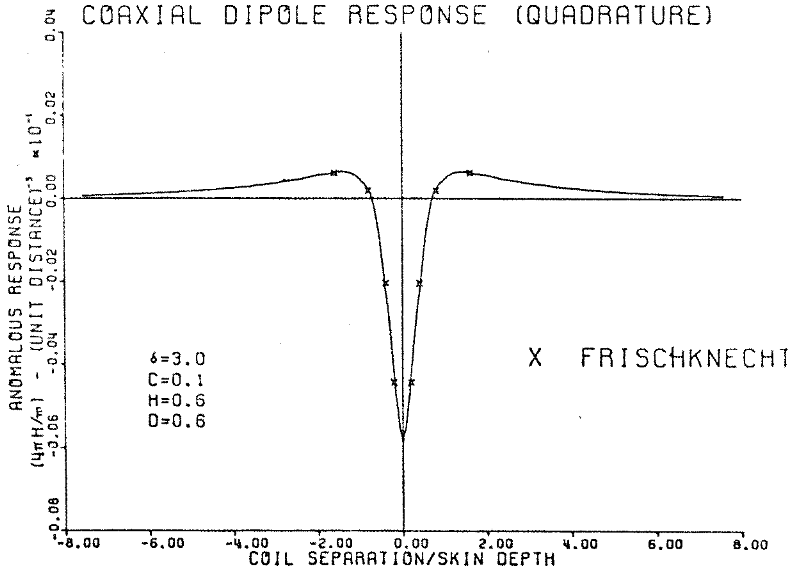

Fig. 3-4c. Splined inverse transform of Figure 3-3a (Quad.).

computed inverse transform of 3-3a with the available tabulated data (Frischknecht, 1967) for this model. The linear interpolation between points plotted by Calcomp is evident. Figure 3-4 shows an example of the response for a conducting layer over an insulating half space which has been cubic spline interpolated.

Figure 3-5 corresponds to the same model as that of Figure 3-3 but with both coils on the surface z=0. The downward continuation is apparent when comparing the transforms of Figures 3-3a and 3-5a. The in-phase transform in Figure 3-5a is still well behaved resulting in a good fit between calculated and tabulated data in Figure 3-5b. The quadrature transform however is truncated at the Nyquist wavenumber. In this case, the anomalous field at all distances is positive except for a negative delta function at zero separation. However, the truncation of the quadrature transform in Figure 3-5a is equivalent to convolving the true spatial response with the sinc function. Thus a broadening of the negative central peak is found in Figure 3-5c. It is therefore necessary to have a record length long enough to properly define the response in the wavenumber domain. The problems of truncation are at their worst when the coil system is on the surface of the earth as shown in the previous examples. Raising the source and/or the receiver

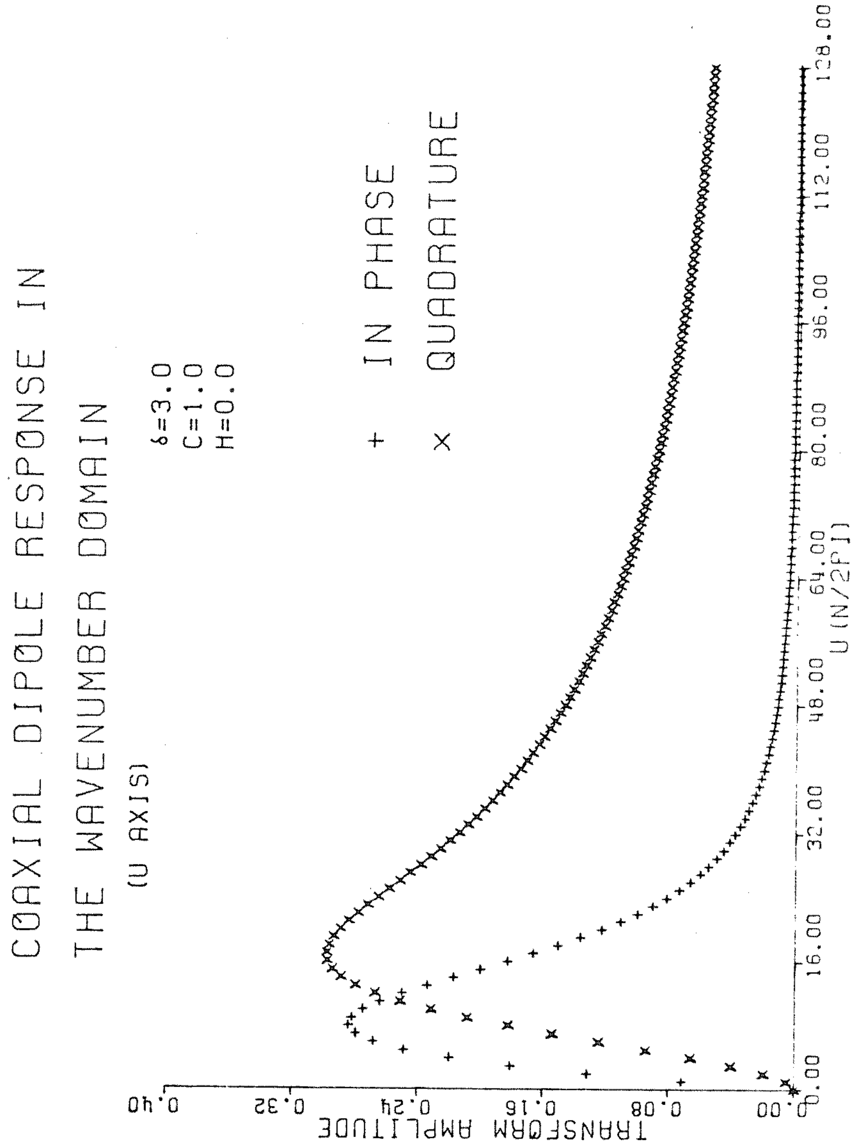

Fig. 3-5a. Wavenumber domain response on the u axis.

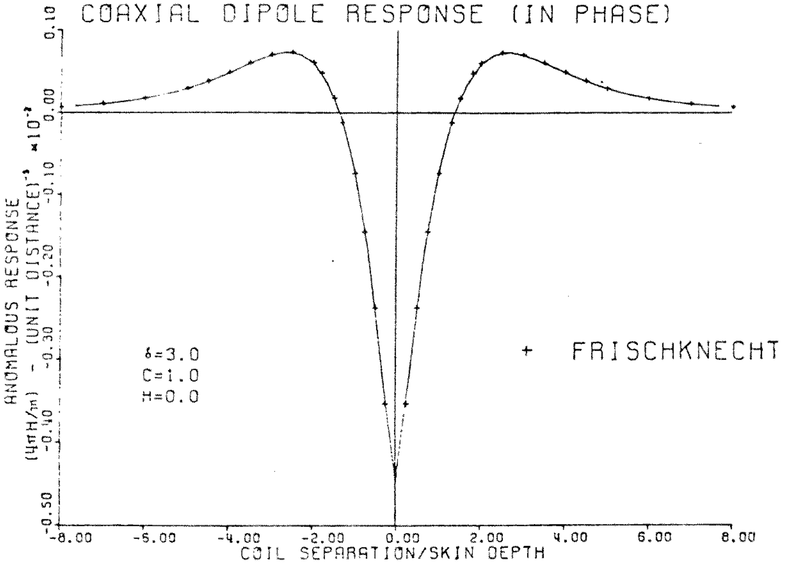

Fig. 3-5b. Inverse transform of Figure 3-5a (IP).

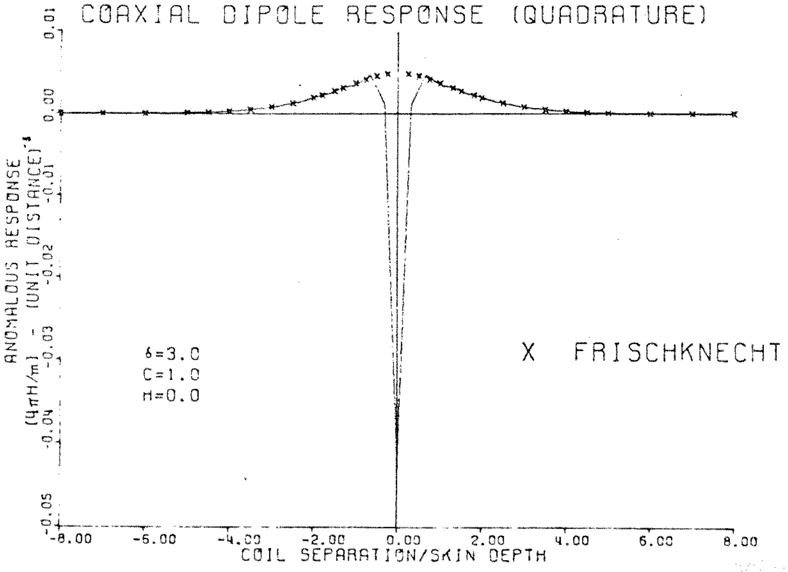

Fig. 3-5c. Inverse transform of Figure 3-5a (Quad.)

will introduce an exponential decay in the transform such that the high wavenumber components tend more rapidly to zero.

Figure 3-6 illustrates the other extreme. In Figure 3-6a the skin depth is 20 sampling units and the wavenumber domain response is such that the lower wavenumbers are undersampled, especially for the in-phase response. The effect on the results is to introduce severe spatial aliasing.

The foregoing examples were presented to demonstrate that care must be taken to obtain satisfactory results with this technique. The parameters and scale of the problem must be adjusted such that the product of source term and filter is well behaved in the wavenumber domain. The accuracy will depend directly on adequate sampling at low wavenumbers (i.e. large enough net) and the amount of cutoff at the Nyquist wavenumber. This is a standard consideration in any Fourier transform technique.

These restrictions are somewhat analogous to those of analogue modelling in an electrolytic tank. If the spatial distribution of the field is too large, edge effects will result from the finite size of the tank. On the other hand, if the spatial distribution is too small, errors will result from the finite size of the pick up coil.

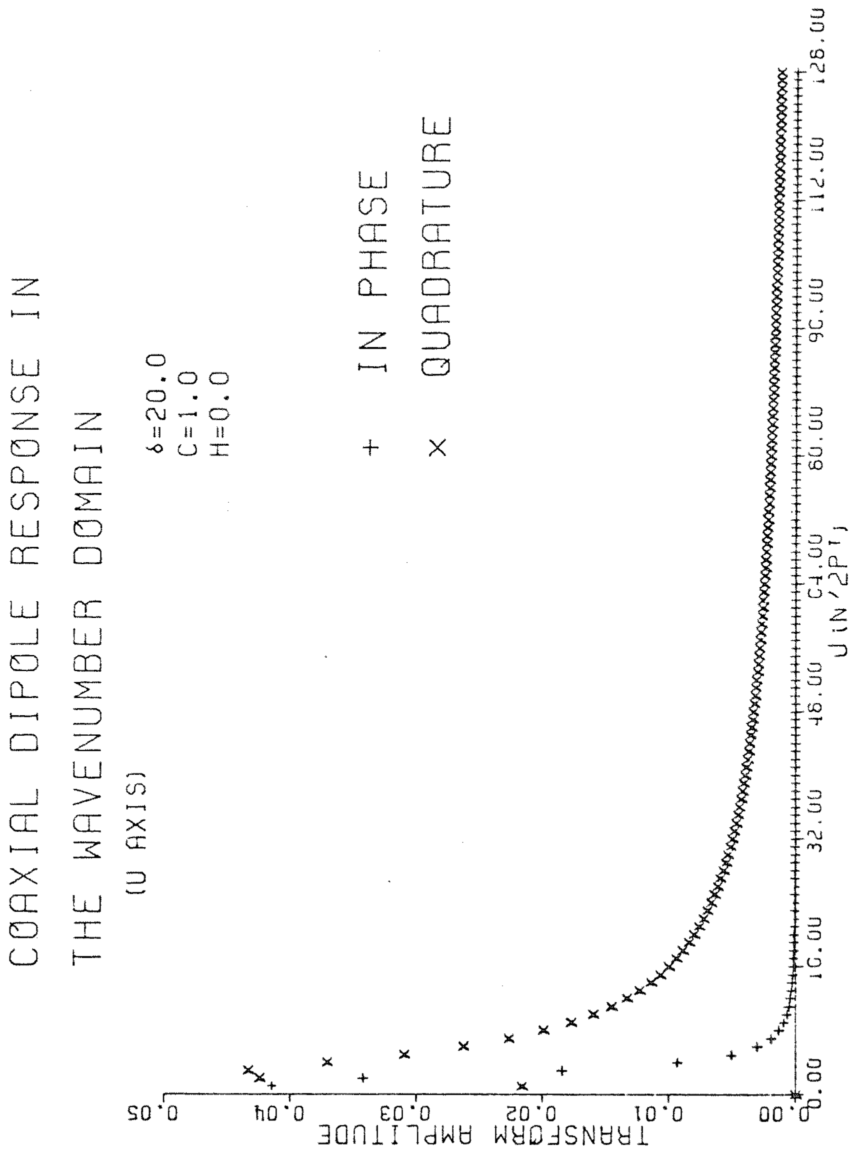

Fig. 3-6a. Wavenumber domain response on the u axis.

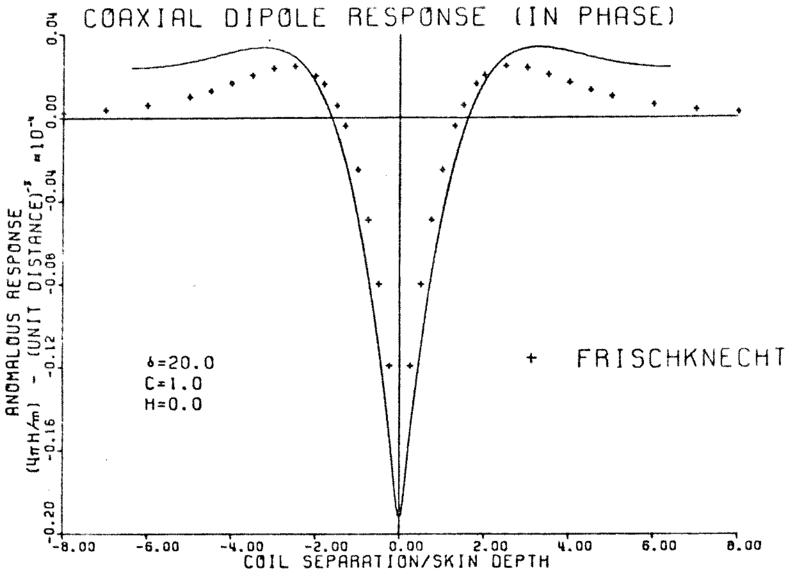

Fig. 3-6b. Inverse transform of Figure 3-6a (IP).

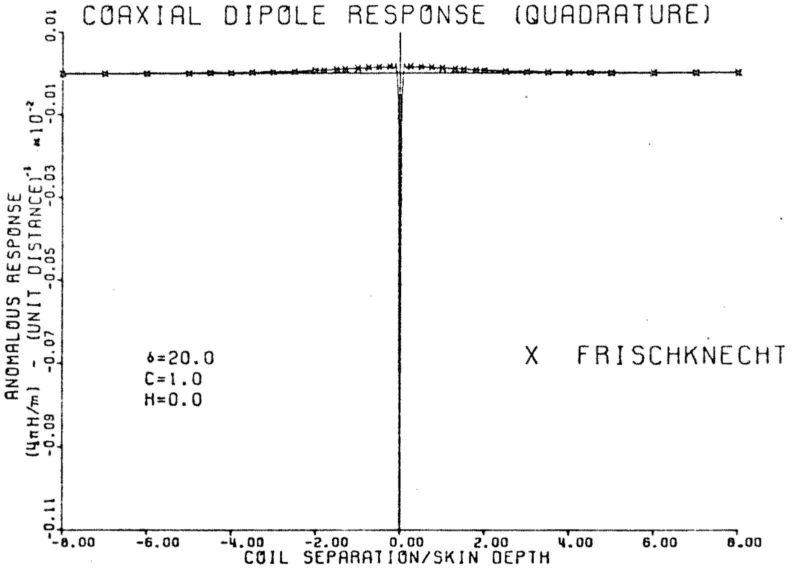

Fig. 3-6c. Inverse transform of Figure 3-6a (Quad.).

Alfonso-Roche (1973) gives an excellent description of the numerical problems involved with finite length records. He also demonstrates how to get around them by folding the data series about the Nyquist frequency so that it becomes artificially "aliased".

The length of record problem can be very serious when computing the fields inside a layered earth. This arises because the continuation operator spreads out the fields and can result in severe spatial aliasing. A simple technique which is used in the models of Chapter 5 to bypass this problem is to begin the FFT filtering approach with the source field at the desired depth inside the layers, as if the layers were absent. An optimum grid size is used to properly sample the source field distribution at this depth. Once in the wavenumber domain, the source field is continued back up to the surface before the filter is applied. The combined filter then considers only the effect of the presence of the layers.

A substantial saving in computation time can be achieved by making use of spline interpolation in obtaining the values on a 128 x 128 grid. Original values may be computed on a 4 x 4 grid size in regions of small spatial variation and a 2 x 2 grid size in regions of faster variation. A spline subprogram is then used to fill in the missing data.

3.3 Comparison of Computational Results with Model Studies in an Electrolytic Tank

Numerical computations are now compared to model studies (Wong, 1973) in the electrolytic tank facility at the Geophysics Lab., U. of Toronto. The electrolyte of course represents a homogeneous earth and a Turam loop source is supported on its surface. Examples of the fit obtained are shown in Figure 3-7.

In this type of computation, problems arise because the source field is singular on the plane z=0. One way to get around this is to raise the loop until the source field on the plane z=0 may be adequately defined by the record length and sampling interval chosen. Once in the wavenumber domain, the source field may be downward continued the distance of the source height. This will result of course in high amplitudes at high wavenumbers, but these will be substantially reduced after multiplication with the reflection filter for the layered earth under consideration. Another method consists of computing the source field directly in the wavenumber domain as is possible with simple sources such as dipoles and line segments making up a loop. The singularity in space is depicted in the wavenumber domain

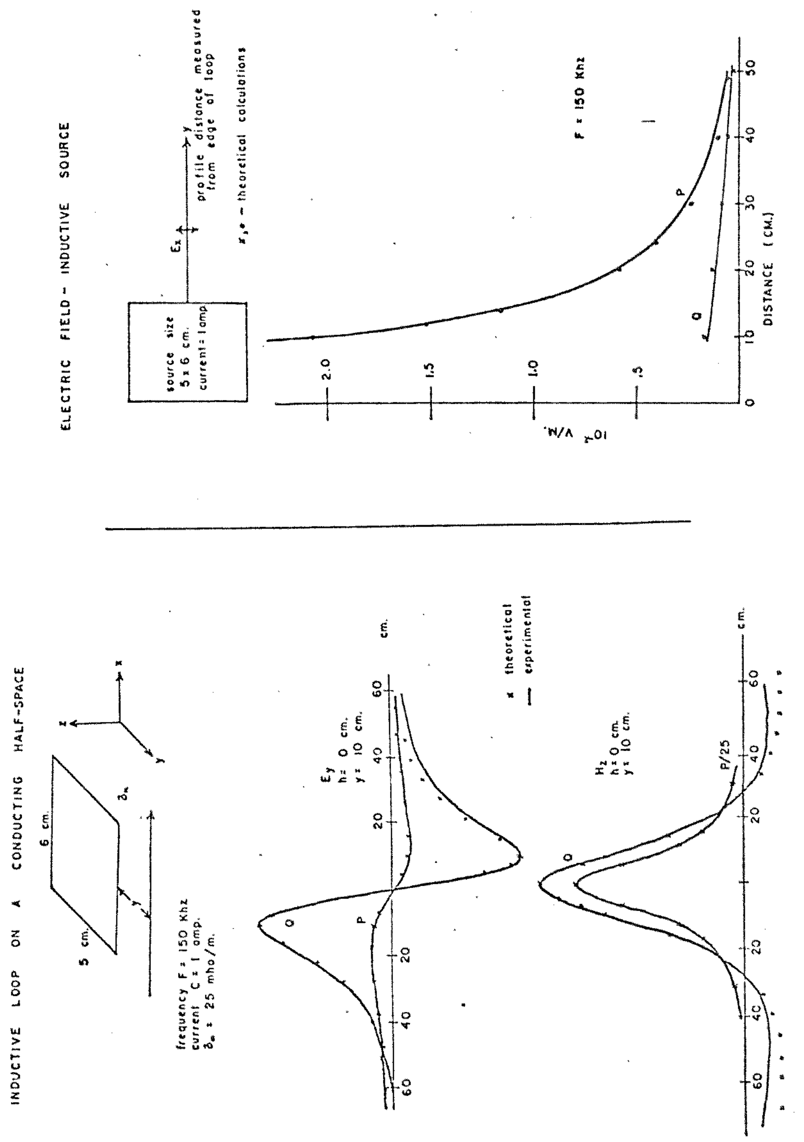

Fig. 3-7. Comparison with tank modelling results (from Wong, 1973)

by increasingly large amplitudes at high wavenumbers. Again, the singularity is removed after multiplication with the reflection filter. If the total field response is desired, as is usually the case, the source fields may be calculated directly and added to the anomalous field.

CHAPTER 4

NUMERICAL RESULTS FOR THE FINITE PLATE IN A CONDUCTIVE HOST MEDIUM OF INFINITE EXTENT

This chapter is a study of the behaviour of electric currents in a plate which is embedded in an infinite host of finite conductivity. It provides a clear picture of the effects of induction in the plate and conduction through it. Also it allows comparison with available theoretical and experimental data.

4.1 Plate in a Uniform Field

a) The V potential

Figures 4-1a and 4-1b give an example of how the contour lines of V, which are normal to the current flow lines, vary with plate conductivity. The contour interval has been adjusted to keep the number of contours constant throughout the six plots in order to demonstrate how the potential surface changes shape as the plate conductivity increases from that of the host conductor ($\sigma_P = \sigma_H = 10^{-3}$ MHO/M) up to 10^{10} MHO/M.

The source field consists of a static, uniform electric field applied parallel to the width of the plate and of amplitude 1 volt per meter. Since there is no time dependence, there is no induction and hence the U potential does not apply. The effect of the plate is to act as a simple

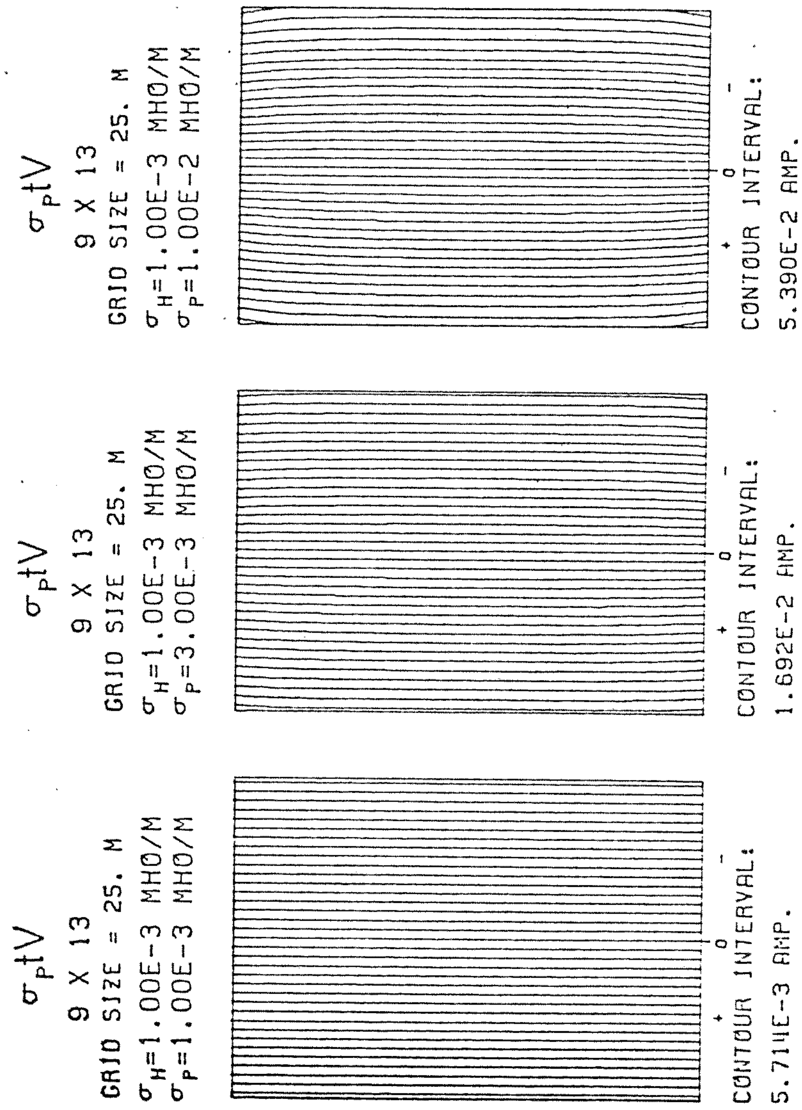

Fig. 4-1a. $\sigma_P tV$ for the plate in a uniform electric source field.

"current collector". Because of the perfect antisymmetry in the V potential for this model, the matrix size reduces to AxA where A = (M-1)XN/2 and M is the number of points along the width of the plate.

The current density may be obtained from the gradient of the σ tV distribution. At zero conductivity contrast, the contours are straight equidistant vertical lines representing the uniform source current. As the conductivity of the plate is increased, the potential surface becomes distorted with the gradient being larger near the center than near the vertical edges. This, of course represents the total accumulated current that has entered the plate between the edge and the center. Another characteristic is the larger gradient near the corners as compared to that near the vertical edges. This shows the tendency for the current to enter and leave through the corners of the plate. The contour plot for $\sigma_p = 10^{10}$ MHO/M gives the saturation σ_ptV surface; i.e., as $\sigma_p \rightarrow \infty$, $V \rightarrow 0$ but the current density in the plate approaches a limiting value.

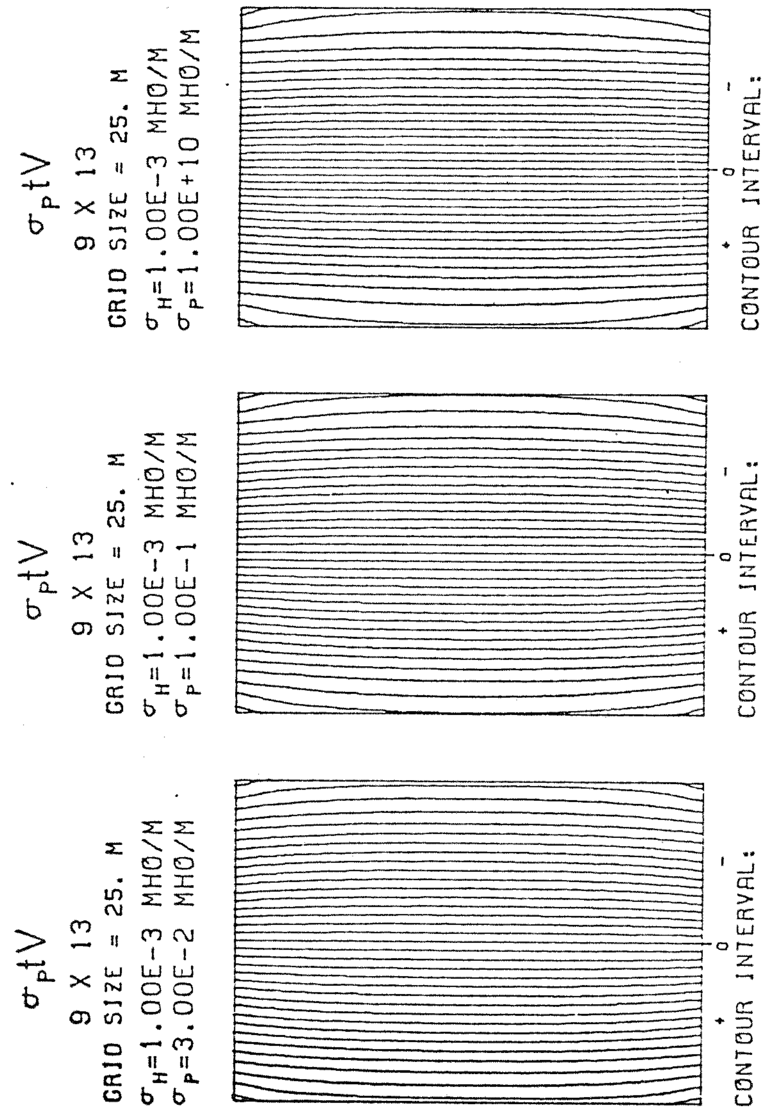

Fig. 4-1b. σ_p tV for the plate in a uniform electric source field.

4.1 b) The U Potential.

Figures 4-2a and 4-2b give a similar example for the U potential. In this case the source field consists of a uniform periodic magnetic field of amplitude 1 AMP/M, perpendicular to the plane of the plate. The conductivity of the host medium is zero and the current is constrained to flow within the plate; therefore, only the U potential applies.

As the conductivity of the plate increases, the induced current flow becomes in phase when the induction parameter θ (=σμωtL) is approximately 10. At very large conductivity the induced current saturates in the plate. A characteristic feature as the conductivity increases is that the current becomes more concentrated near the edges of the plate as seen in Figure 4-2b. Figure 4-3 gives an example of the typical response of the plate in air for a uniform inducing field perpendicular to it.

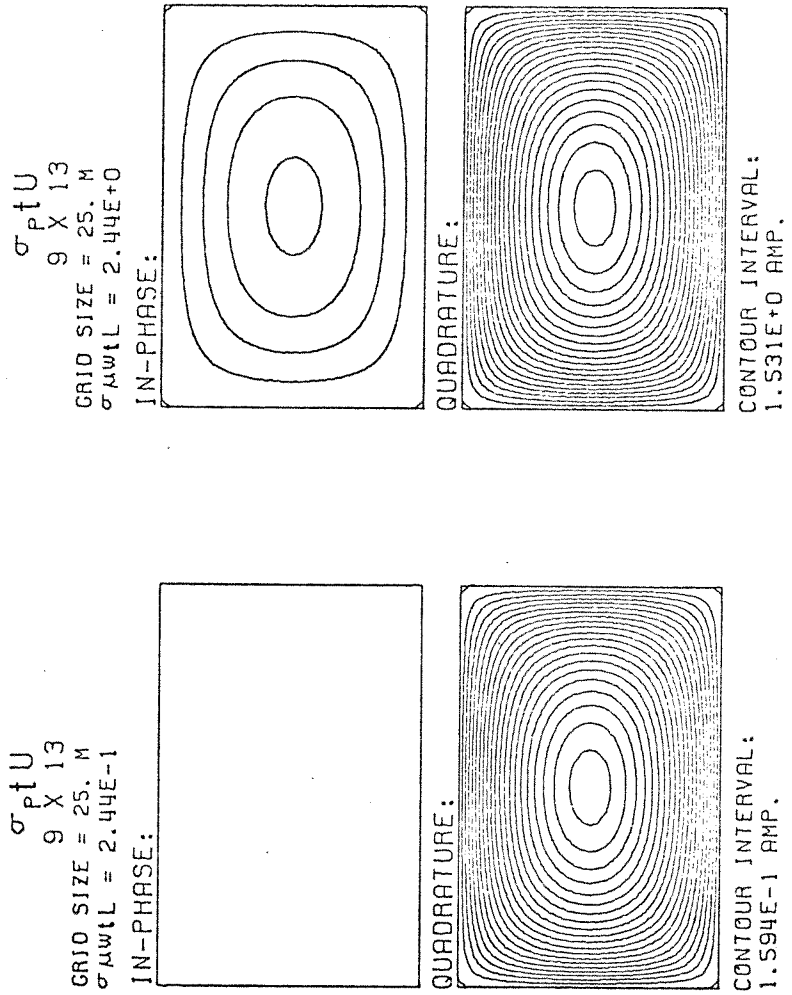

Fig. 4-2a. σ_p tU for the plate in a uniform magnetic field.

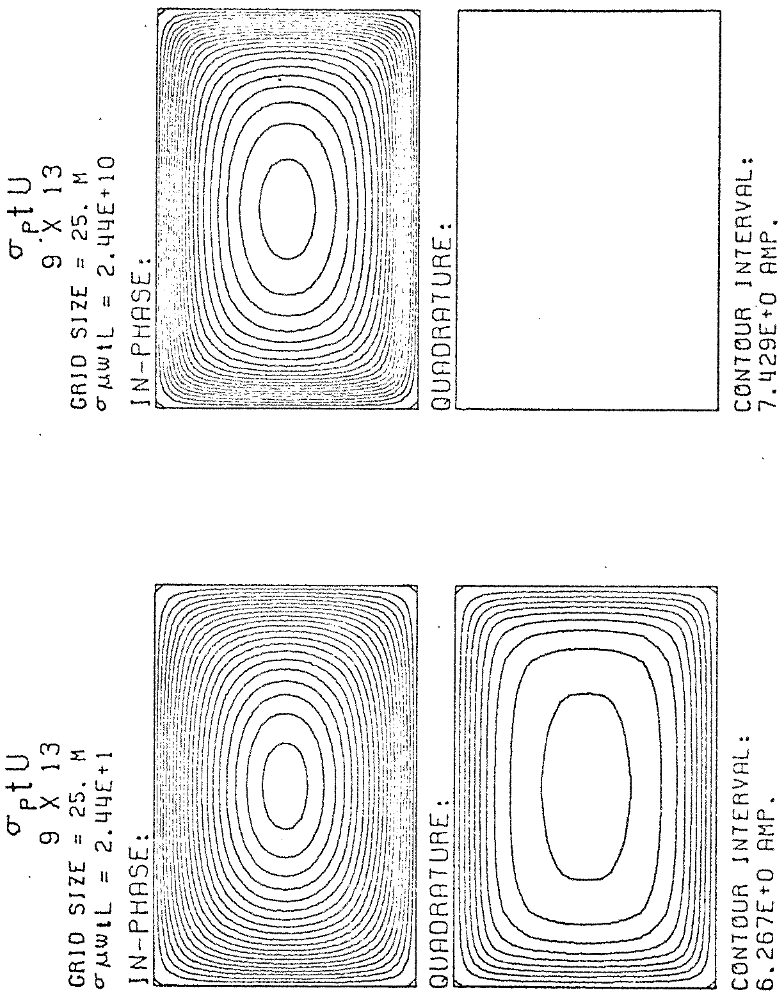

Fig. 4-2b. σ_p tU for the plate in a uniform magnetic field.

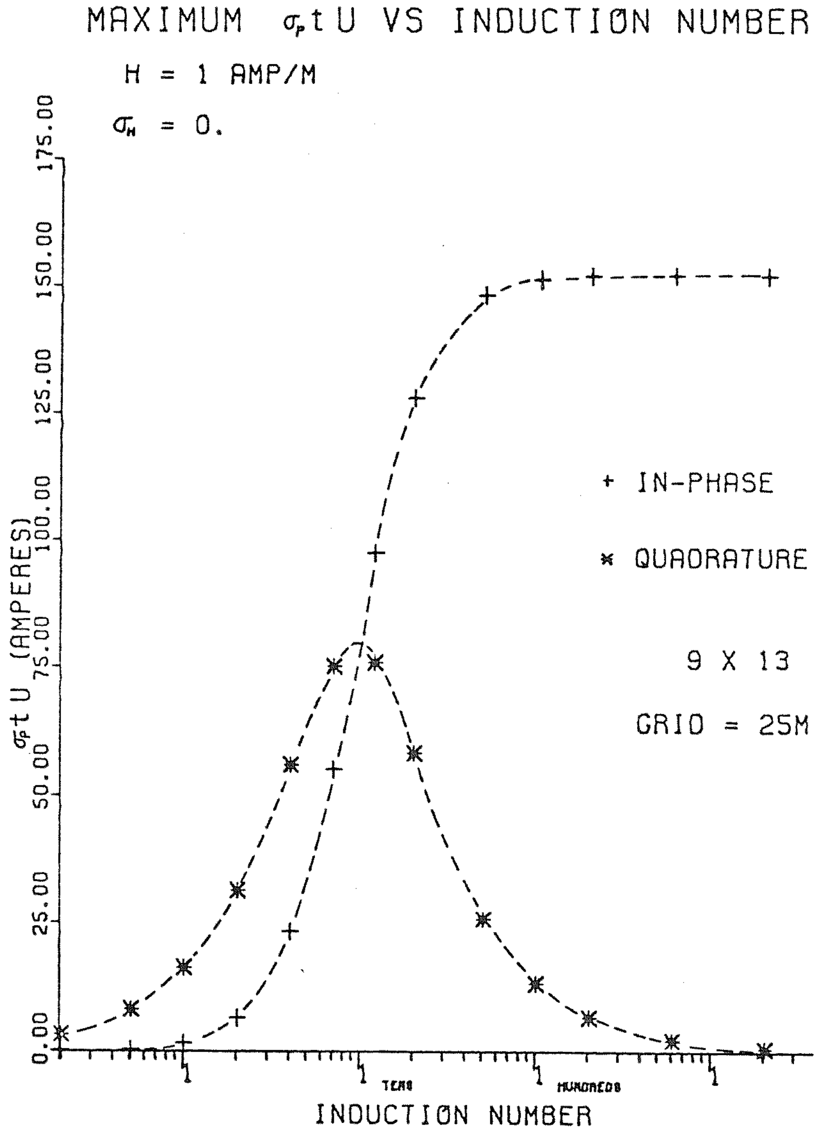

Fig. 4-3. The response of the plate in air to a uniform magnetic field.

4.2 Comparison with Theoretical Ribbon Model

Analytical solutions for an infinitely long ribbon in a uniform field are not too difficult to obtain, (Appendix A), and the numerical solutions may be compared to these results. The conductivity of the ribbon must be assumed high enough such that the saturation point is reached. The width of the ribbon and plate is 250M. The length of the plate is 500M giving only a length to width ratio of 2.

In Figures 4-4 and 4-5 the solid line is the solution for the infinite ribbon model along a profile through the center and parallel to the width of the ribbon. The points for the numerical solution are for a profile through the center of the plate and parallel to its width. Various grid sizes have been used.

Figure 4-4 compares numerical and theoretical results for the V potential distribution at saturation, i.e. in the limit of infinite plate conductivity. The source field consists of a static electric field parallel to the width of the plate and ribbon. The background conductivity, σ_H, is 10^{-3} MHO/M. The results show that the potential on a profile through the center of the plate is not very much affected by the plate not being infinite in length.

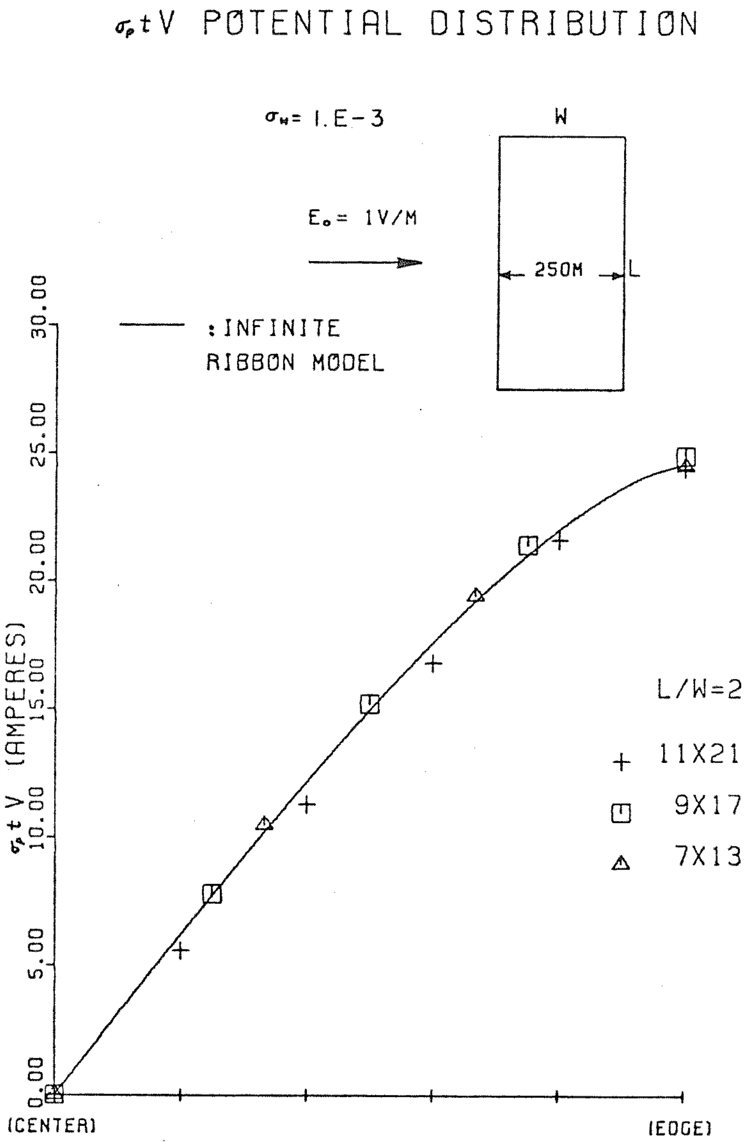

Fig. 4-4 Comparison with ribbon model for the V potential.

This may be seen in the contour plots of the last section where the curvature of the contours is small in the central region. The numerical results for various grid spacings cluster around the theoretical solution.

Similar results for the U potential are shown in Figure 4-5. The inductive limit is assumed such that the U potential is in phase with the incident field. The source field is a uniform periodic magnetic field of amplitude 1 AMP/M perpendicular to the plane of the plate and ribbon. In this case, the finite length of the plate prevents a good match between numerical and theoretical results. The results show that less current is induced in the plate than in the ribbon although the form is almost identical in both cases. The numerical results for a plate of length to width ratio of 2, using different grid sizes cluster closely together. When the length to width ratio is increased to 3, allowing greater freedom to current flowing along the length of the plate, the numerical solution is seen to approach that of the infinite ribbon model.

An interesting characteristic which is demonstrated in these models is that the amplitude of the solution varies little with grid size. This indicates that the special moment functions that were used to compute the

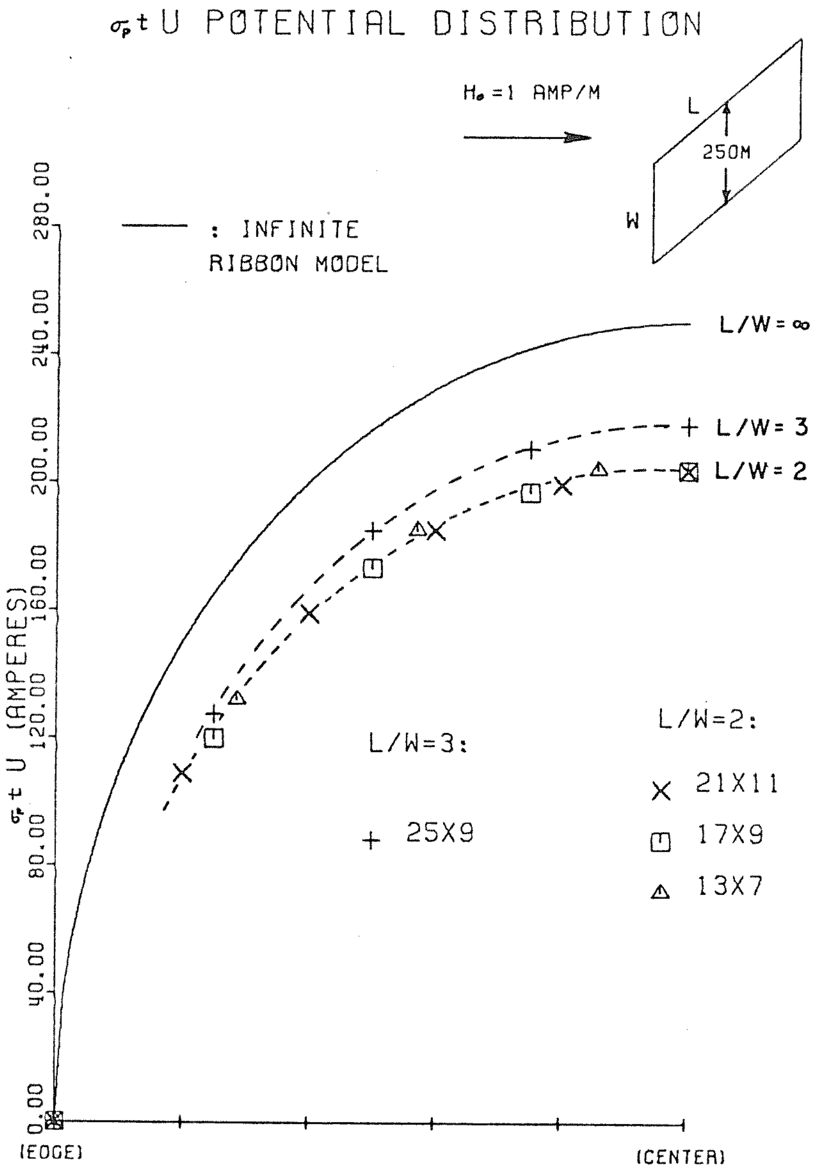

Fig. 4-5 Comparison with ribbon model for the U potential

Green's tensor arrays are successful in interpolating the field between grid points. However, as will be seen in the next section, a reasonably dense grid spacing is required in order to compute the scattered fields outside the plate.

4.3 Comparison with Experimental Data

The numerical results are now compared with laboratory model measurements by Lamontagne (1970). The geometry consists of a horizontal rectangular loop source in the vicinity of a vertical plate in air, as shown in Figure 4-6. The experimental points are laboratory measurements of the anomalous vertical magnetic field intensity along a profile in the plane of the loop as shown in Figure 4-6. The response is expressed as a percentage of the incident vertical field at $X=X_0$.

The anomalous field along the profile was computed by integrating the U solution digitally. The top two rows of elements were further subdivided into 5 rows using the Type 1 spline interpolation of figure 2-4. This was done in order to obtain a better representation of the U potential solution along the top edge of the plate, as this is the most important region, especially if the top edge of the plate is close to the profile.

Figure 4-6 compares results for two plate conductivities, using three different grid spacings. The odd values of conductivity were required to obtain the same induction numbers for the plate as was used by Lamontagne. For the plate of lower conductivity, $\sigma_p = 9.42$ MHO/m, a very good fit is obtained for the in-phase component. The quadrature component converges to the experimental

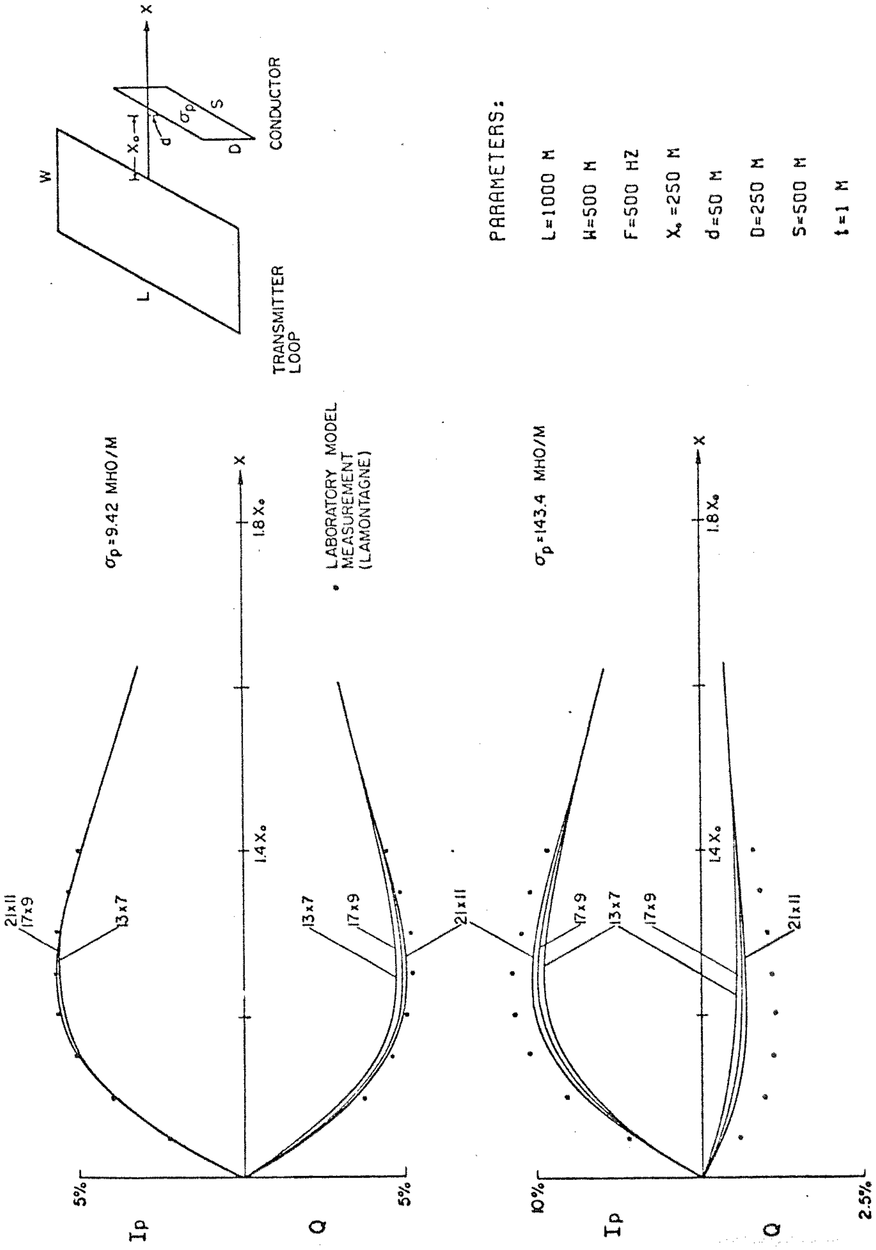

Fig. 4-6. Comparison with experimental data.

data as the grid size is reduced. The grid size is more important for the quadrature component because the quadrature current flow is concentrated closer to the edge (Lamontagne, 1970).

As the plate conductivity increases, the use of a smaller grid size becomes important, since both in-phase and quadrature current flow become more concentrated on the edges of the plate. The U potential solution has a steeper gradient near the edge, and a larger number of points is required to adequately represent it. This is evident in the numerical results for the plate of high conductivity σ_p = 143.4 MHO/M in Figure 4-6. Again, the error is greater in the quadrature component. In this case, the fit could be improved by a larger subdivision along the top edge of the plate, and of course, a smaller grid size.

It would be possible to have a different grid spacing for the vertical and horizontal directions. Lamontagne(1970) has shown that the longer the horizontal extent of the plate, the more important it is to have a smaller sampling interval in the vertical direction. On the other hand, the sampling in the horizontal direction could be proportionally increased.

However, in the integral equation technique, the same Green's function data banks are used for all sides of the plate. If the plate is not equisampled in both directions, the cost of generating the Green's function matrix would be doubled.

The foregoing results are presented in order to demonstrate the care that must be taken in order to accurately compute the anomalous fields outside the plate. Lamontagne (1970) suggests that for reasonable accuracy ($\pm$ 5% of the % anomaly magnitude), the product $\sigma\mu\omega t\Delta$, where Δ is the grid size, should be less than 6. The present work supports this statement since for the 21 x 11 grid size, the product is approximately 1 for σ_ρ = 9.42 MHO/M and 16 for σ_ρ = 143.4 MHO/M.

4.4 Electric Current Density in the Plate

In this section, numerical results are presented for the plate embedded in an infinite host medium of finite conductivity. Four series of solutions are presented to demonstrate the behaviour of the electric currents in the plate due to magnetic dipole excitation.

The format for presenting the solutions is the same throughout Figures 4-7 to 4-10. In each plot, the boxes outline the plate for both in-phase and quadrature components. Because both potentials exist the current in the sheet cannot be represented by stream lines. Thus, at each sample point a vector is drawn representing the amplitude and direction of the current density. It is effectively the amplitude of the 5th degree spline moment function centred at the grid point. The arrow is omitted if the current amplitude is less than the length of the arrow. The maximum amplitude for the plot is given at the top of each figure. The current density vectors are derived from curl U and grad V which are computed by finite difference differentiation.

In series #1 (Figures 7), the magnetic dipole source is close to the plate. The magnetic coupling with the plate is strong as the lines of incident magnetic field cut

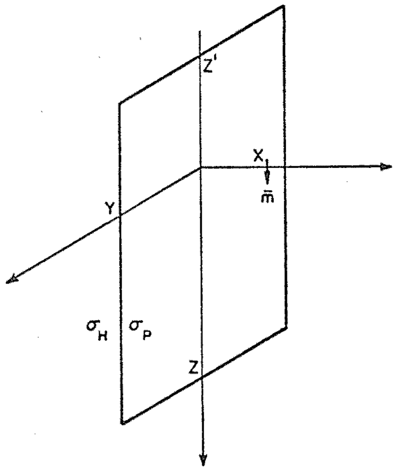

SERIES #1

7 X 11

GRID=25.0 M
F=1000. CPS
σ_H=1.000E-3 MHO/M
σ_P-VARIABLE
δ_H=4.948E+2 M
m=1 AMP-M^2

X=50 M
Y=75 M
Z=162.5 M
Z'=-87.5 M

Fig. 4-7a. Geometry for series #1.

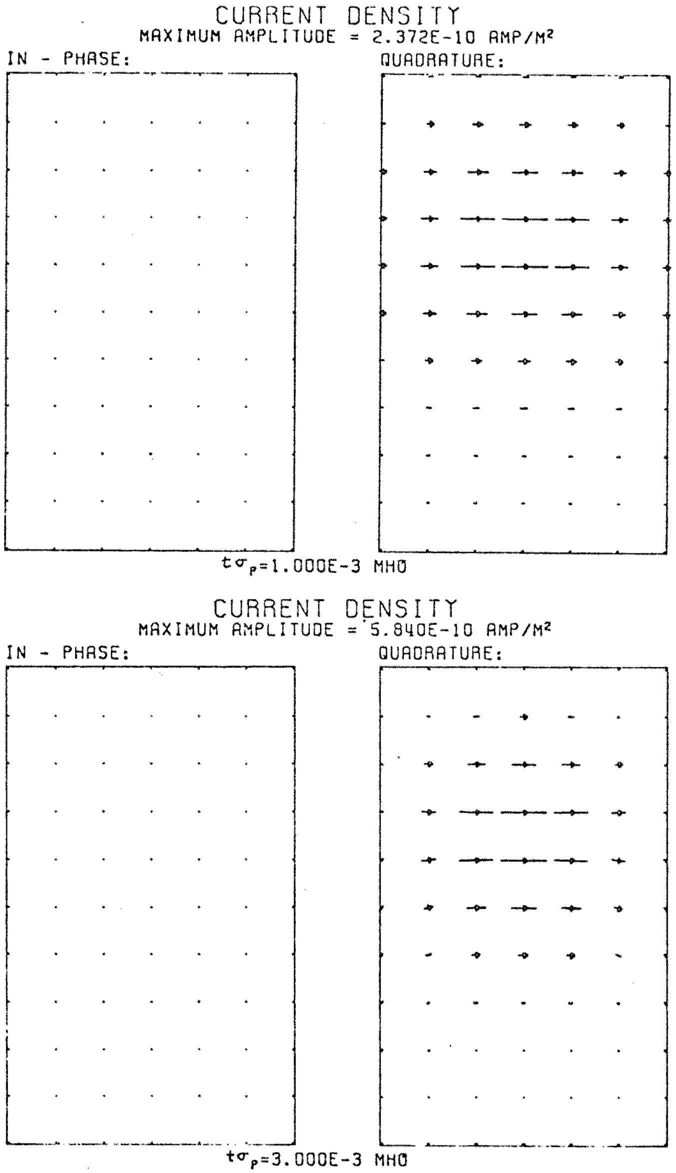

Fig. 4-7b. Series #1.

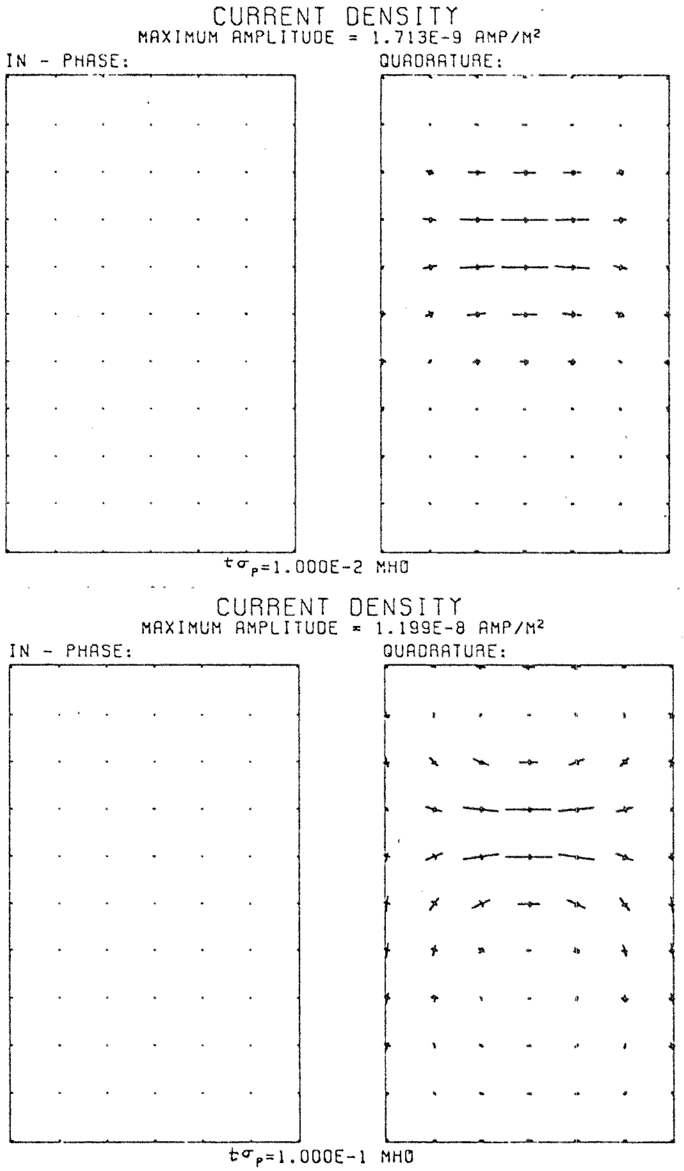

Fig. 4-7c. Series #1.

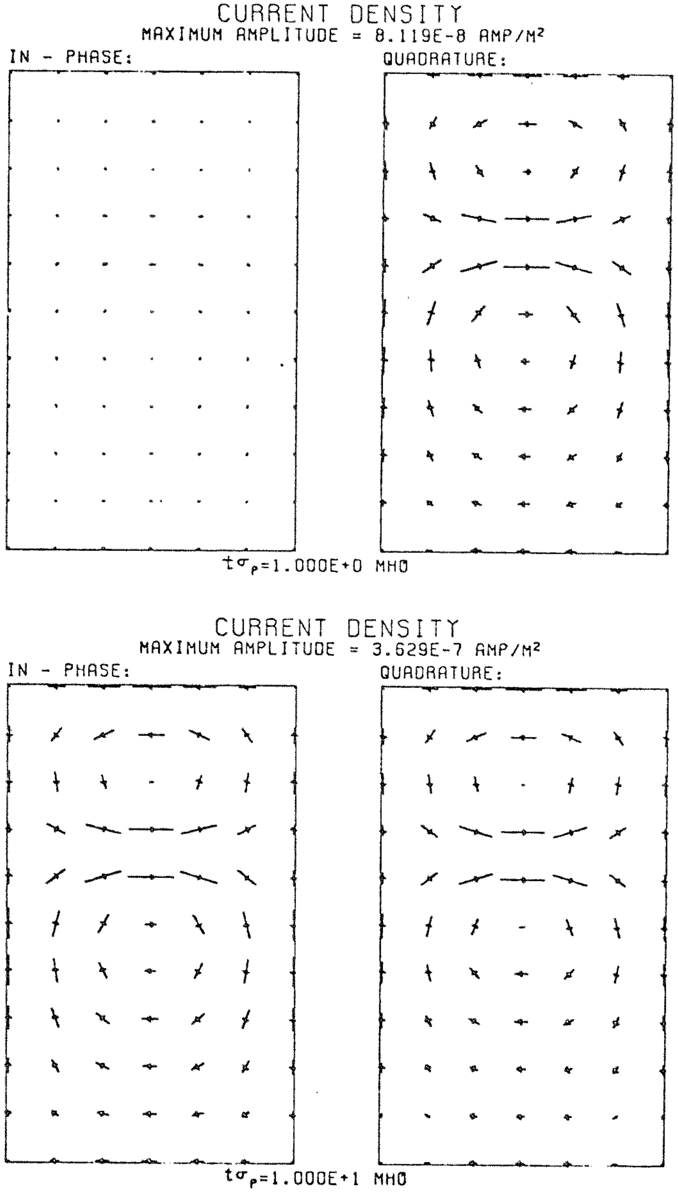

Fig. 4-7d. Series #1.

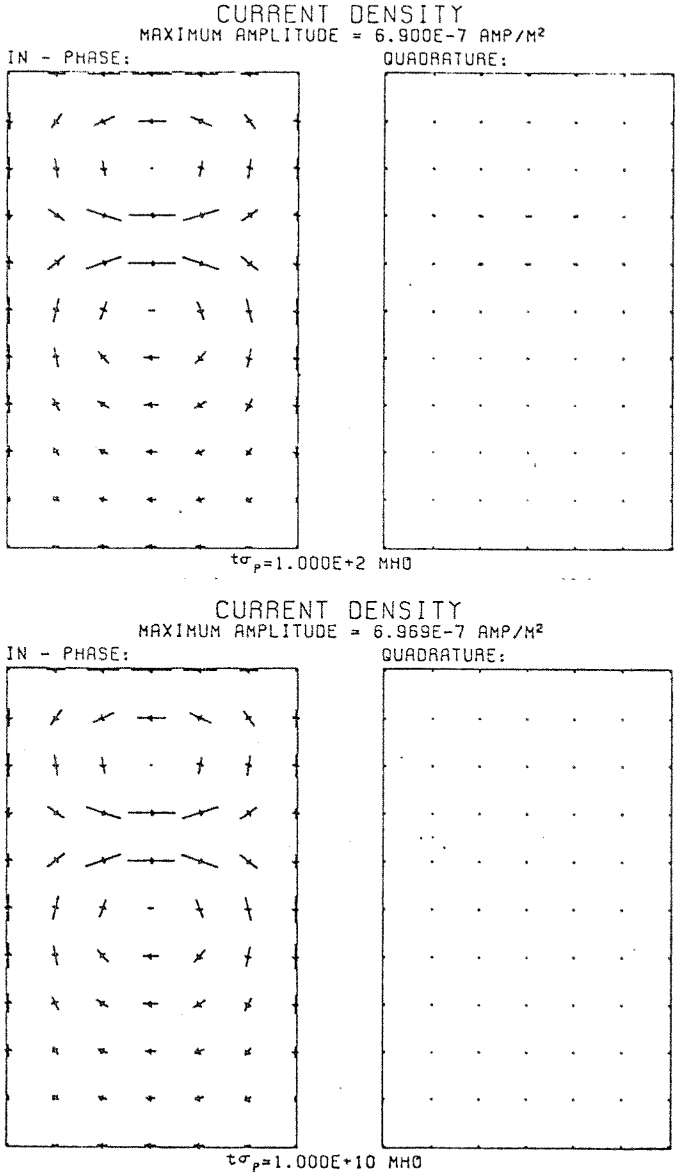

Fig. 4-7e. Series #1.

the plate almost perpendicularly over most of the surface.

In the first figure, the plate conductivity $t\sigma_p = 10^{-3}$ MHO is the same as that of the host medium (zero anomalous σt). Therefore, the electric current density in the region of the plate is simply the current induced in the host conductor, which is flowing circularly around the magnetic dipole, in planes perpendicular to the dipole moment. Due to the close proximity of the source, there is a large gradient over the plate for the component of current density in the plane of the plate. The current is chiefly in the quadrature phase since the plate-dipole distance is a small fraction of the skin depth in the host conductor.

At $t\sigma_p = 3\times10^{-3}$ MHO, the plate acts primarily as a current collector for the current flowing in the host conductor, thereby increasing the plate current density. The total electric field, however, has decreased slightly. The amplitude of the maximum in comparison to the other sampled points is now relatively larger than before since the host current around this point is larger. This region of the plate then pulls in relatively more current. As the conductivity increases to $t\sigma_p = 10^{-2}$ MHO the conduction currents begin to show a tendency to spread out across the width of the plate.

At $\sigma_p = 10^{-1}$ MHO two induction vortices begin to take shape in the quadrature component. The direction of each vortex is such that the magnetic field generated by it will tend to cancel the incident magnetic field on the plate. The two vortices are not completely closed inside the plate. The current vectors show that current is leaking outside the plate over its surface and edges. At $\sigma_p = 1$ MHO, the induction current becomes fairly well contained within the plate. At $\sigma_p = 10$ MHO, the current becomes in phase. At $\sigma_p = 100$ MHO and higher the current density is fully in phase and the amplitude saturates.

In series #2 (Figures 8), the dipole source is farther away from the plate. For this case, the magnetic coupling with the plate is poorer as the lines of incident magnetic field on this plate are mostly parallel to it. The first plot in this series, for zero anomalous conductivity, $\sigma_p = 10^{-3}$ MHO, shows the incident current density on the plate, which is fairly uniform. There is an in-phase incident current component since the plate-dipole distance is half a skin depth in the host conductor. Up to a plate conductivity of $\sigma_p = 1$ MHO, the plate acts primarily as a current collector. This is in contrast to series #1 where at this conductivity, two current vortices were fairly

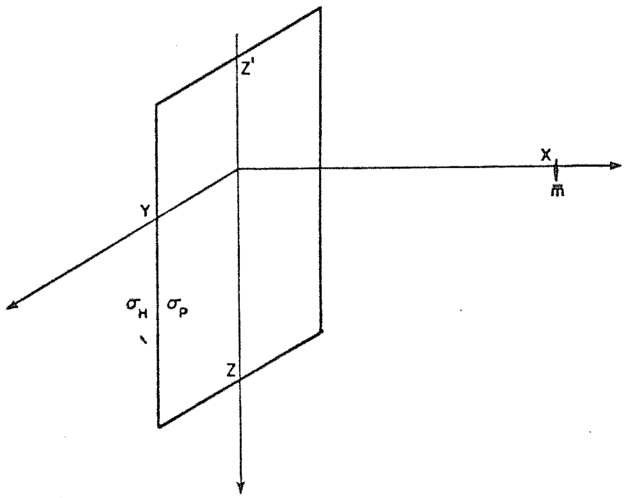

SERIES #2

7 X 11

GRID=25.0 M
F=1000. CPS
σ_H=1.000E-3 MHO/M
σ_P-VARIABLE
δ_H=4.948E+2 M
m=1 AMP-M^2

X=250 M
Y=75 M
Z=162.5 M
Z'=-87.5 M

Fig. 4-8a. Geometry for series #2.

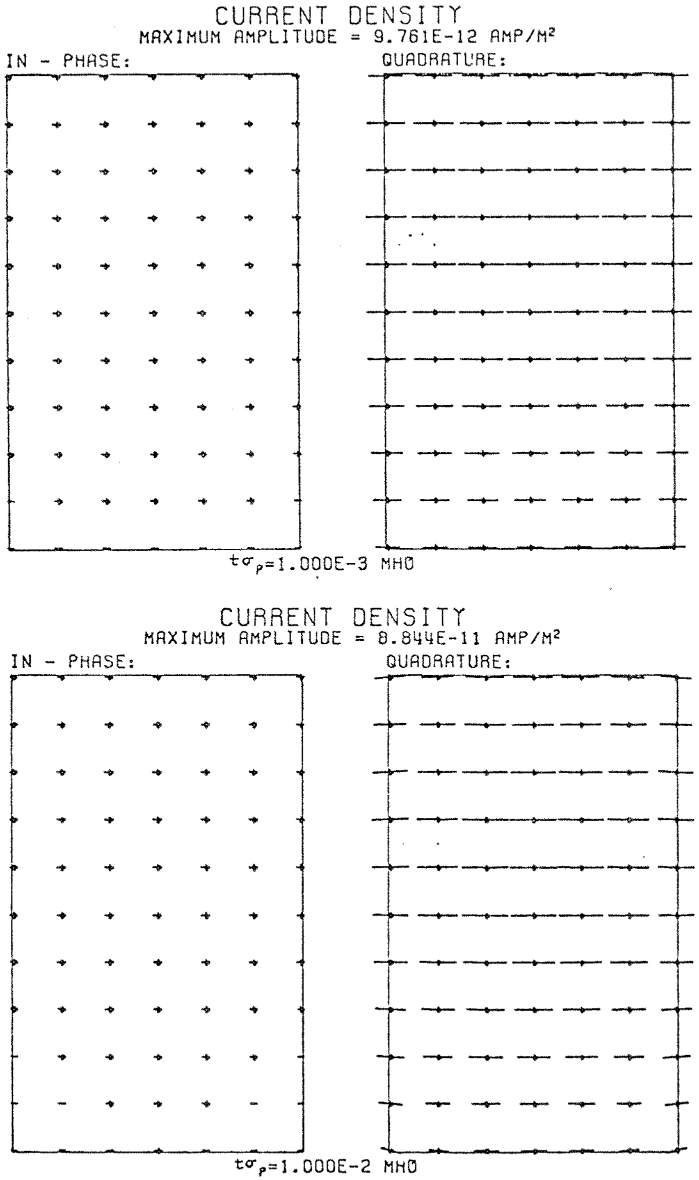

Fig. 4-8b. Series #2.

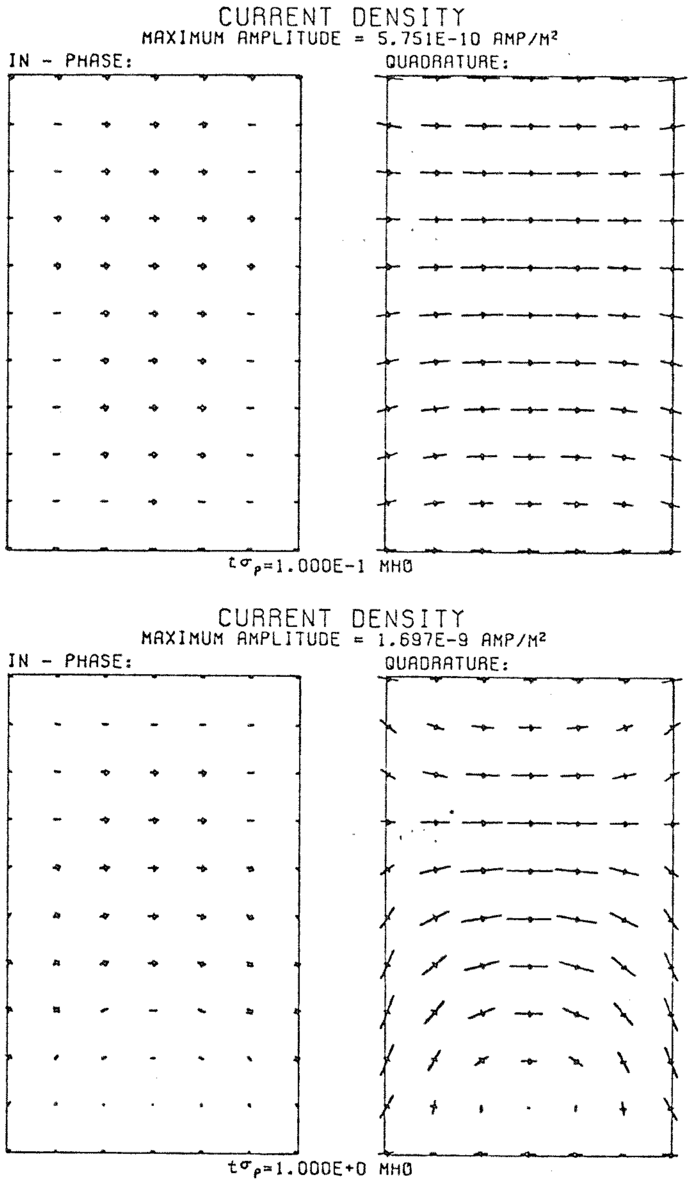

Fig. 4-8c. Series #2.

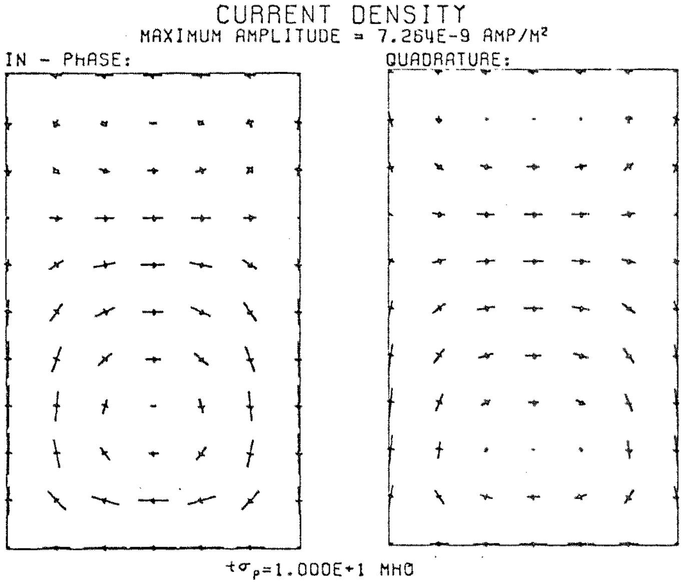

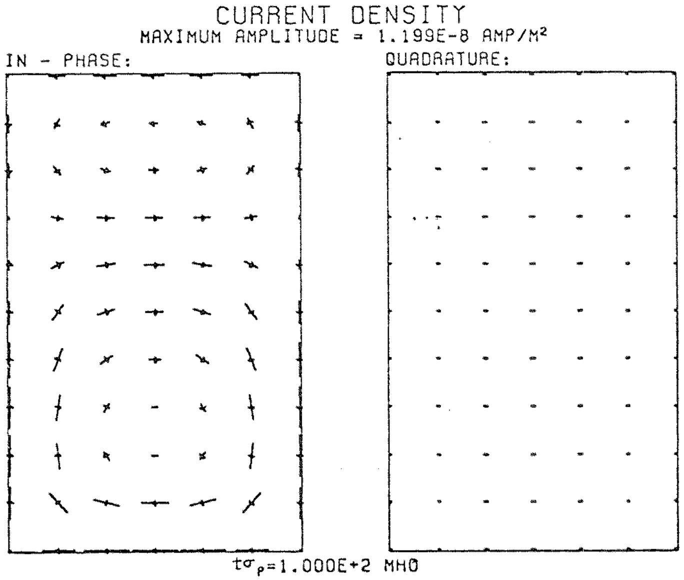

Fig. 4-8d. Series #2.

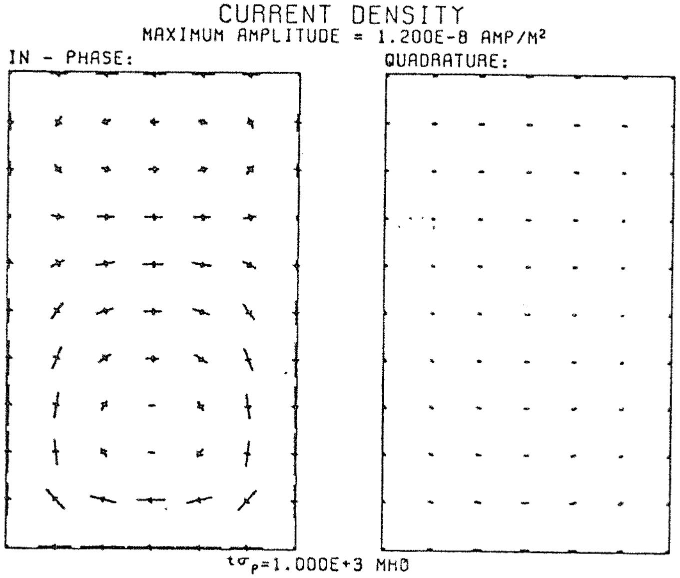

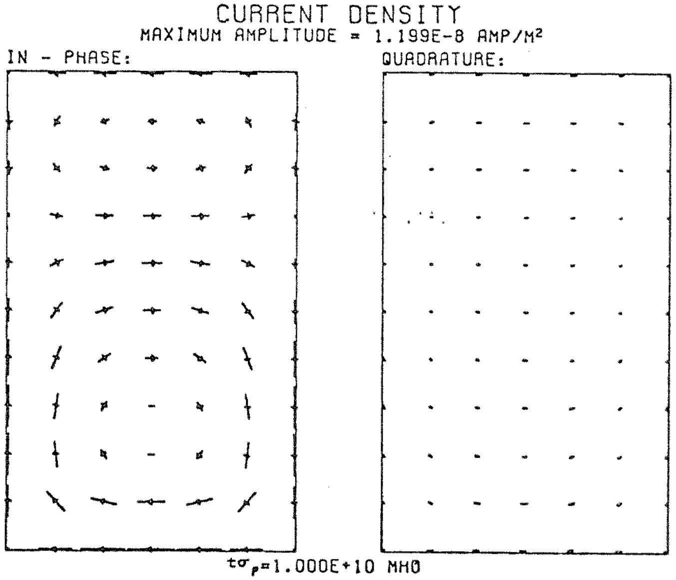

Fig. 4-8e. Series #2.

well contained within the plate. In series #2, at σ_p = 1 MHO the current vortices begin to take shape but most of the current is leaking out of the edges. This is a result of the poorer magnetic coupling for this series and the relatively stronger and fairly uniform incident current density.

At σ_p = 10 MHO , the current vortices become in phase. At σ_p = 100 MHO and higher, the current density saturates in the plate. The center of each vortex is now closer to the upper and lower edge than for series #1.

The geometry for series #3 (Figures 9) and #4 (Figures 10) is more representative of the typical exploration problem, a magnetic dipole source above and to the side of a conductor whose strike length is greater than its depth.

In series #3, the plate conductivity is varied as before. At low contrasts, the conduction currents through the top edge of the plate are predominant, with the induction effect superimposed. As the conductivity increases, the current vortex closes itself inside the plate, becomes in phase and saturates.

In series #4, the plate conductivity is constant at 1 MHO/M and the host conductivity is varied. Varying the host conductivity in the numerical computation is considerably more costly, since a new Green's function matrix must be

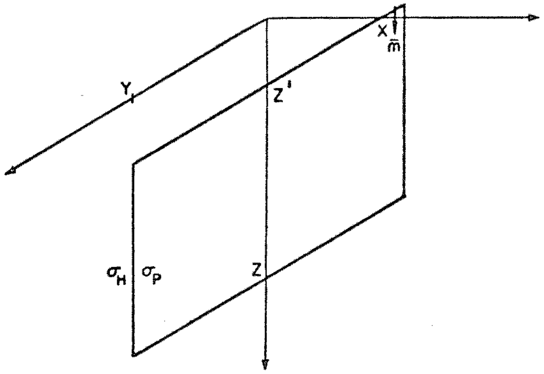

SERIES #3

7 X 11

GRID=25.0 M
F=1000. CPS
σ_H=1.000E-3 MHO/M
σ_P-VARIABLE
δ_H=4.948E+2 M
m=1 AMP-M^2

X=100 M
Y=125 M
Z=200 M
Z'=50 M

Fig. 4-9a. Geometry for series #3.

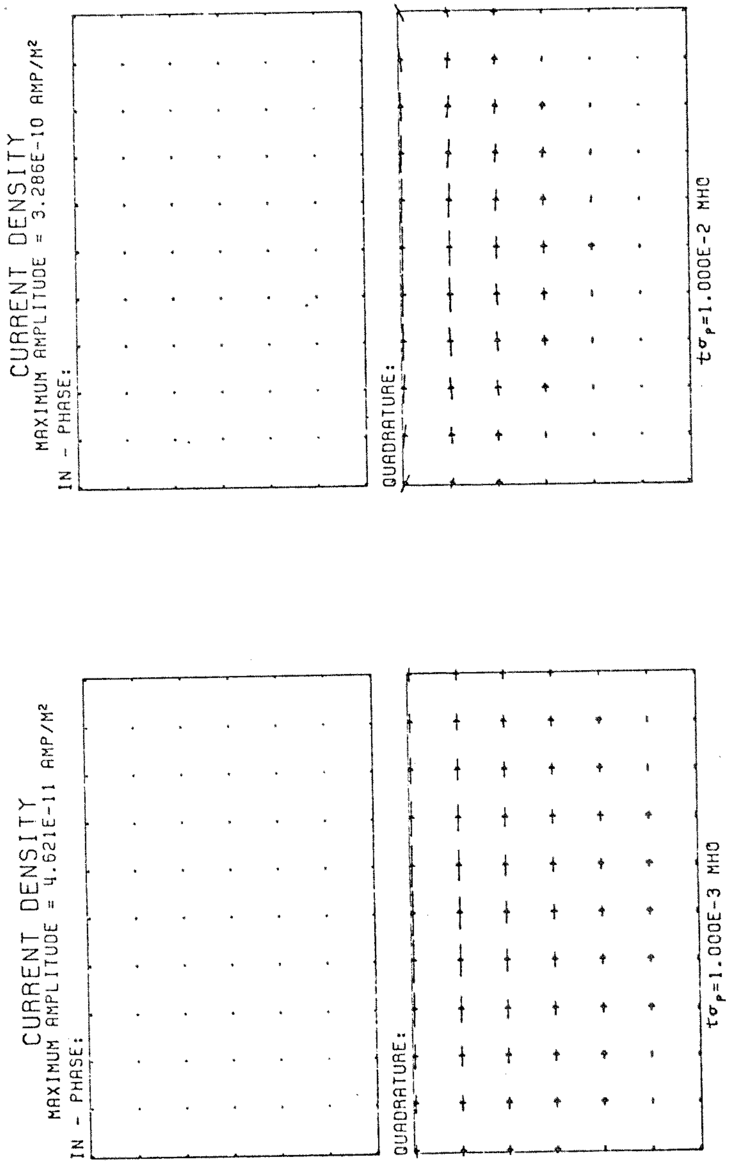

Fig. 4-9b. Series #3.

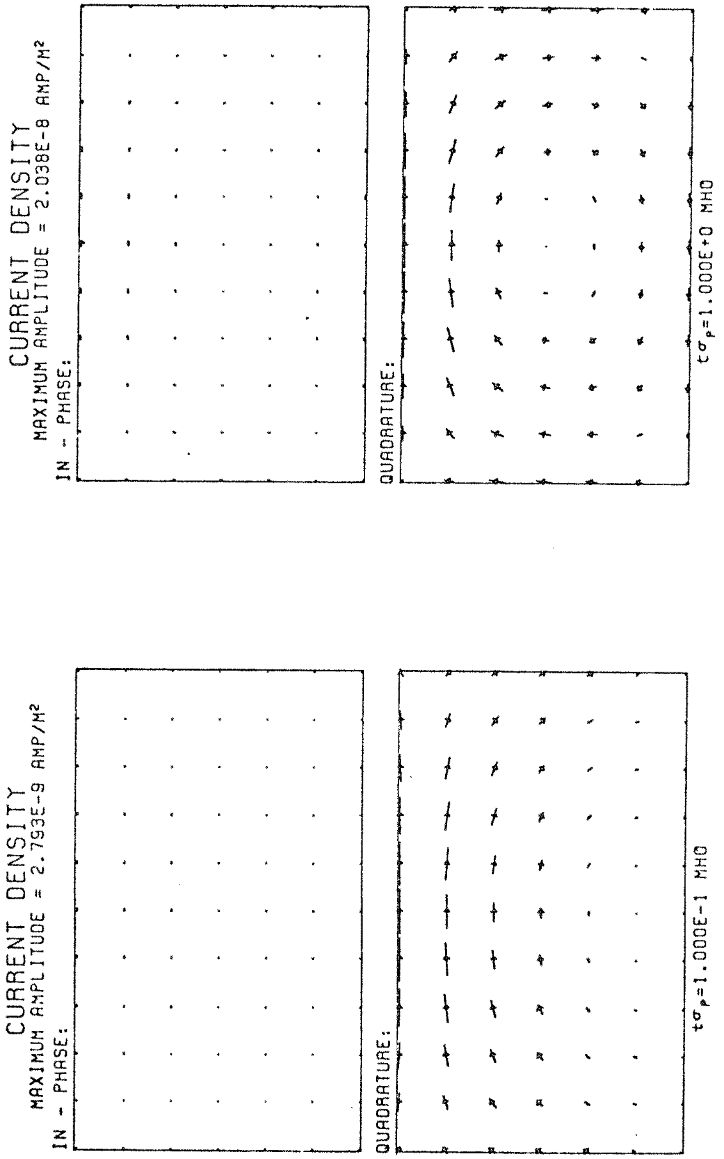

Fig. 4-9c. Series #3.

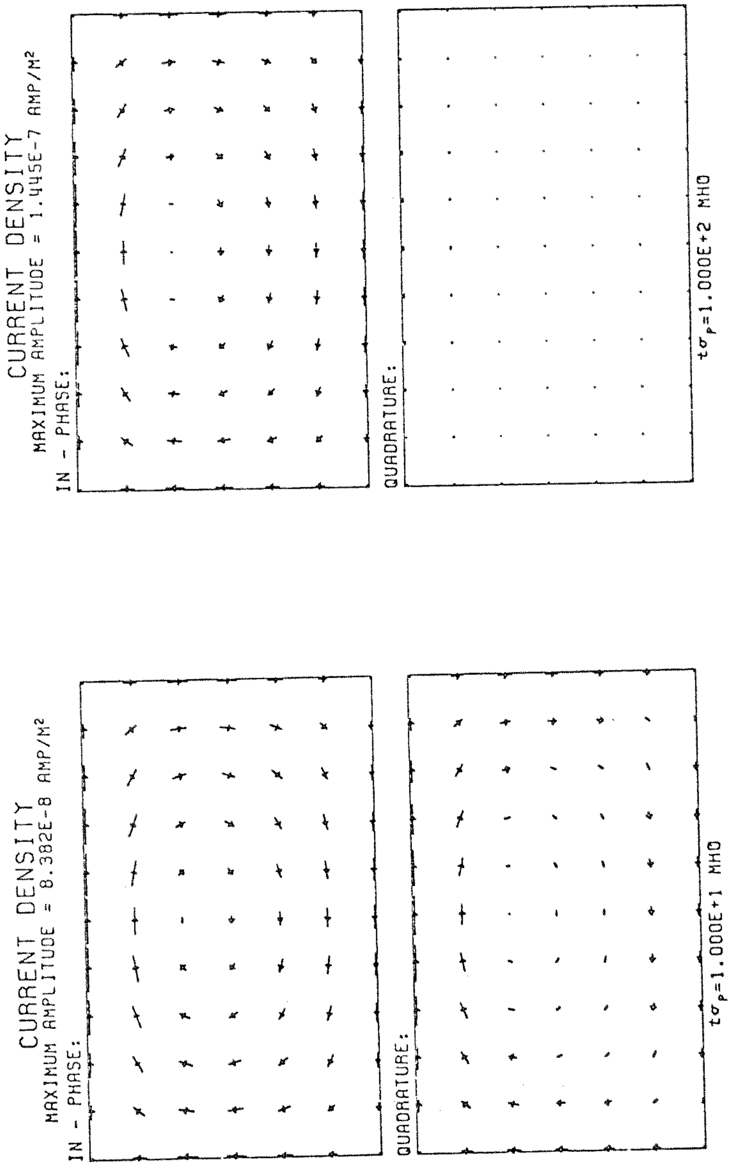

Fig. 4-9d. Series #3.

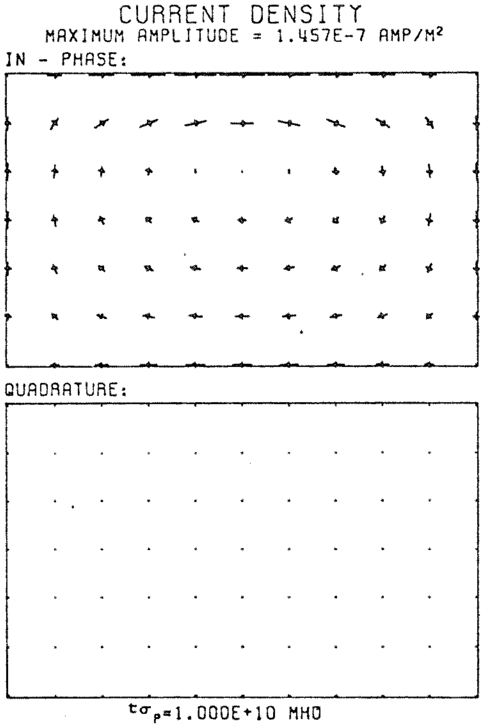

Fig. 4-9e. Series #3.

SERIES #4

SAME AS SERIES #3 EXCEPT:

σ_H-VARIABLE

$t\sigma_P$=1.000E+0 MHO

Fig. 4-10a. Geometry for series #4

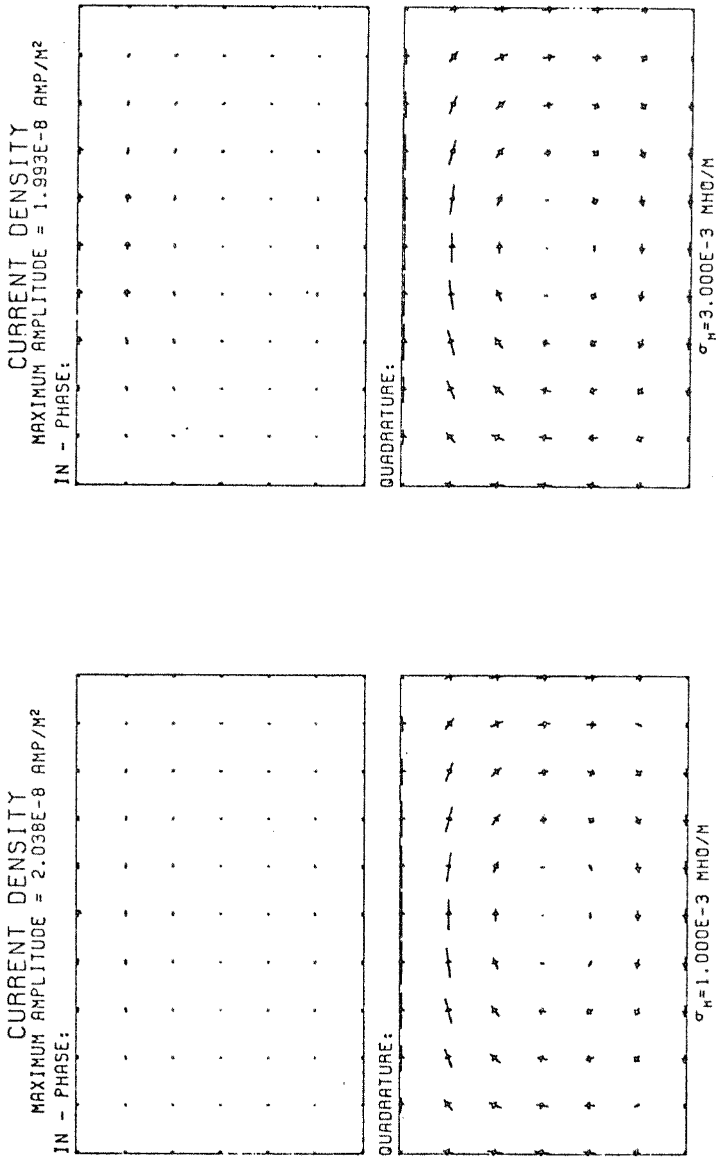

Fig. 4-10b. Series #4.

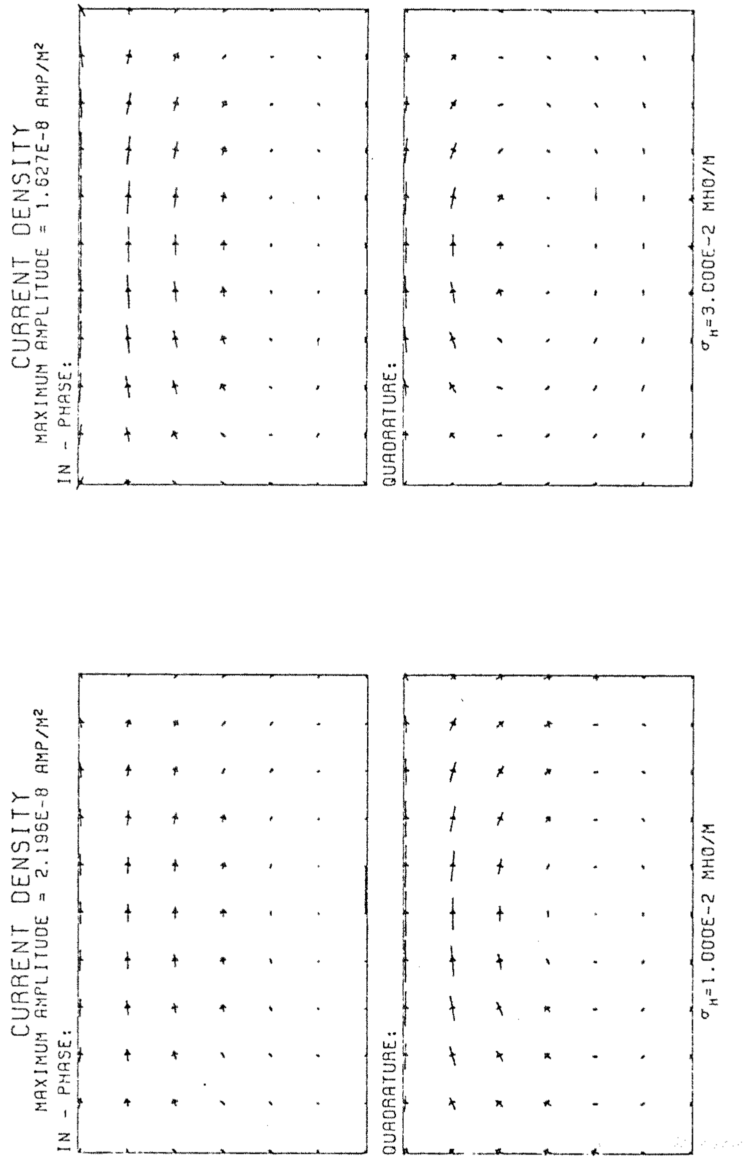

Fig. 4-10c. Series #4.

generated. The matrices are stored onto on-line disk space and later dumped onto magnetic tape. An important point to remember when varying the host conductivity is that the incident electromagnetic field on the plate is changing in both amplitude and phase. When the host reaches $\sigma_H = 10^{-2}$MHO/M, the skin depth is approximately equal to the depth extent of the plate and conduction type currents are predominant. An induction vortex can still be seen in the quadrature component, however. As the host conductivity increases to $\sigma_H = 3 \times 10^{-2}$ MHO/M the skin depth is approximately one third of the depth extent. The induction vortex has shifted from quadrature to in-phase and the conduction quadrature currents are flowing in the opposite direction. This is due to the phase change of the incident electromagnetic field between the dipole and the plate.

CHAPTER 5

NUMERICAL RESULTS FOR THE FINITE PLATE IN A CONDUCTIVE EARTH ENVIRONMENT

5.1 General Comments

The operating cost of the present system of computer programs is such that the routine production of type curves of high accuracy is formidably expensive, especially when considering the large number of independent variables in such problems. Considerable further development and optimization would be required to achieve an economical method. However, the present system can clearly demonstrate the general effect of a conductive environment on the anomaly due to a finite plate. The models chosen for this chapter are therefore intended to give insight into the underlying physical processes of this important geophysical problem. Hopefully, this will result in a better intuitive interpretation and a greater understanding of electromagnetic data from the field.

The system of computer programs is broken up into many steps each with its associated on-line disk storage. The reason for this is that it is frequently unnecessary to change the complete system to obtain the solution for a different mode. When a dataset is no longer required,

it is dumped onto magnetic tape for permanent storage and future use, to avoid having to regenerate it. The simplest procedure for obtaining sets of solutions with the integral equation method is to prepare the on-line datasets for a particular background environment and then to obtain solutions for varying plate conductivity. Then, the appropriate datasets are changed for a different background and the process is repeated. This is in contrast to analogue modelling in a electrolytic tank where the simplest procedure is to vary the operating frequency.

A plate of length to width ratio of 2 with a corresponding grid size of 13x7 is chosen. As was shown in the previous chapter, this grid size leaves something to be desired for numerical accuracy especially at the higher plate conductivities when the currents are more concentrated near the edges of the plate. For an equispaced grid, however, a large number of grid points would be required to adequately represent the edge currents. In any case, the 13x7 grid is sufficient for the purpose herein. Although absolute accuracy of the anomaly intensity in the following models is probably not better than about 10%, the relative accuracy between curves for different background environments is certainly much better.

The electromagnetic source is a fixed rectangular loop on the ground surface, commonly known as a Turam loop (Bosschart, 1964). The repetitive computation for a moving source system would have greatly increased computation costs. Besides, the effects of finite host conductivity are suspected to be greater for the larger sources and thus more important to investigate. The model scale has been chosen to present results for a typical field situation. The simulated field data are anomalous vertical component measurements of the magnetic field, on profiles perpendicular to the strike of the plate, and crossing it at its center. The results are summarized as phasor diagrams of the peak to peak anomaly amplitude expressed as a percentage of the free space vertical field directly over the plate.

The following summary gives an idea of the computer costs involved with the present system. It is based on the low priority commercial user rate (1973) for the IBM 370/ Model 165 at the U. of Toronto. The plate is a 13x7 grid. Generating the basic coefficient matrix costs approximately $25., and the same again for the plate layer interaction matrix. The source vector for the matrix equation costs approximately $15. These are stored for use onto on-line

disk and later dumped onto tape. Once the datasets are ready, the cost of solving for the scattered fields in the plate, when operating in a loop, is approximately $3. Finally, the cost of obtaining the anomalous fields at the surface, on a 128x128 grid, is approximately $3. for each solution.

5.2 The Shallow Conductor in a Half-Space (Model 1)

Figure 5-1 shows the geometrical parameters for model 1, a relatively shallow conductor buried in a halfspace. Figure 5-2 is the phasor diagram corresponding to this model. The solid curves correspond to varying plate conductivity while keeping the host conductivity constant. Alternately, the dashed curves correspond to varying host conductivity only. A characteristic of the phasor curves is the break when the anomaly changes sign. This is because the anomaly amplitude does not pass through zero when changing sign but rather degenerates into two maxima of opposite sign, one decreasing while the other increases. This is considered in more detail in a later section.

Solid curve 1 of Figure 5-2 is the phasor curve for the plate in air. Solid curves 2 to 6 demonstrate the effect on curve 1 as the conductivity of the host halfspace increases. The initial effect of increasing the host conductivity is an increase in the quadrature component of the anomaly. At low host conductivities, the background current flow is mostly in the quadrature phase and this current is being channelled through the plate. As the host conductivity increases further, the current collection by the plate greatly increases the amplitude of the anomaly phasor and clockwise phase rotation begins.

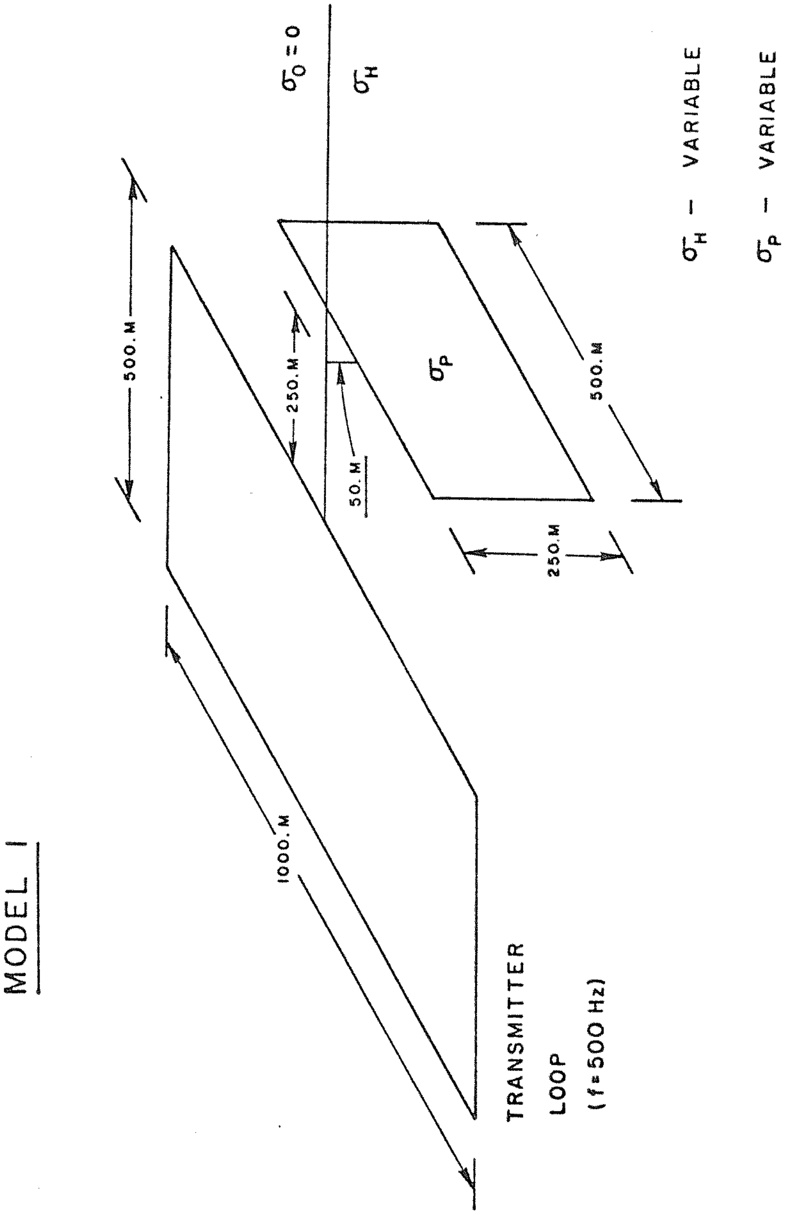

Fig. 5-1. Geometry for Model 1.

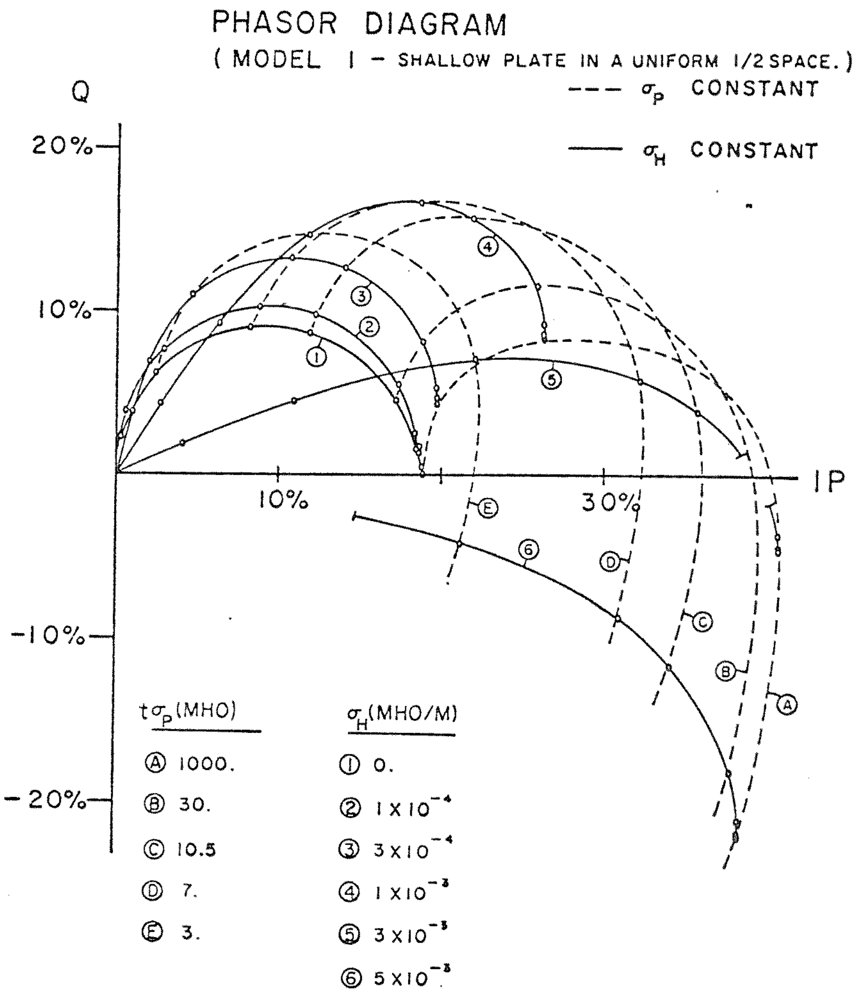

Fig. 5-2. Phasor diagram for Model 1.

The rotation is due both to the phase rotation of the currents flowing in the host conductor and to the phase rotation of the magnetic field causing induction in the plate, which changes phase by the time it reaches the plate through the conductive host. The scattered fields must also change phase between the plate and the surface.

The conductive host obviously has a significant effect on the anomaly from a buried conductor. It can increase the amplitude of the anomaly, which may be thought of as a greater possibility of anomaly detection in the field or, alternatively, as the possibility that weakly conductive features will produce strong unwanted response. Either way, interpretation of anomaly amplitude and width based on the usual model of a plate in air will be erroneous. These observations have also been confirmed by Ward (1973). Eventually, of course, if the host conductivity becomes very large the anomaly must vanish as the skin depth in the halfspace becomes a fraction of the plate depth.

A different method of presenting these results is to express them as a function of independent response parameters for the plate, θ_P and host, θ_H, as suggested by Wong (1973). These parameters are defined by

$$\theta_P = \mu_0 \omega \sigma_P t L$$

and

$$\theta_H = \mu_0 \omega \sigma_H L^2 ,$$

RESPONSE DIAGRAM
(MODEL 1)

IN-PHASE

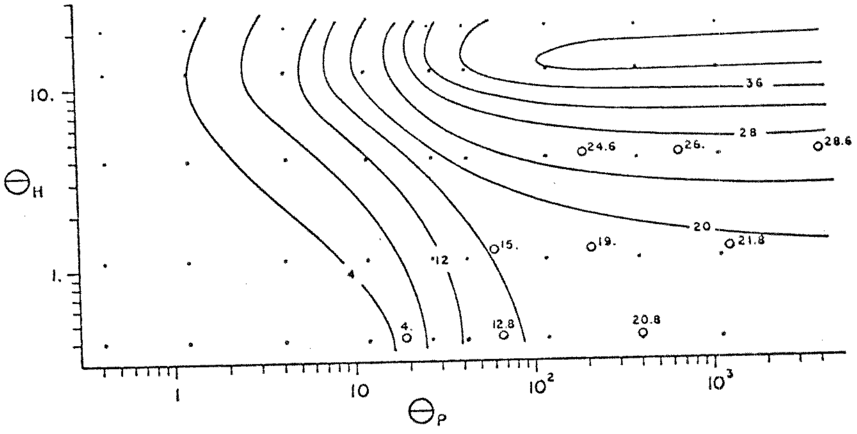

QUADRATURE

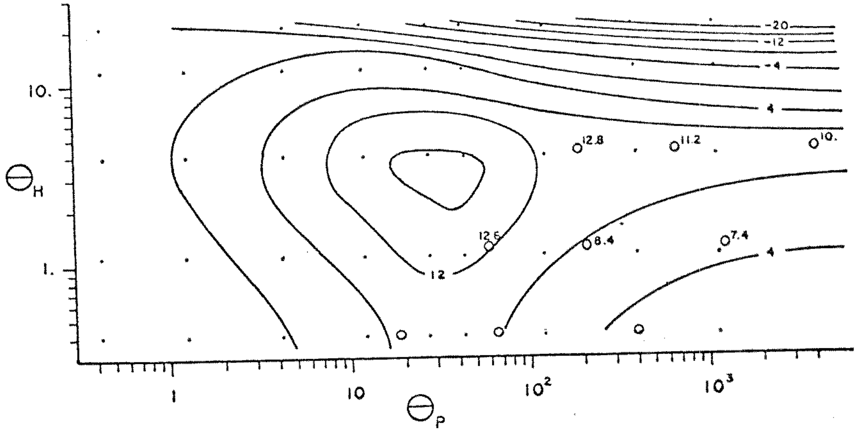

Fig. 5-3. Response disgram for Model 1.

where L is the length of the Turam loop. The numerical model results are shown contoured in Figure 5-3, where measurements from tank model studies by Wong (1973) are shown superimposed. These lie on lines of increasing frequency, at 45^0 to the θ_P and θ_H axes. The fit shows fairly good agreement in both amplitude and phase, especially when considering the many possible sources of error when attempting to compare with tank model data. Besides the computational errors of numerical modelling due to a large grid size, the problems in the tank are mainly those of geometrical positioning, phase stability and the possible existance of surface impedance between the conductor and the host.

5.3 The Deep Conductor in a Half Scace (Model 2)

As shown in Figure 5-4, Model 2 is the same as Model 1 except that the plate is buried deeper. The corresponding phasor and response diagrams are whown in Figure 5-5 and 5-6 respectively. The results are very similar to those of Model 1. The increase in anomaly amplitude is comparatively larger for this model since there is more conduction type current available to the plate. Also, the phase rotation is more advanced since the plate is deeper.

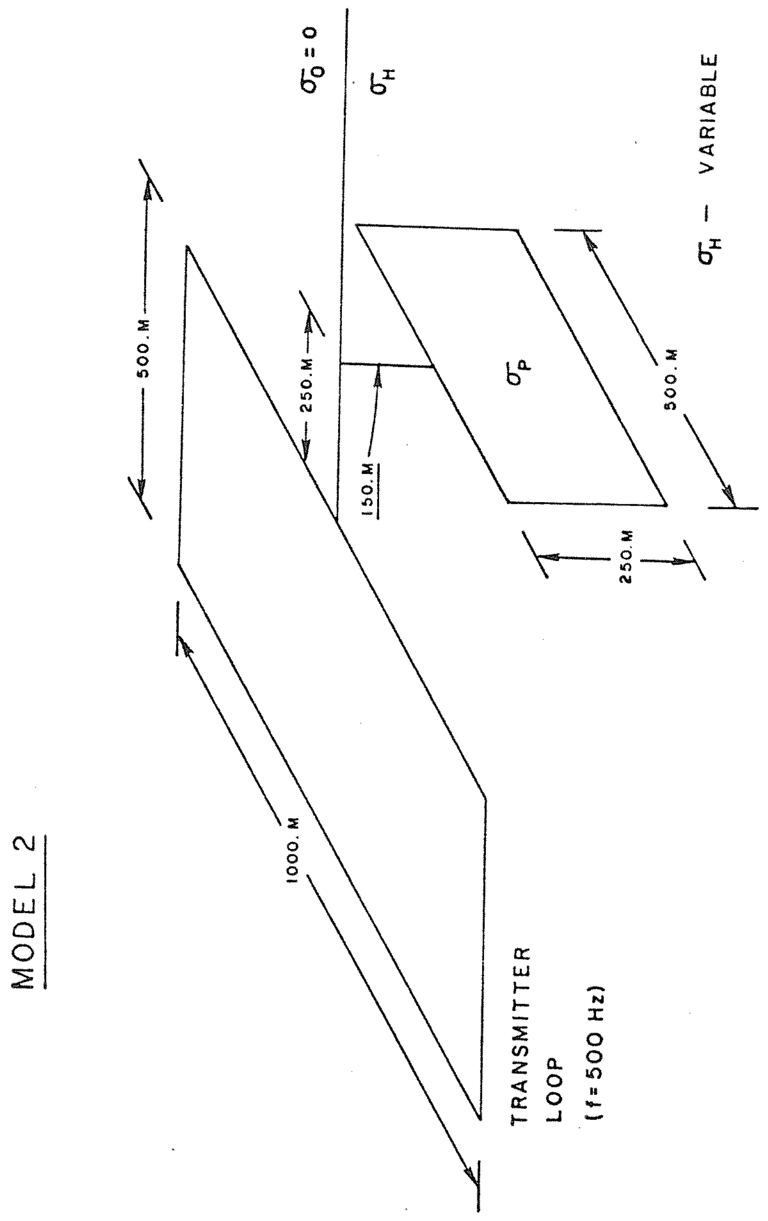

Fig. 5-4. Geometry for Model 2.

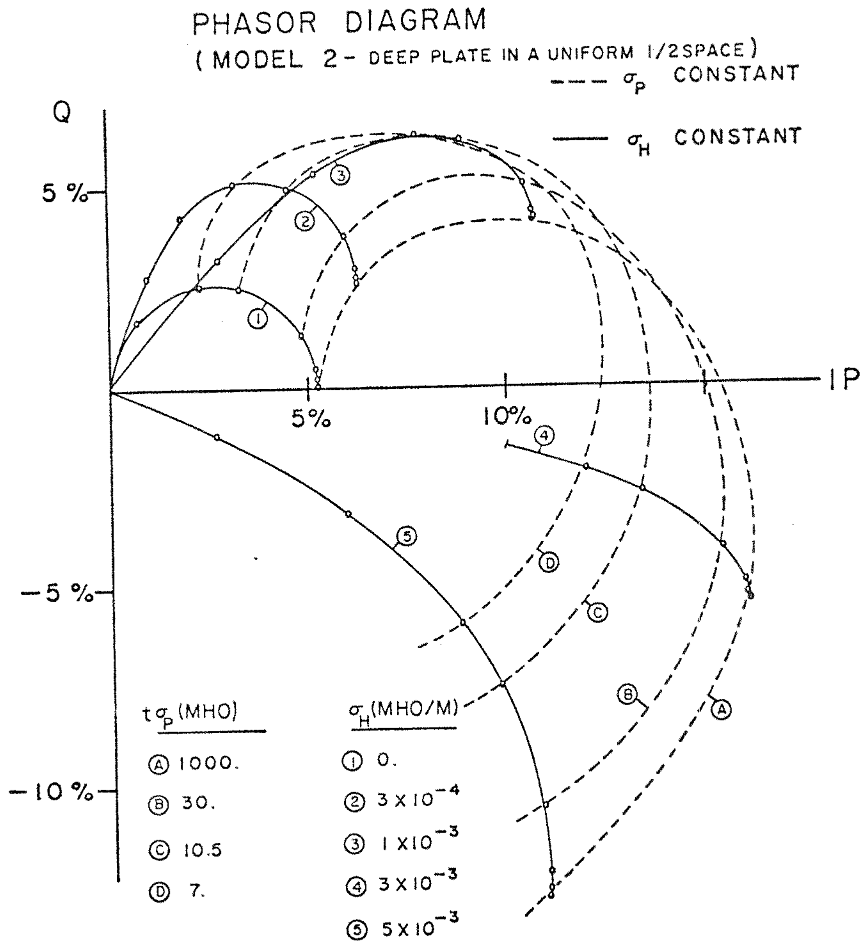

Fig. 5-5. Phasor diagram for Model 2.

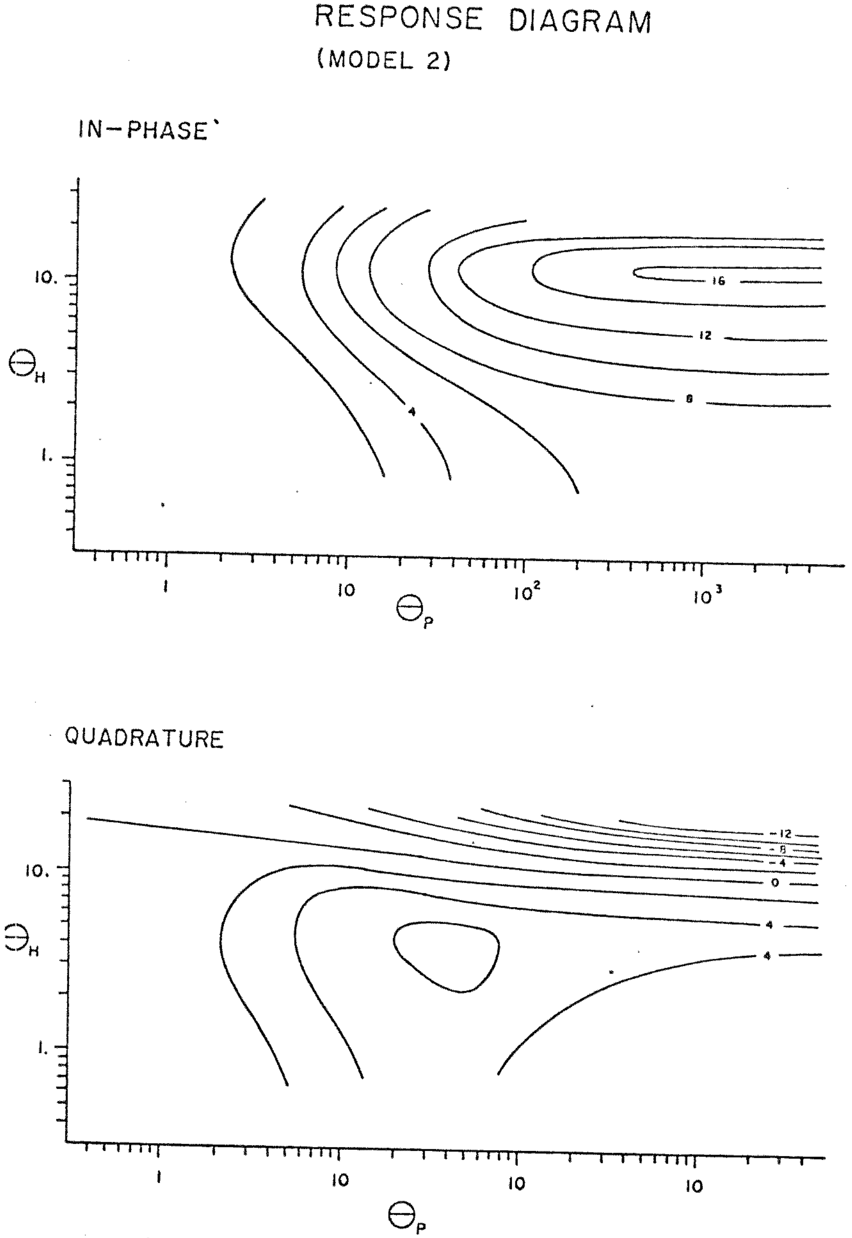

Fig. 5-6. Response diagram for Model 2

5.4 The Effect of Conductive Overburden with Zero Host Rock Conductivity (Model 3)

Figure 5-7 shows the geometry for Model 3, a plate buried under overburden of variable conductivity. The host halfspace under the overburden has zero conductivity in this model. The results are summarized in the phasor diagram of Figure 5-8. The difference between this model and the previous two is evident. When the host rock conductivity is zero, there is no conduction type current available to increase the amplitude of the anomaly. The effect of the layer is to attenuate and rotate the phase of the electromagnetic fields passing through it, this applying of course to both source fields and scattered fields. As shown in Figure 5-8, the anomaly amplitude is attenuated and rotated in phase for increasing layer conductivity, until of course it must reach zero amplitude.

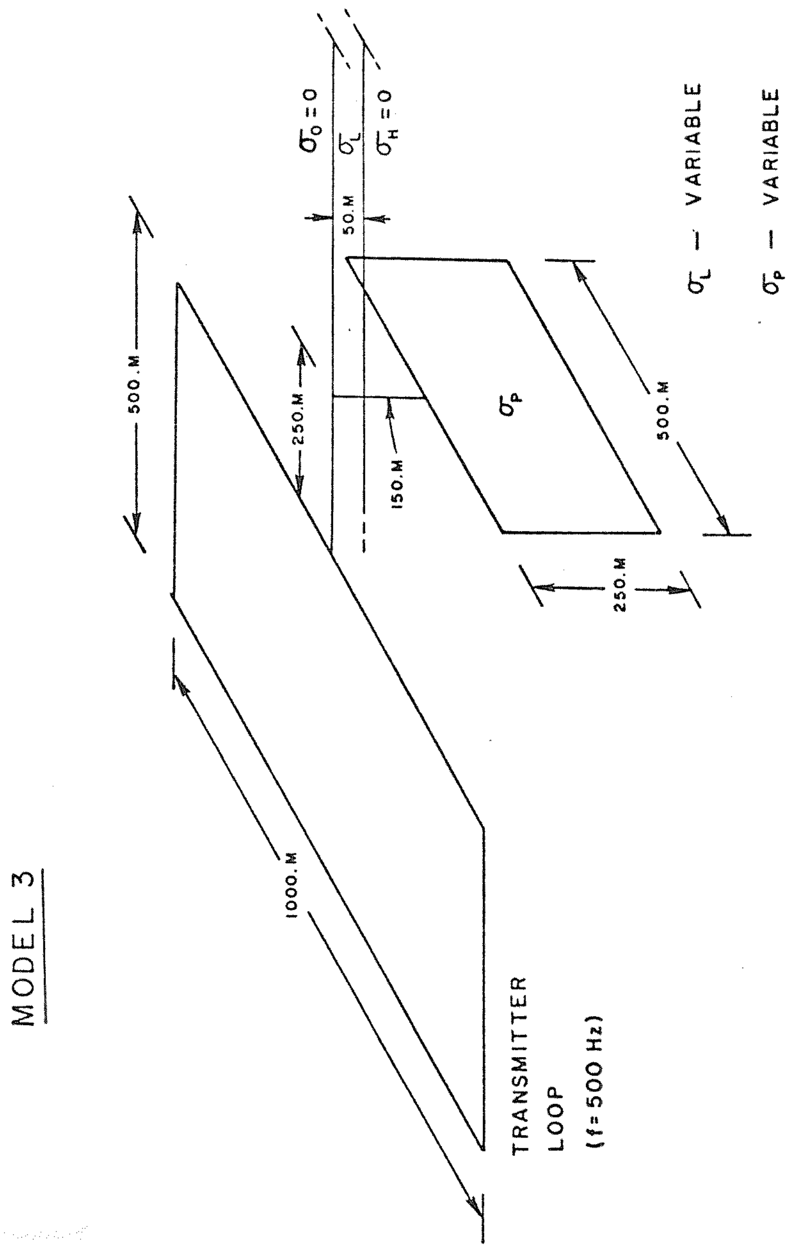

Fig. 5-7. Geometry for Model 3.

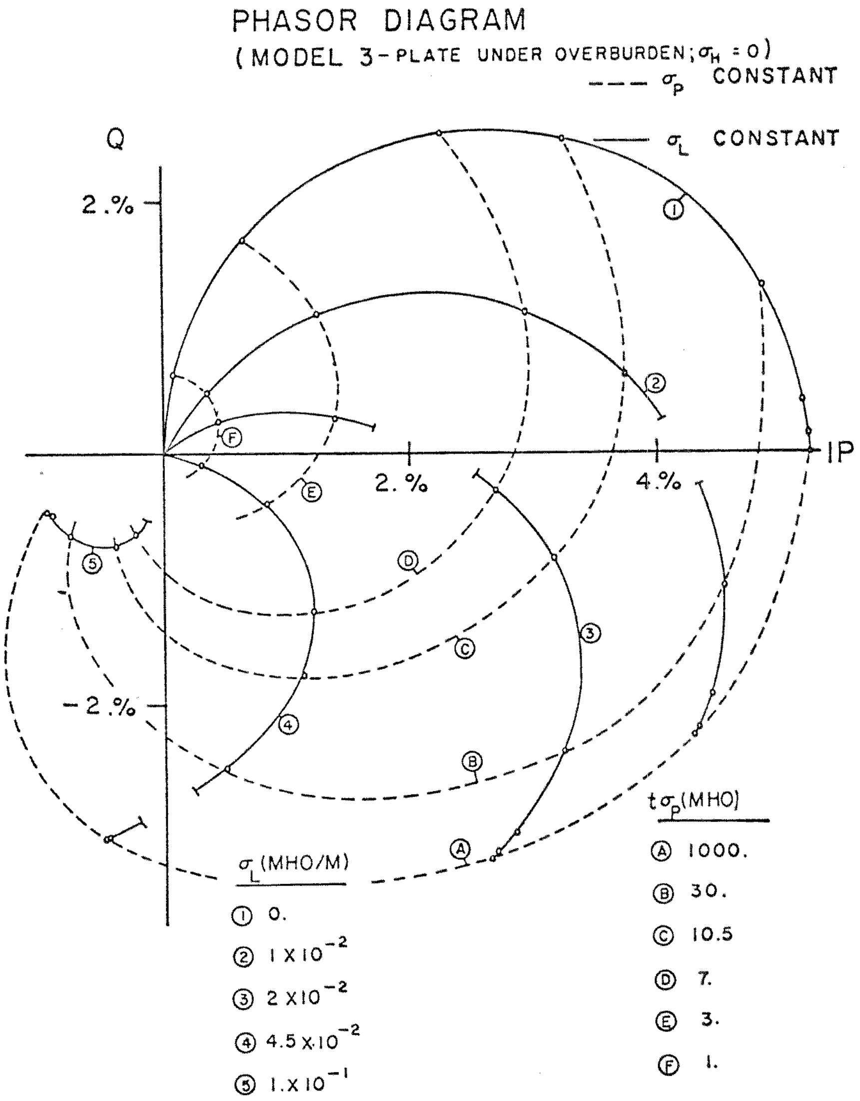

Fig. 5-8. Phasor diagram for Model 3.

5.5 Conductive Overburden with Variable Host Rock Conductivity (Model 4)

Figure 5-9 shows the geometry for Model 4. The conductivity of the 50M thick layer is kept constant at σ_L= .002 MHO/M. In the phasor diagram of Figure 5-10, curve 1 corresponds to curve 3 of Figure 5-8, i.e. for zero host rock conductivity. Phasor curves 2 to 4 demonstrate what happens to curve 1 as the host conductivity is increased. The conduction type currents increase the anomaly amplitude which also rotates in phase. This result is very similar to that of Models 1 and 2. At intermediate host rock conductivities, the conductive layer probably acts as a current source and sink for current channelling through the plate.

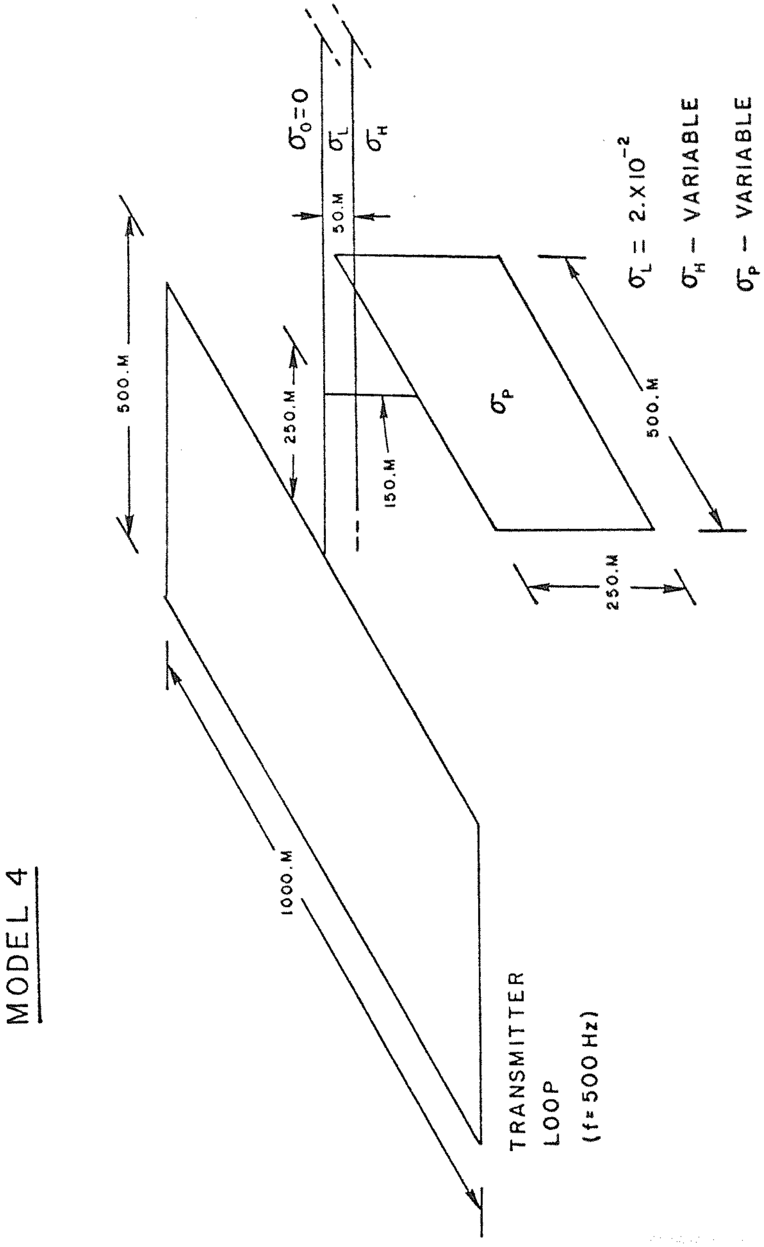

Fig. 5-9. Geometry for Model 4.

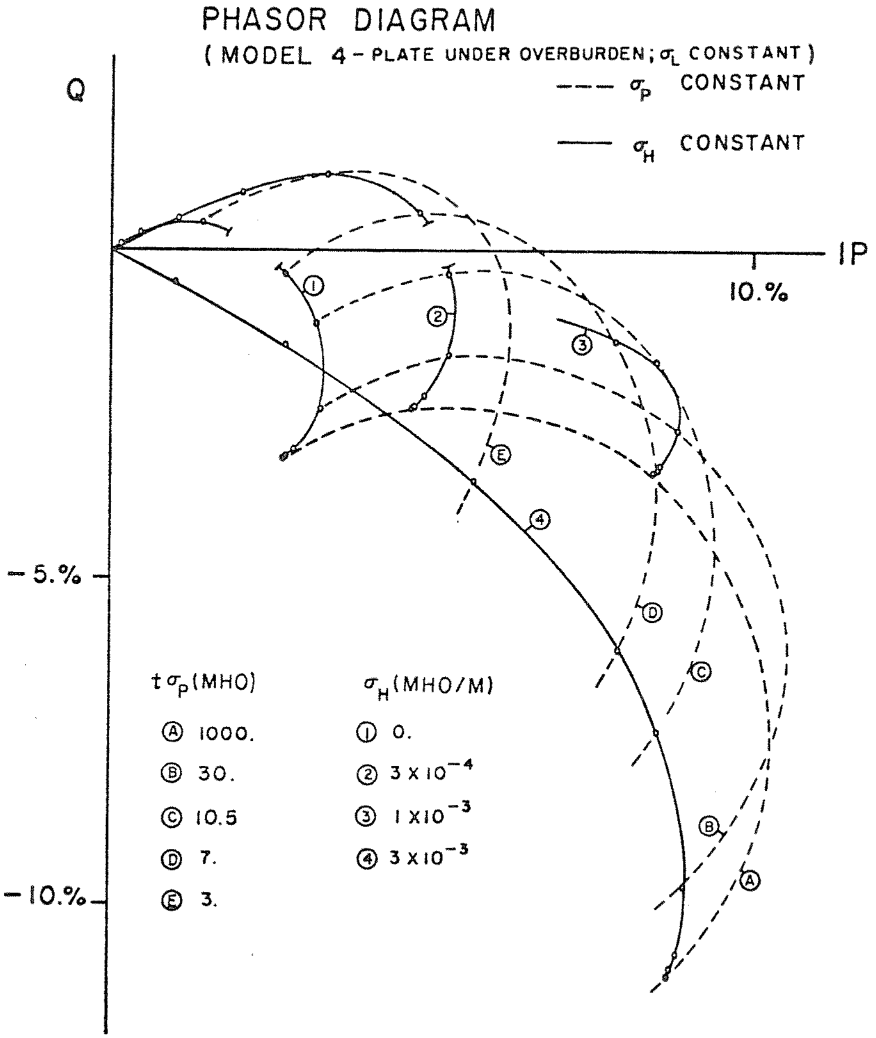

Fig. 5-10. Phasor diagram for Model 4.

5.6 Effect of Source Dimensions (Models 5 & 6)

In this section, the effect of varying source size is investigated for the case of a halfspace host environment and the case of a layer over a non conducting host, as shown in Figure 5-11. Figures 5-12 and 5-13 are the phasor diagrams corresponding to Models 5 and 6 respectively. The results are similar in character in both cases. The percentage anomaly amplitude is largest for some intermediate sized loop and a small positive phase rotation is observed as the source dimension becomes relatively larger. This is because the lower spatial wavenumbers of the electromagnetic field undergo a greater phase change while passing through the layer and halfspace than the higher wavenumbers.

In Model 5 the infinite line results in a larger percentage anomaly amplitude than the dipole. For Model 6, it is the opposite. Also the maximum anomaly corresponds to a larger loop size in Model 5 than in Model 6. This is attributed to the increased coupling with conduction type currents as the loop size increases in the case of the conducting host halfspace of Model 5.

The results seem to indicate that there is an optimum source dimension for maximizing the possibility of anomaly detection. However, much more investigation is required to provide conclusive information.

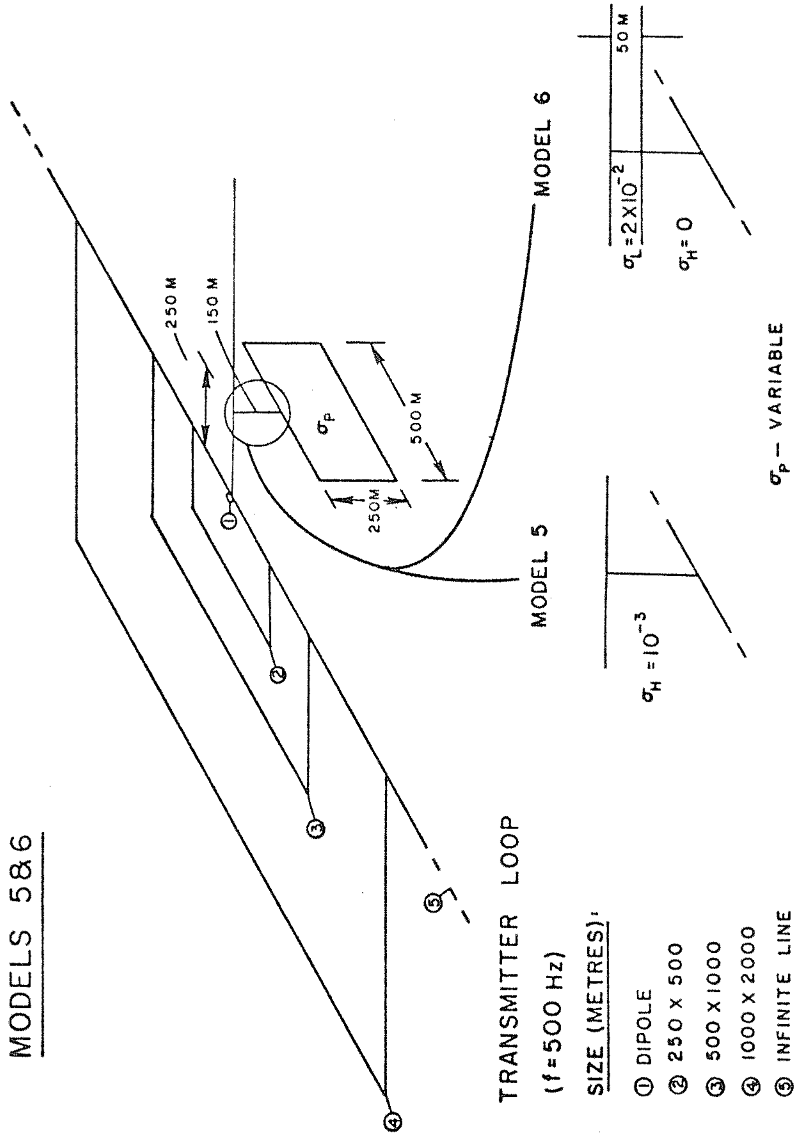

Fig. 5-11. Geometry for Models 5 and 6.

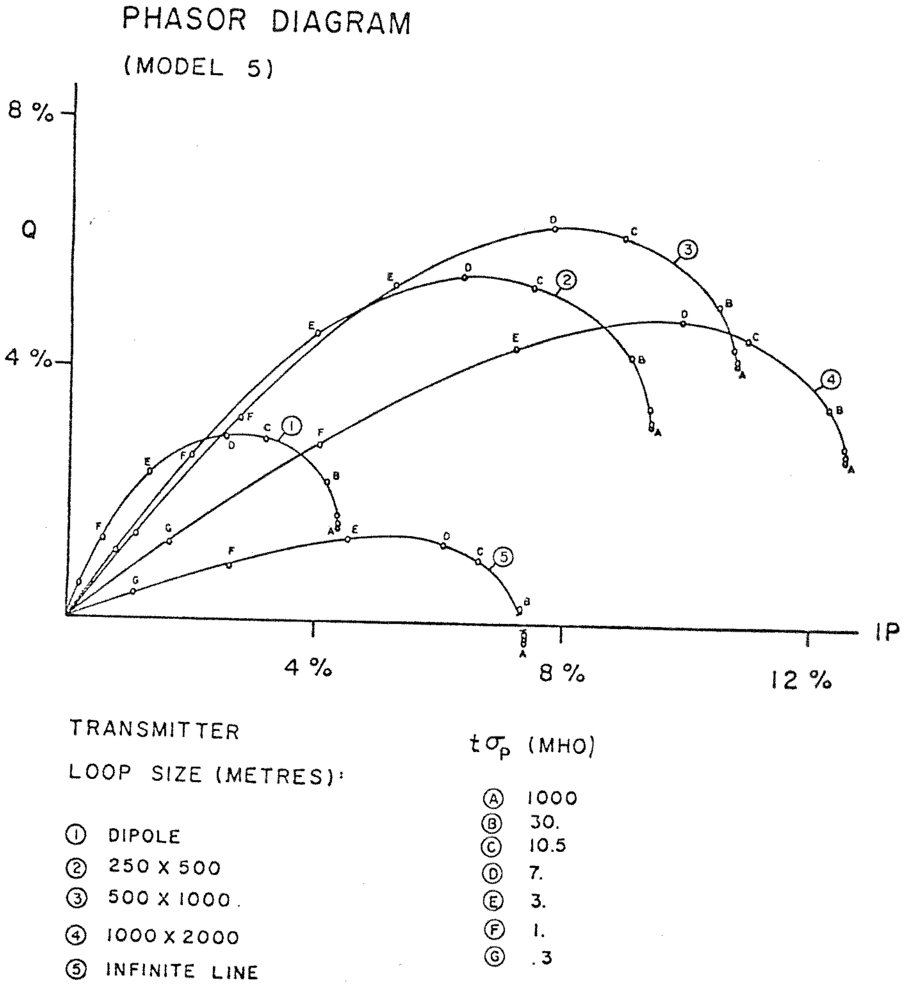

Fig. 5-12. Phasor diagram for Model 5.

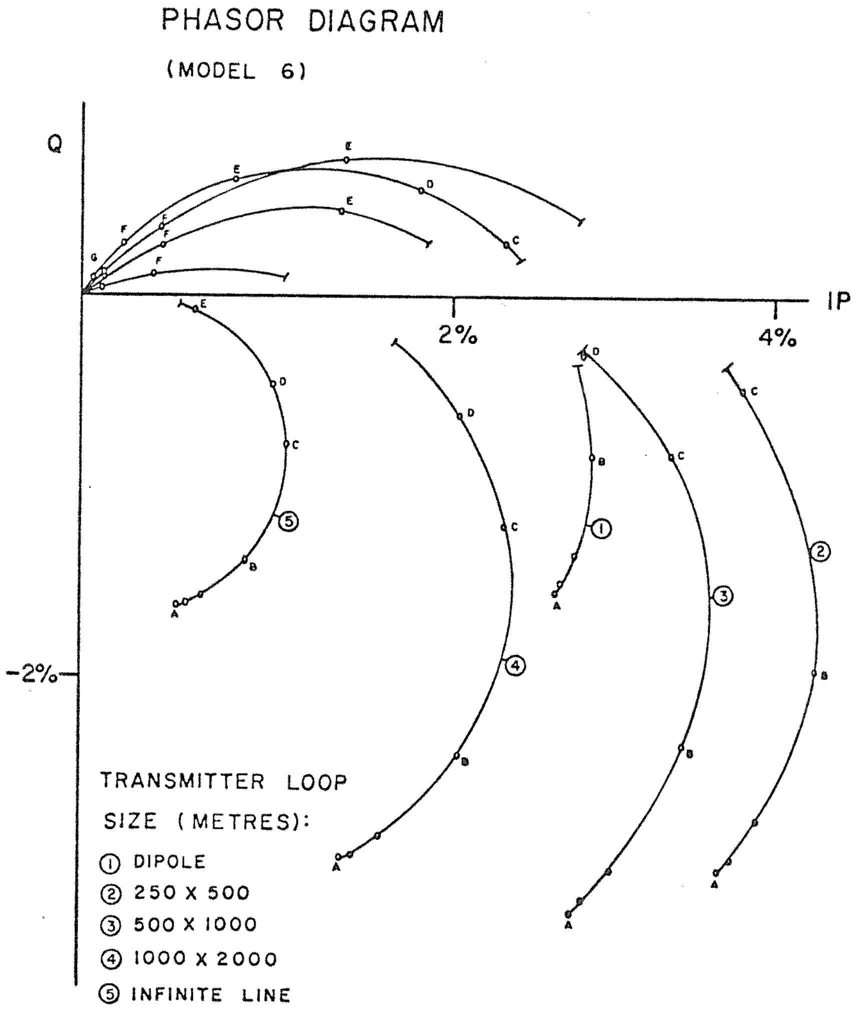

Fig. 5-13. Phasor diagram for Model 6.

5.7 Profile Examples

This section gives examples of centre profiles for the case of the homogeneous halfspace (Model 2) and for the conductive overburden (Model 3). These are shown in Figures 5-14 and 5-15 respectively. The behaviour of the anomaly profiles is similar in both cases. In general, the position of the maximum drifts farther away from the plate as the conductivity of the halfspace or layer increases. This trend becomes interrupted, however, when the anomaly is changing sign. As the conductivity increases, the maximum becomes sharper and shrinks towards the plate. At the same time, a broader peak of opposite sign gains in amplitude farther away from the plate. The latter eventually converges towards the plate and dominates the other in amplitude. This is demonstrated in the quadrature profiles of Figure 5-14, curves 3, 4, and 5, and Figure 5-15, curves 2, 3, and 4.

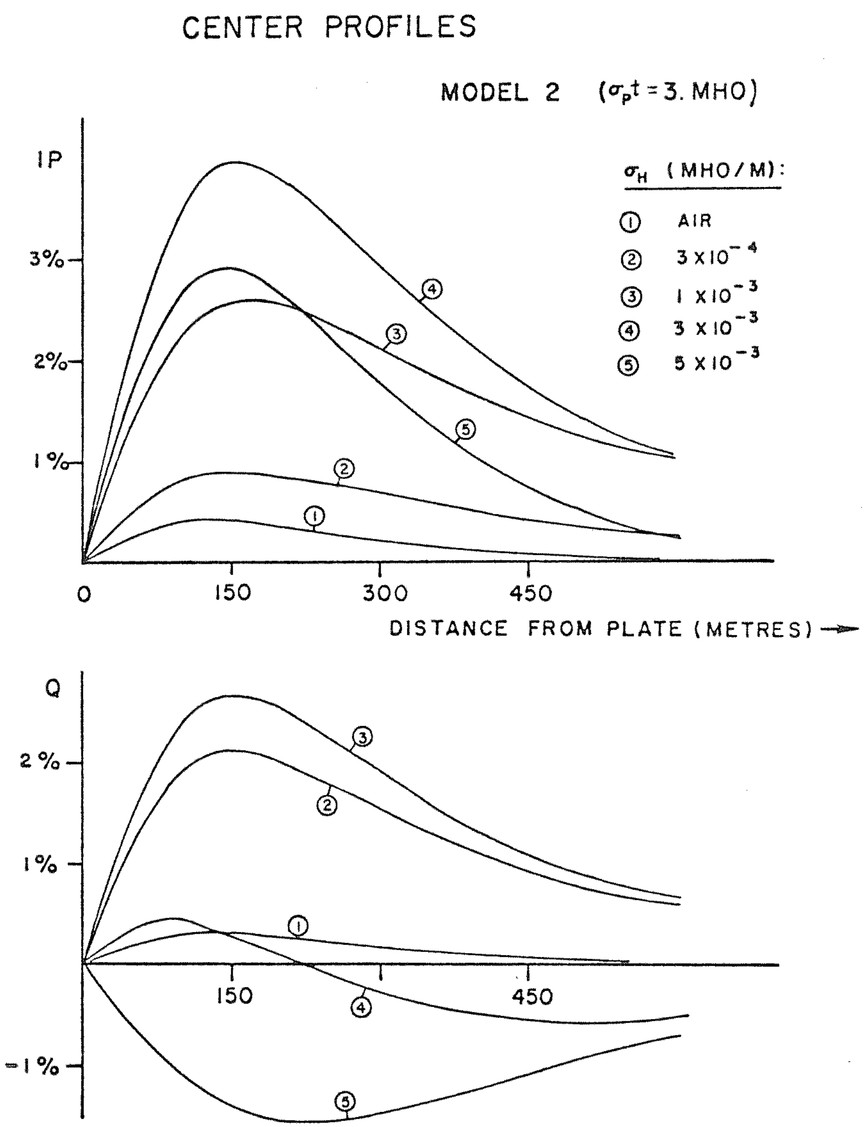

Fig. 5-14. Center anomaly profiles for Model 2.

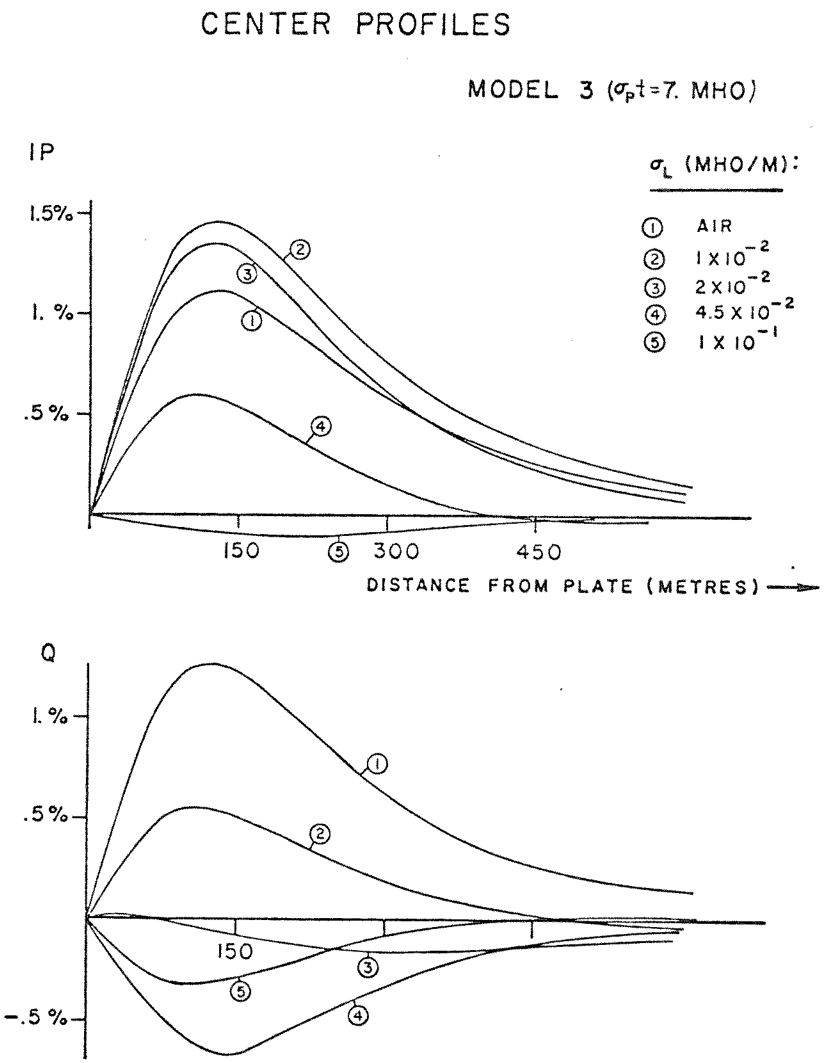

.Fig. 5-15. Center anomaly profiles for Model 3.

CHAPTER 6

CONCLUSIONS

There are two main conclusions to draw from this thesis.

Firstly, the integral equation approach, where the electromagnetic fields in the zone of anomalous conductivity are found, followed by the computation of the secondary fields outside the conductor, has proven very successful. Two chief obstacles have been overcome. In order to bypass the numerical problems encountered with the coefficient matrix, the scattering currents were expressed in terms of two potential functions to represent curl free and divergence free current flow in the anomalous conductor. Also, the computation of large Green's function tensor matrices for the layered earth was overcome through the use of the Fast Fourier Transform. The numerical solution for the scattering current was obtained using a square grid which was interpolated by a fifth degree spline.

Secondly, the physics of the geophysical problem has become somewhat clearer. When a conductive target is shielded by overburden and/or is in contact with a conductive host, the amplitude of the anomaly is altered and the phase is rotated. Two effects are superimposed; first, the phase rotation and attenuation of the primary field in reaching the conductor and the scattering field in reaching the receiver; second, the channelling of regional induced currents in the host medium into the anomalous conductor. Both of these effects occur when a host conductor is in contact with the target while only the first occurs in the case of conductive overburden with zero host rock conductivity.

This thesis has investigated one of many possible approaches for solving electromagnetic problems involving finite targets and finite sources. Alternative approaches may well prove more efficient. Although considerable care was taken to minimize the computer time, now that the first prototype program system is operational, a redesigning of the system with implementation of new ideas could reduce costs and increase the accuracy substantially. The future will undoubtedly see many new developments in the computation of these problems. It is hoped that, eventually, a level of sophistication will be reached whereby they may be solved on a computer interactive system for ease of interpretation. Examples of important problems requiring further research are those of a conductor in contact with the overburden and the response to grounded

sources. With the development of multifrequency and time domain types of instrumentation, coincident with research efforts to increase computational capabilities, the optimal inversion of electromagnetic data may one day become reality.

APPENDIX A

Theoretical Solutions for the Infinite Ribbon Model

The basic formulation for the ribbon model may be found in Grant and West (1965) or Morse and Feshback (1953). A summary of the development as it applies to this study is presented in this appendix.

a) V Potential

The ribbon of infinite conductivity is embedded in a background medium of conductivity σ_H, and lies in the plane y=0 between x=-f and x=+f, as shown in Figure A-1. A uniform source electric field E_o is applied parallel to the x axis.

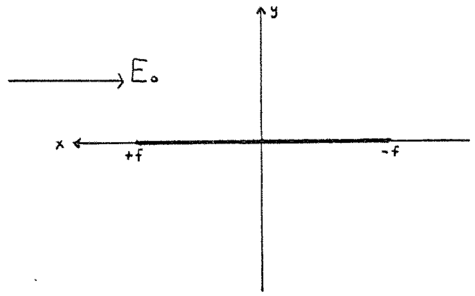

Fig. A-1

From the conservation of stationary electric fields,

The $\bar{E}$ vector may be expressed as the negative gradient of a scalar potential function υ:

$$\bar{E} = -\bar{\nabla}\upsilon \qquad \text{A-1}$$

(note that υ is not the same as V in the integral equation formulation). The problem reduces to solving Laplace's equation for υ subject to the boundary condition that $\upsilon \to 0$ as the ribbon is approached.

The problem is simplified by considering a conformal transformation to the elliptical coordinate system defined by:

$$x = f \cosh\mu \cos\gamma \qquad \text{A-2}$$

and

$$y = f \sinh\mu \sin\gamma \;. \qquad \text{A-3}$$

The lines of constant μ and γ are shown in Figure A-2.

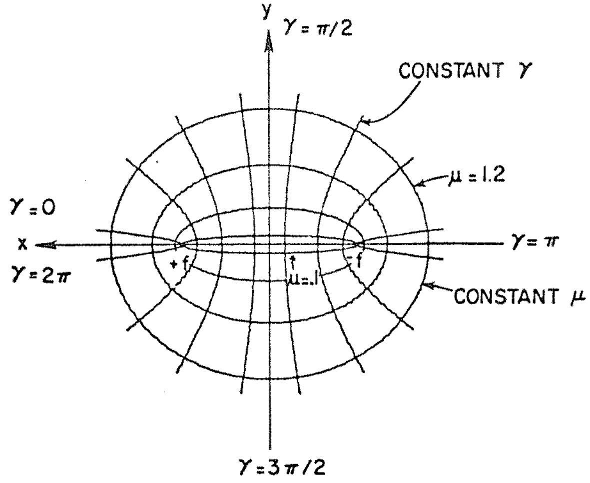

Fig. A-2. Elliptical coordinate system for the V potential.

In the elliptical coordinate system, the ribbon is defined by the thin ellipse $\mu = \mu_0$ where in the limit $\mu_0 \to 0$.

The potential at large distances from the ribbon may be written as

$$\upsilon_0 = - E_0 x \qquad \text{A-4}$$

$$= - f E_0 \cosh\mu \cos\gamma \quad . \qquad \text{A-5}$$

From the characteristic function of Laplace's equation in the elliptical coordinate system and equation A-5, the secondary potential υ^s must be of the form

$$\upsilon^s = e^{-\mu} (A \cos\gamma + B \sin\gamma) \quad . \qquad \text{A-6}$$

Applying the boundary condition $\upsilon = \upsilon^s + \upsilon_0 = 0$ at $\mu = \mu_0$, it follows that B = 0 and

$$A = E_0 f \cosh\mu_0 \, e^{+\mu_0} \quad . \qquad \text{A-7}$$

In the limit $\mu_0 \to$, equation A-6 reduces to

$$\upsilon^s = - E_0 f \, e^{-\mu} \cos\gamma \quad . \qquad \text{A-8}$$

In the elliptical coordinate system, the gradient operator is defined by

$$\bar{\nabla} \Psi = \frac{1/f}{(\cosh^2\mu - \cos^2\gamma)^{1/2}} \left[\bar{\mu} \frac{\partial \psi}{\partial \mu} + \bar{\gamma} \frac{\partial \psi}{\partial \gamma} \right] ; \qquad \text{A-9}$$

where $\bar{\mu}$ and $\bar{\gamma}$ denote the unit vectors in the μ and γ directions respectively.

The current density $\bar{J}$ passing through a surface μ = constant is then

$$J_\mu(\mu, \gamma) = - \sigma_H \frac{(1/f)}{(\cosh^2\mu - \cos^2\gamma)^{1/2}} \frac{\partial}{\partial \mu} (\upsilon^s + \upsilon^0) \qquad \text{A-10}$$

$$= \frac{- \sigma_H E_0}{(\cosh^2\mu - \cos^2\gamma)^{1/2}} \left\{ e^{-\mu} \cos\gamma - \sinh\mu \cos\gamma \right\} . \qquad \text{A-11}$$

When $\mu \to \mu_0$, J_μ represents the current density entering the ribbon from the background medium of conductivity σ_H. Considering both surfaces, the current density J^E entering the plate, for μ_0 small, is

$$J^E(\gamma) = \frac{- 2 \sigma_H E_0 \cos\gamma}{(1 - \cos^2\gamma)^{1/2}} \quad . \qquad \text{A-12}$$

Transforming back to the Cartesian coordinate system, using the inverse relation:

$$2 f \cos\gamma = (y^2 + (f + x)^2)^{1/2} - (y^2 + (f - x)^2)^{1/2} \quad , \qquad \text{A-13}$$

we obtain

$$J^E(x) = \frac{- 2 \sigma_H E_0 x}{(f^2 - x^2)^{1/2}} \quad . \qquad \text{A-14}$$

The total current accumulated in the ribbon per unit strike length is

$$\int^{x} J^{E}(x)\,dx \quad . \qquad \text{A-15}$$

The current density J^{I} in the ribbon is therefore given by

$$J^{I}(x) = \frac{1}{t}\int^{x} J^{E}(x)\,dx \quad ,$$

$$= \frac{2\sigma_H E_0}{t}\left(f^2-x^2\right)^{1/2} \quad . \qquad \text{A-16}$$

where t is the thickness of the ribbon. Note that J^{I} is equal to zero at the edges of the ribbon.

J^{I}, however, must also be given by

$$J^{I} = -\sigma_p \frac{\partial V}{\partial x} \quad , \qquad \text{A-17}$$

where V is the potential used in the integral equation formulation and σ_p is large. Equating A-16 and A-17,

$$\sigma_p t V = -2\sigma_H E_0 \int^{x} \left(f^2-x^2\right)^{1/2} dx \quad . \qquad \text{A-18}$$

From integral tables (Dwight, 350.01) equation A-18 reduces to

$$\sigma_p t V = -2\sigma_H E_0 \left\{ \frac{x\left(f^2-x^2\right)^{1/2}}{2} + \frac{f^2}{2}\sin^{-1}\frac{x}{f} \right\} \qquad \text{A-19}$$

From equation A-16, the current density at the center of the ribbon is given by

$$J_c = \sigma_H E_0 \frac{\ell}{t} \quad , \qquad \text{A-20}$$

where ℓ is the width of the ribbon.

From equation A-19, the potential at the edge of the ribbon is given by

$$t\sigma_p V = \pm\, \sigma_H E_0 f^2 \frac{\pi}{2} \quad . \qquad \text{A-21}$$

b) U Potential

In this case the conductivity of the background medium is zero and the ribbon is in the plane x=0, from y=-f to y=f, as shown in Figure A-3. A uniform alternating magnetic source field H is applied parallel to the x axis.

In the limit of high conductivity, the saturation limit is reached, i.e. the current flow in the ribbon is in phase with the incident H field and acts in such a way as to completely cancel it inside the ribbon.

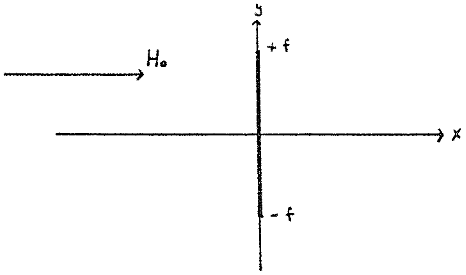

Fig. A-3

As in the last section, H is expressed in terms of the negative gradient of a scalar potential υ:

$$\overline{H} = -\nabla \upsilon .$$

The problem now reduces to solving Laplace's equation subject to the boundary condition that $\partial \psi / \partial \bar{n} \rightarrow 0$ where $\bar{n}$ is the unit vector normal to the surface of the ribbon.

The transformation to the elliptical coordinate system is defined by:

$$x = f \sinh \mu \sin \gamma \qquad \text{A-23}$$

and $$y = f \cosh \mu \cos \gamma ,$$

as shown in Figure A-4.

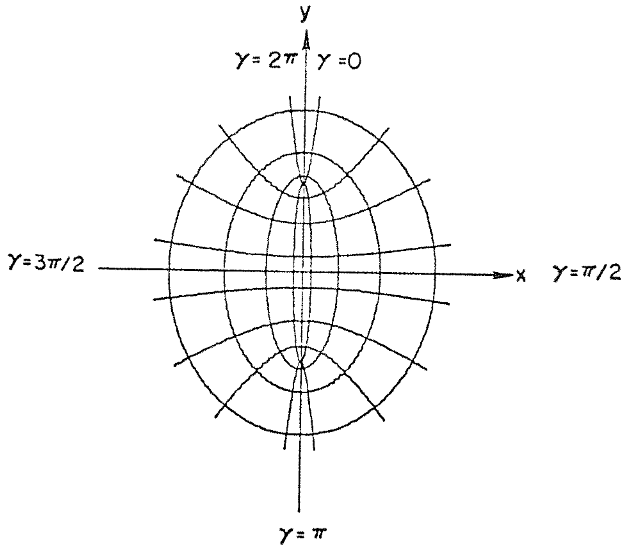

Fig. A-4

The potential at large distances from the ribbon may be written as

$$\begin{aligned} \nu_o &= -H_o x \\ &= -H_o f \sinh \mu \sin \gamma . \end{aligned} \qquad \text{A-24}$$

As in the last section, the secondary potential must be of the form

$$\nu^s = e^{-\mu} (A \cos \gamma + B \sin \gamma) . \qquad \text{A-25}$$

Applying the boundary condition $\frac{\partial}{\partial \mu} (\nu = \nu^o + \nu^s) = 0$ at $\mu = \mu_o$, it follows that

$$A = 0$$

and $$B = -H_o f \cosh \mu_o e^{\mu_o} . \qquad \text{A-26}$$

Therefore, in the limit $\mu_o \rightarrow 0$, equation A-25 becomes

$$\nu^s = -H_o f e^{-\mu} \sin \gamma . \qquad \text{A-27}$$

In order to find the current density in the ribbon, we now consider a small section transverse to its strike as shown in Figure A-5.

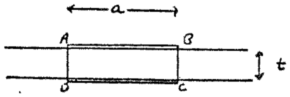

Fig. A-5

From Ampere's law,

$$\oint_{ABCD} H \cdot dl = I^t \quad , \qquad \text{A-28}$$

where I^t is the transverse current flowing in the ribbon. Since H is zero inside the ribbon, there is no contribution to the integral from the arms BC and DA. We may assume that a is small enough such that H is constant over the distance a. Equation A-28 reduces to

$$a\{H_y(y,+t/2) - H_y(y,-t/2)\} = J_z(y)\, t \cdot a \quad . \qquad \text{A-29}$$

From the symmetry of the ribbon in a uniform field,

$$H_y(y,+t/2) = -H_y(y,-t/2) \quad . \qquad \text{A-30}$$

Therefore, equation A-29 reduces to

$$2H_y(x,+t/2) = t\, J_z(y) \quad , \qquad \text{A-31}$$

where J is the current density inside the ribbon.

The magnetic field component parallel to the ribbon in the limit $\mu \rightarrow \mu_o$ is obtained from

$$H_\gamma(\mu,\gamma) = \frac{1/f}{(\cosh^2\mu - \cos^2\gamma)^{1/2}} \frac{\partial V^s}{\partial \gamma} \quad , \qquad \text{A-32}$$

since υ^a does not contribute in the limit $\mu \rightarrow \mu_o$.

Therefore,

$$H_\gamma(\mu_o,\gamma) = -\frac{H_o \cos\gamma}{(1-\cos^2\gamma)^{1/2}} \quad . \qquad \text{A-33}$$

Transforming back to the Cartesian coordinate system,

$$H_y(y) = \frac{-H_o y}{(f^2-y^2)^{1/2}} \quad . \qquad \text{A-34}$$

Equating equations A-31 and A-34,

$$J_z(y) = -\frac{2H_o}{t} \frac{y}{(f^2-y^2)^{1/2}} \quad . \qquad \text{A-35}$$

$J_z(y)$, however, must be equal to $-\sigma_p \partial U/\partial y$ where U is the potential in the integral equation formulation and σ_p is large. Therefore,

$$\sigma_p\, t\, U(y) = 2H_o(f^2-y^2)^{1/2} \quad . \qquad \text{A-36}$$

At the center of the ribbon,

$$\sigma_p\, t\, U_c = 2H_o f \quad . \qquad \text{A-37}$$

REFERENCES

Alfonso-Roche, J.R., 1973, A study of the electromagnetic fields generated by a finite grounded wire source: M.Sc. thesis, U. of Toronto.

Annan, P., 1973, Personal communication.

Bosschart, R.A., 1964, Analytical interpretation of fixed source electromagnetic data: Ph.D. thesis, U. of Delft, Holland.

Coggon, J.H., 1971, Electromagnetic and electrical modelling by the finite element method: Geophysics, v.36, 1, p 132-155.

Dosso, H.W., 1966, Analogue model measurements for electromagnetic variations near a coastline; Can. J. Earth Sci., v.3, 7, 917-936.

Dwight, H.B., 1969, Tables of integrals and other mathematical data: The Macmillan Company, Toronto.

Frischknecht, F.C., 1967, Fields about an oscillating magnetic dipole over a two-layer earth, and application to ground and airborne ele-tromagnetic surveys: Quarterly of Colorado School of Mines, v.62, no.1.

Geyer, R.G., 1972, The effect of a dipping contact on the behaviour of the electromagnetic field: Geophysics, v.37, 2, 337-350.

Goldstein, M.A., 1971, Magnetotelluric experiments employing an artificial dipolar source: Ph.D. thesis, U. of Toronto.

Ghosh, M.K., West, G.F., 1972, AEM analogue model studies: N. Paterson and Assoc., Toronto.

Gupta, C.P., Raval, U., Ramachandra, Y.M., 1973, Quantitative identification of some inherent ambiguities in induction prospecting data: Symposium on Electromagnetic Exploration Methods, University of Toronto.

Harrington, R.F., 1961, Time harmonic electromagnetic fields: McGraw Hill, New York.

1968, Field computation by moment methods: The MacMillan Co., New York.

Hohmann, G.W., 1970, Electromagnetic scattering by two-dimensional inhomogeneities in the earth; Ph.D. thesis, University of California, Berkely.

Jordan, E.C., Balmain, K.G., 1968, Electromagnetic waves and radiating systems: Prentice-Hall, New Jersey.

Lamontagne, Y., 1970, Model studies of the Turam electromagnetic method: M.A.Sc. thesis, U. of Toronto.

1972, Personal communication

1973, A wide-band, time domain ground EM system: Symposium on Electromagnetic Exploration Methods, U. of Toronto.

REFERENCES

Alfonso-Roche, J.R., 1973, A study of the electromagnetic fields generated by a finite grounded wire source: M.Sc. thesis, U. of Toronto.

Annan, P., 1973, Personal communication.

Bosschart, R.A., 1964, Analytical interpretation of fixed source electromagnetic data: Ph.D. thesis, U. of Delft, Holland.

Coggon, J.H., 1971, Electromagnetic and electrical modelling by the finite element method: Geophysics, v.36, 1, p 132-155.

Dosso, H.W., 1966, Analogue model measurements for electromagnetic variations near a coastline; Can. J. Earth Sci., v.3, 7, 917-936.

Dwight, H.B., 1969, Tables of integrals and other mathematical data: The Macmillan Company, Toronto.

Frischknecht, F.C., 1967, Fields about an oscillating magnetic dipole over a two-layer earth, and application to ground and airborne ele-tromagnetic surveys: Quarterly of Colorado School of Mines, v.62, no.1.

Geyer, R.G., 1972, The effect of a dipping contact on the behaviour of the electromagnetic field: Geophysics, v.37, 2, 337-350.

Goldstein, M.A., 1971, Magnetotelluric experiments employing an artificial dipolar source: Ph.D. thesis, U. of Toronto.

Ghosh, M.K., West, G.F., 1972, AEM analogue model studies: N. Paterson and Assoc., Toronto.

Gupta, C.P., Raval, U., Ramachandra, Y.M., 1973, Quantitative identification of some inherent ambiguities in induction prospecting data: Symposium on Electromagnetic Exploration Methods, University of Toronto.

Harrington, R.F., 1961, Time harmonic electromagnetic fields: McGraw Hill, New York.

1968, Field computation by moment methods: The MacMillan Co., New York.

Hohmann, G.W., 1970, Electromagnetic scattering by two-dimensional inhomogeneities in the earth; Ph.D. thesis, University of California, Berkely.

Jordan, E.C., Balmain, K.G., 1968, Electromagnetic waves and radiating systems: Prentice-Hall, New Jersey.

Lamontagne, Y., 1970, Model studies of the Turam electromagnetic method: M.A.Sc. thesis, U. of Toronto.

1972, Personal communication

1973, A wide-band, time domain ground EM system: Symposium on Electromagnetic Exploration Methods, U. of Toronto.

Lowrie, W., West, G.F., 1965, The effect of a conducting overburden on electromagnetic prospecting measurements, Geophysics, v.30, 4, 624-632.

Morse, P.M., Feshback, H., 1953, Methods of theoretical physics: McGraw Hill, New York.

Nabighian, M.N., 1971, Quasi-transient response of a conducting permeable two-layer sphere in a dipolar field: Geophysics, v.36, 1, 25-37.

Negi, J.G., 1967, Electromagnetic screening due to a desseminated spherical zone over a conducting sphere: Geophysics, v.32, 1, 69-87.

Parry, J.R., 1969, Integral equation formulations of scattering from two-dimensional inhomogeneities in a conductive earth: Ph.D. thesis, U. of California, Berkely.

Paterson, N.R., 1972, Extra low frequency (ELF) EM surveys with the EM-25: Paper M1, 42nd Annual SEG Meeting, Anaheim, California.

Sunde, E.D., 1968, Earth conduction effects in transmission systems: Dover Publications Inc., New York.

Swift, C.M., Jr., 1971, Theoretical magnetotelluric and Turam responses from two-dimensional inhomogeneities: Geophysics, 36, 1, 38-52.

Wait, J.R., 1951, A basis of electrical prospecting methods employing time-varying fields: Ph.D. thesis, U. of Toronto.

1970, Electromagnetic waves in stratified media: Pergamon Press, New York.

Ward, S.H., 1967, Electromagnetic theory for geophysical applications: Mining Geophysics, v.2, p.10-196, SEG, Tulsa, Oklahoma.

Ward, S.H., Ryu, J., Glenn, W.E., Hohmann, G.W., Dey, A., Smith, B.D., 1973, Electromagnetic methods in conductive Terraines: Symposium on Electromagnetic Exploration Methods, U. of Toronto.

Weaver, J.T., 1970, The general theory of electromagnetic induction in a conducting half-space: Geophys. J. R. Astr. Soc., V.22, p. 83-100.

West, G.F., 1960, Quantitative interpretation of electromagnetic prospecting measurements: Ph.D. thesis, U. of Toronto.

Wong, J., 1973, Electromagnetic model experiments in an electrolytic tank: M.Sc. thesis, U. of Toronto.